Induction Machine Speed Estimation

Observations on Observers

Bo Peterson

Department of
Industrial Electrical Engineering and
Automation (IEA)
Lund Institute of Technology (LTH)
Box 118
S-221 00 LUND
Sweden

http://www.iea.lth.se/

Abstract

This work focuses on observers estimating flux linkage and speed for induction machines, mainly in the low speed region. With speed estimation, sensorless control is possible, meaning that the speed of induction machines without mechanical speed sensors can be controlled. The observer based sensorless drive system has superior dynamic performance compared to a system with an open loop frequency inverter, yet it is neither more complex nor expensive. Using mechanical equivalent models of the induction machine and observers, an accurate flux observer working in the entire speed region of the induction machine is presented. The flux observer is expanded into a combined flux and speed observer, measuring only stator current and voltage. A method for sensorless control is proposed, analyzed and experimentally verified. Observer and controller calculations are performed by a digital signal processor.

Contents

Acknowledgements

I would like to thank my supervisors Jari Valis and Gustaf Olsson for introducing me to the problems associated with control of electrical drives and for guiding me through the rocky roads of research. I would also like to thank everybody at the Department of Industrial Electrical Engineering and Automation for helping me with all kinds of practical problems.

1

Introduction

The induction motor is the most widely used electrical motor in industrial applications. The majority of induction machines are used in constant speed drives, but during the last decades the introduction of new semiconductor devices has made variable speed drives with induction machines available.

Variable speed induction motors are usually fed by open loop frequency inverters. The rotor speed of the machine is not measured, and a change in load torque will result in a change in speed. The dynamic performance is weak and problems such as oscillations are common.

The work presented in this thesis is a continuation of a work that started with studies of the oscillatory behaviour of inverter fed induction machines (Peterson, 1991). Methods were presented for damping of the oscillations. However, there is more to improve in open loop drives; fast acceleration, fast braking, fast reversal and constant speed independent of load changes are all desirable properties of a drive system. This requires a *fast-acting* and accurate *torque control* in the *low speed region*.

All those properties are obtained with vector controlled induction machines (Leonhard, 1985). The drawback of this method is that the rotor speed of the induction machine must be measured, which requires a speed sensor of some kind, for example a resolver or an incremental encoder. The cost of the speed sensor, at least for machines with ratings less than 10 kW, is in the same range as the cost of the motor itself. The mounting of the sensor to the motor is also an obstacle in many applications. A *sensorless* system where the speed is *estimated* instead of *measured* would essentially reduce the cost and complexity of the drive system. One of the main reasons that inverter fed induction motor drives have become popular is that any standard induction motor can be used without modifications. Note that the term *sensorless* refers to the absence of a speed sensor on the motor shaft, and that motor currents and voltages must still be measured. The vector control method requires also estimation of the flux linkage of the machine, whether the speed is estimated or not.

Research on sensorless control has been ongoing for more than 10 years (Haemmerli, 1986 and Tamai et al, 1987), and it is remarkable that reliable sensorless induction motor drive systems are not readily available. The aim of the work presented here is to derive an applicable method for sensorless control of induction machines. The system must work with standard induction machines and the inverter hardware should not be considerably more complex than present-day open loop frequency inverters.

Problems associated with sensorless control systems have mainly included parameter sensitivity, integrator drift, and problems at low frequencies. Some have tried to solve these problems by redesigning the induction machine (Jansen et al, 1994a).

As it is most unfavourable using anything but standard machines, re-designed motors are not considered the best solution. The questions raised in this work are: what is the best possible solution using standard motors? To what extent can the problems at low frequencies, and the parameter sensitivity problems be reduced?

The feasibility of such a solution is highly facilitated by the arrival of inexpensive digital signal processors. Even though basically the same hardware can be used for a sensorless system and a standard open loop drive, the sensorless system requires substantially more computation capacity.

Overview of the Thesis

After a general discussion on the induction machine model, an introduction to flux estimation is given, with the assumption that rotor current is zero. A discussion on flux estimation, now considering the fact that the rotor current may differ from zero follows, assuming that the rotor speed can be measured. In the next chapter, methods for speed and flux estimation are described when the measured speed signal is no longer available. A combined speed and flux observer overcoming accuracy problems and integrator drift problems at low frequencies in earlier attempts is presented. This is followed by a description of an experimental set-up used for testing the proposed sensorless drive system. Finally the results obtained by experiments are presented. Throughout the thesis, mechanical equivalent models are used to clarify the behaviour of the induction machine and the flux and speed estimators.

2

Induction Machine Models

It is crucial to start with a good and appropriate model of the induction machine when designing flux observers. In this chapter a complete model for the induction machine as well as simplified models assuming that the rotor current is zero will be discussed. The simplified models will later be used as a start when analyzing flux observers.

Dynamic Model of the Induction Machine

The standard vector equations (2.1)-(2.2) relating stator and rotor currents and flux linkages (Kovács, 1984), including stator and rotor leakage inductances L_{sl} and L_{rl}, are written

$$\boldsymbol{\Psi}_s^T = \left(L_{sl} + L_m\right)\mathbf{i}_s^T + L_m\mathbf{i}_r^T \tag{2.1}$$

$$\boldsymbol{\Psi}_r^T = L_m\mathbf{i}_s^T + \left(L_{rl} + L_m\right)\mathbf{i}_r^T \tag{2.2}$$

and sometimes called the *T-model*, indicated by the *T*-superscript. This set of equations has one redundant parameter and can be rearranged into a set of equations with only one leakage inductance, L_L (Slemon et al, 1980 and Peterson, 1991). The corresponding equations for this *Γ-model* with only one leakage inductance are

$$\boldsymbol{\Psi}_s = L_M\left(\mathbf{i}_s + \mathbf{i}_r\right) \tag{2.3}$$

$$\boldsymbol{\Psi}_r = \boldsymbol{\Psi}_s + L_L\mathbf{i}_r \tag{2.4}$$

The vector differential equations for the stator flux $\boldsymbol{\Psi}_s$, and the rotor flux $\boldsymbol{\Psi}_r$, here in the stator reference frame, and the torque equation are the same for both models,

$$\frac{d\boldsymbol{\Psi}_s}{dt} = \mathbf{u}_s - R_s\mathbf{i}_s \tag{2.5}$$

$$\frac{d\boldsymbol{\Psi}_r}{dt} = jz_p\omega\boldsymbol{\Psi}_r - R_r\mathbf{i}_r \tag{2.6}$$

$$J\frac{d\omega}{dt} = T - T_{load} \tag{2.7}$$

where ω is the mechanical angular velocity of the rotor (rotor speed for short). The scaling of the vectors is chosen so that the magnitude of the stator voltage vector is equal to the *peak value* of the *phase-to-neutral voltage*, and the magnitude of the current vector is equal to the *peak value* of the *line current* (Kovács, 1984). With this scaling, the driving torque T of the motor can be expressed

$$T = \frac{3}{2} z_p \Im\left(\boldsymbol{\Psi}_s^* \mathbf{i}_s\right) = \frac{3}{2} z_p \Im\left(\mathbf{i}_r^* \boldsymbol{\Psi}_s\right) = \frac{3}{2} z_p \Im\left(\mathbf{i}_r^* \boldsymbol{\Psi}_r\right) \tag{2.8}$$

where z_p is the number of pole *pairs*. Throughout this thesis, voltage, current and flux vectors are represented as complex numbers. The complex conjugate of a vector $\mathbf{v} = v_x + jv_y$ is denoted $\mathbf{v}^* = v_x - jv_y$, and $\Im$ denotes imaginary part. The expression $\Im\left(\mathbf{v}^* \mathbf{w}\right) = v_x w_y - v_y w_x$ of the complex variables **v** and **w** is equivalent to the magnitude of the cross product of the vectors **v** and **w**.

A block diagram of the Γ-model, equations (2.3)-(2.7), is shown in Fig. 2.1, where the upper part of the diagram is the real part of the vector equations, and the lower part is the imaginary part of the equations.

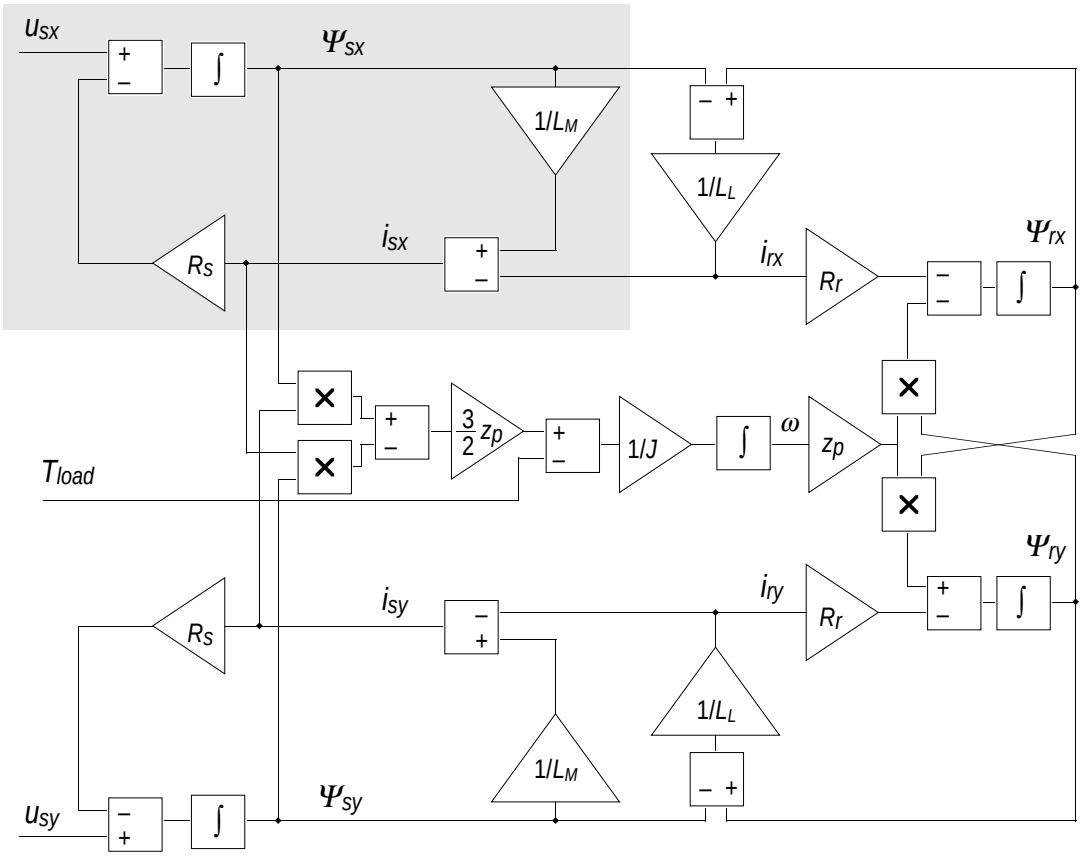

Fig. 2.1 Block diagram of the Γ-model.

The correspondence between the parameters and variables of the two models is described by Table 2.1.

	Model with one leakage inductance (Γ)		Model with two leakage inductances (T)
magnetizing inductance	L_M	=	$\frac{L_m}{k_\gamma}$
leakage inductance	L_L	=	$\frac{L_{sl}}{k_\gamma} + \frac{L_{rl}}{k_\gamma^2}$
stator resistance	R_s	=	R_s^T
rotor resistance	R_r	=	$\frac{R_r^T}{k_\gamma^2}$
stator flux	$\boldsymbol{\Psi}_s$	=	$\boldsymbol{\Psi}_s^T$
rotor flux	$\boldsymbol{\Psi}_r$	=	$\frac{\boldsymbol{\Psi}_r^T}{k_\gamma}$
stator current	$\mathbf{i}_s$	=	$\mathbf{i}_s^T$
rotor current	$\mathbf{i}_r$	=	$k_\gamma \mathbf{i}_r^T$

$$k_\gamma = \frac{L_m}{L_m + L_{sl}}$$

If $L_{sl} = L_{rl}$, it also holds that $k_\gamma = \sqrt{\frac{L_M}{L_M + L_L}}$

Table 2.1 Correspondence between models with one leakage inductance (Γ-model) or two leakage inductances (T-model).

In matrix notation, the Γ-model is described by

$$\frac{d\boldsymbol{\Psi}}{dt} = A(\omega)\boldsymbol{\Psi} + B\mathbf{u}_s \tag{2.9}$$

$$\mathbf{i}_s = C\boldsymbol{\Psi} \tag{2.10}$$

where

$$A(\omega)=\begin{bmatrix} -R_s\left(\frac{1}{L_M}+\frac{1}{L_L}\right) & \frac{R_s}{L_L} \\ \frac{R_r}{L_L} & \frac{-R_r}{L_L}+jz_p\omega \end{bmatrix} \tag{2.11}$$

$$B=\begin{bmatrix} 1 \\ 0 \end{bmatrix} \tag{2.12}$$

$$C=\begin{bmatrix} \frac{1}{L_M}+\frac{1}{L_L} & \frac{-1}{L_L} \end{bmatrix} \tag{2.13}$$

$$\Psi=\begin{bmatrix} \boldsymbol{\Psi}_s \\ \boldsymbol{\Psi}_r \end{bmatrix}=\begin{bmatrix} \Psi_{sx}+j\Psi_{sy} \\ \Psi_{rx}+j\Psi_{ry} \end{bmatrix} \tag{2.14}$$

Note that the system described by equation (2.9) is a non-linear system, as the rotor speed ω is varying. Saturation leads to variations in the inductances, and the resistances will vary with temperature, introducing additional non-linearities.

A First Approach to a Mechanical Model of the Induction Machine

Matrices and equations give limited insight into the behaviour of a dynamic system. A mechanical equivalent model of the induction machine can be used to get a better understanding (Török et al, 1985 and Peterson, 1991).

A simplified example where the rotor current is assumed to be zero is used as an introduction to the mechanical model. With this assumption, equations (2.3) and (2.5) give

$$\frac{d\boldsymbol{\Psi}_s}{dt}=\mathbf{u}_s-R_s\mathbf{i}_s=\mathbf{u}_s-\frac{R_s}{L_M}\boldsymbol{\Psi}_s \tag{2.15}$$

With zero rotor current, there is no cross coupling between the x-axis and the y-axis of equation (2.15). A block diagram of the x-axis (real axis) equation,

$$\frac{d\Psi_{sx}}{dt}=u_{sx}-R_s i_{sx}=u_{sx}-\frac{R_s}{L_M}\Psi_{sx} \tag{2.16}$$

is shown in Fig. 2.2, which basically is the shaded area of Fig. 2.1.

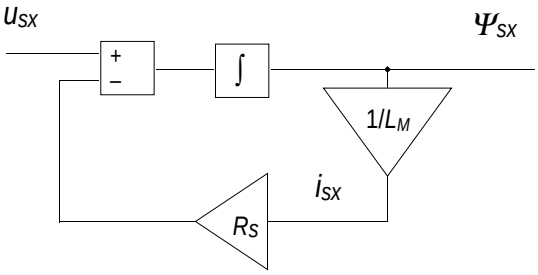

Fig. 2.2 Block diagram of the x-axis equation

In the mechanical model, a coil is represented by a spring. The length of the spring is equivalent to the flux linkage of the coil, and the force acting on the spring represents the current of the coil. Resistance is represented by a viscous damper. The speed difference of the damper's ends is equivalent to the voltage over the resistance. A complete description of the mechanical analogy is found in Appendix B.

A mechanical model of equation (2.16) is shown in Fig. 2.3.

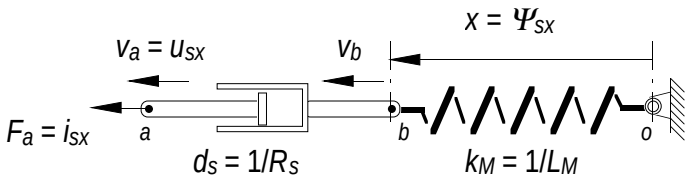

Fig. 2.3 Mechanical model of equation (2.16).

This mechanical system is described by

$$F_{spring} = k_M x \tag{2.17}$$

$$F_{damper} = d_s\left(v_a - v_b\right) \tag{2.18}$$

$$F_a = F_{spring} = F_{damper} \tag{2.19}$$

$$v_b = \frac{dx}{dt} \tag{2.20}$$

Combining equations (2.19)-(2.20) gives

$$\frac{dx}{dt} = v_a - \frac{F_a}{d_s} = v_a - \frac{k_M}{d_s} x \tag{2.21}$$

With the substitutions shown in Fig. 2.3, equation (2.21) is equal to equation (2.16). The mechanical model will be used later to clarify some properties of a flux observer.

A complete mechanical model of the induction machine, including rotor current and rotor flux, is found in Appendix C.

3

An Introduction to Flux Estimation

In order to have a fast acting and accurate control of the induction machine, the flux linkage of the machine must be known. It is, however, expensive and difficult to measure the flux. Instead, the flux can be *estimated* based on measurements of voltage, current and angular velocity. There are different control strategies for the induction machine. Some prefer stator flux control, while others prefer rotor flux control (Leonhard, 1985, Takahashi, 1989 and Lorenz, 1994). The estimators discussed in this chapter are mainly stator flux estimators, since stator flux control is used in later chapters. Throughout this chapter, it is assumed that the rotor current is zero, meaning that the induction machine is running at no load. In Chapter 4, a more accurate estimator will be analyzed.

Estimator A - the Voltage Model

A first simple flux estimator is obtained from equation (2.5) in integral form,

$$\hat{\boldsymbol{\Psi}}_s = \int \left(\mathbf{u}_s - R_{se} \mathbf{i}_s \right) dt \tag{3.1}$$

often referred to as the *voltage model*. The ^ superscript denotes estimated values, and index *e* denotes estimator parameter. Again, we consider only the real part of the equation, and assume the rotor current to be zero (no load torque). Most of the results obtained are valid for the imaginary axis as well, and also when load torque is present.

The estimator for the real axis

$$\hat{\Psi}_{sx} = \int \left(u_{sx} - R_{se} i_{sx} \right) dt \tag{3.2}$$

is shown as a block diagram in Fig. 3.1.

The input to the estimator is the measured current and voltage of the machine. If the stator resistance R_{se} of the estimator is identical to the resistance R_s of the machine, and if the measured current and voltage are without any errors such as noise and offset errors, the output of this estimator would be a perfect estimate of the stator flux, even if the rotor

current differs from zero. This is seen in equation (3.1), where the rotor current does not appear.

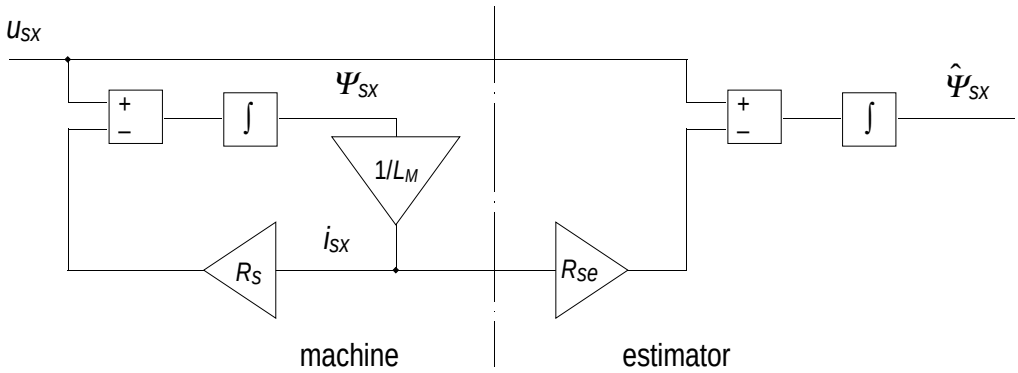

Fig. 3.1 Block diagram of estimator A.

Even the slightest error in R_{se} would cause the estimator to drift at low frequencies. Fig. 3.2 shows the drift of the estimate if the estimator resistance parameter differs from the true resistance with 5 percent. The input voltage u_{sx} is a step from zero at $t = 0$, and then held constant.

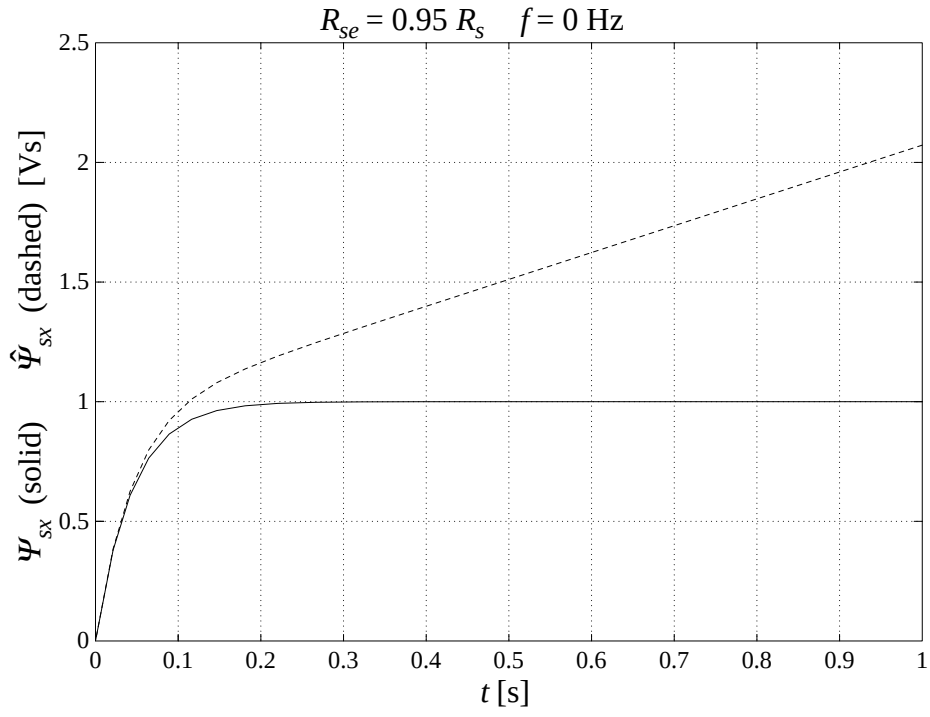

Fig. 3.2 Simulation of estimator A, starting from zero. R_{se} = 0.95 R_s, f = 0 Hz (u_{sx} is constant).

The machine parameters used throughout this thesis are for the IMEP induction machine in Δ-connection, described in Appendix D. This 0.75 kW machine is not representative to all induction machines. The p.u. stator

resistance is much higher for such a small machine than for a larger one. However, the challenges in flux estimation appear at low frequencies, when the term $R_s\mathbf{i}_s$ of equation (2.5) is in the same order of magnitude as $\mathbf{u}_s$. A large value of the stator resistance accentuates this problem.

Initially the estimate tracks the flux, but then drifts to infinity, or until the integrator saturates. The influence of the resistance parameter error is decreasing as the frequency is increasing. Fig. 3.3 shows that the estimate tracks the flux well already at 5 Hz. The error in the resistance is still 5 percent.

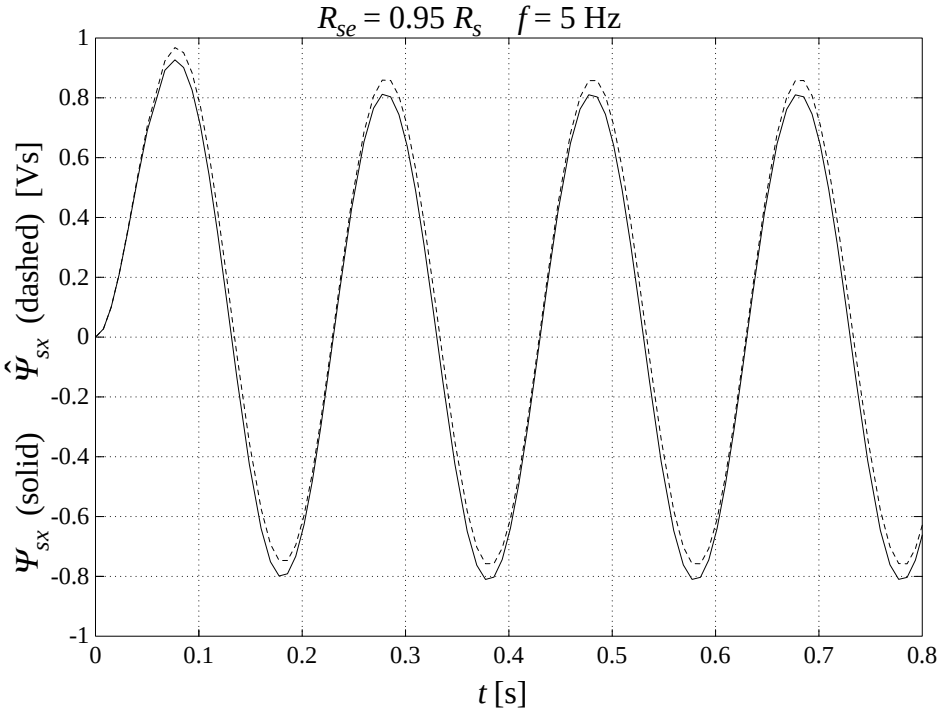

Fig. 3.3 Simulation of estimator A, starting from zero. R_{se} = 0.95 R_s, f = 5 Hz.

Offset in the current measurement will cause drift at all frequencies. The drift at 5 Hz is shown in Fig. 3.4. The offset of the measured current is 5 percent of the current peak value.

It is obvious that this method is of no practical use due to the shown limitations. The problems related to the drifting integrators are often pointed out as the main difficulties with flux estimation at low speeds. (Bausch et al, 1994). In fact, the drift can easily be mastered, as will be shown. The real problems at low frequencies will be discussed in Chapter 5.

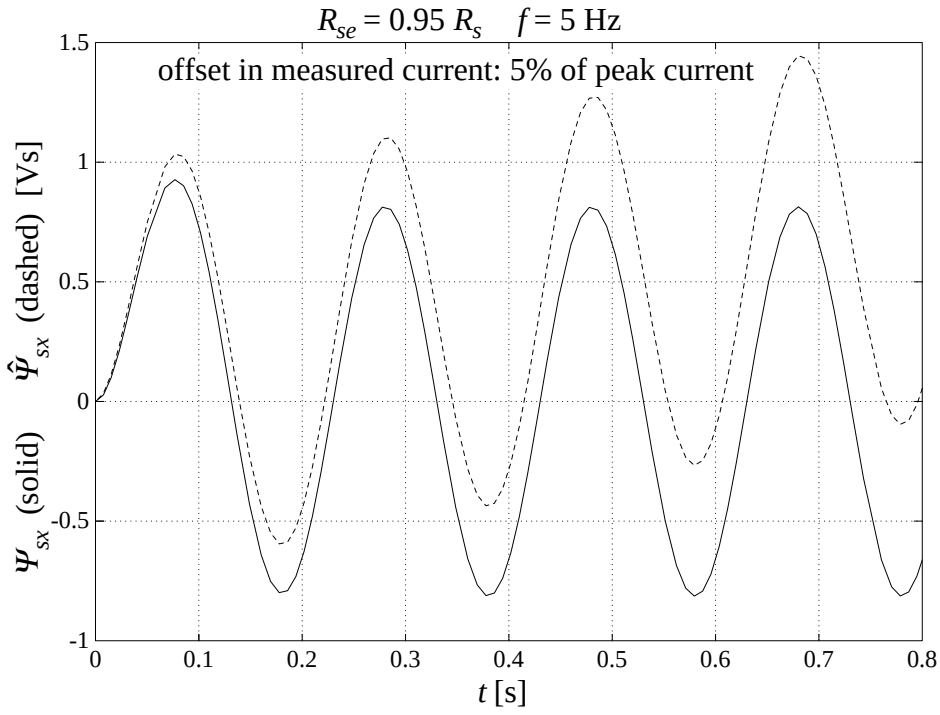

Fig. 3.4 Simulation of estimator A, starting from zero. R_{se} = 0.95 R_s, f = 5 Hz, 5% offset in measured current.

Estimator B - the Current Model

One way to eliminate the drift is to use equation (2.3) as a base for the estimator. Assuming zero rotor current, the estimated flux can be calculated,

$$\hat{\Psi}_{sx} = L_{me} i_{sx} \tag{3.3}$$

shown in Fig. 3.5. Only the measured stator current is used as input to the estimator.

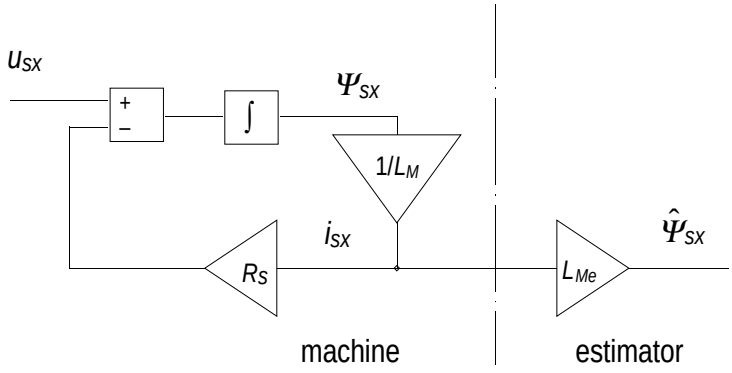

Fig. 3.5 Block diagram of estimator B.

One of the drawbacks of this estimator is that a correct flux estimate requires a correct value of the magnetizing inductance L_M. Due to magnetic saturation in the machine, the inductance is varying, making it difficult to obtain a correct parameter L_{Me}. Fig. 3.6 shows the estimated flux at an error of five percent in the magnetizing inductance.

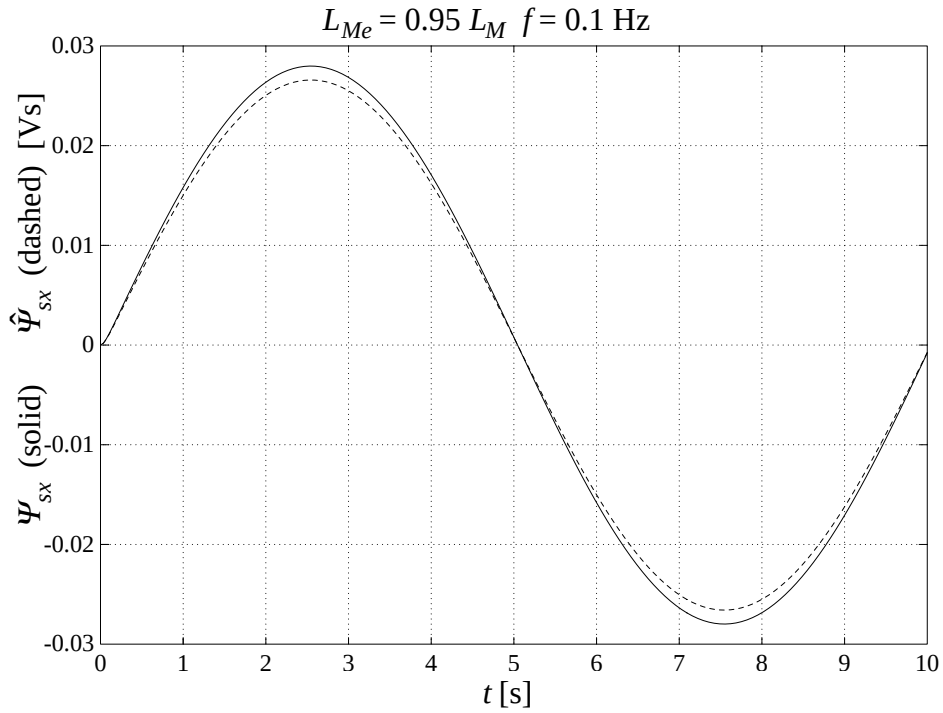

Fig. 3.6 Simulation of estimator B, $L_{Me} = 0.95\ L_M$.

Another drawback of the estimator in (3.3) is that it will produce poor results when the rotor current differs from zero. To compensate for the rotor current, which usually cannot be measured, the angular velocity of the rotor must be measured. Estimator A has the advantage of not being dependent on the speed or rotor current. Equations (2.3) and (2.4) give

$$\boldsymbol{\Psi}_s = \left(L_L \mathbf{i}_s + \boldsymbol{\Psi}_r\right) \frac{L_M}{L_L + L_M} \tag{3.4}$$

In order to calculate the rotor flux in (3.4), equation (2.6) is combined with (2.3) and (2.4) which gives the differential equation

$$\frac{d\boldsymbol{\Psi}_r}{dt} = \mathbf{i}_s \frac{R_r L_M}{L_L + L_M} - \boldsymbol{\Psi}_r \left(\frac{R_r}{L_L + L_M} - j z_p \omega \right) \tag{3.5}$$

We now have the following estimator:

$$\hat{\boldsymbol{\Psi}}_s = \left(L_{Le}\mathbf{i}_s + \hat{\boldsymbol{\Psi}}_r \right) \frac{L_{Me}}{L_{Le} + L_{Me}} \tag{3.6}$$

$$\frac{d\hat{\boldsymbol{\Psi}}_r}{dt} = \mathbf{i}_s \frac{R_{re} L_{Me}}{L_{Le} + L_{Me}} - \hat{\boldsymbol{\Psi}}_r \left(\frac{R_{re}}{L_{Le} + L_{Me}} - jz_p\omega \right) \tag{3.7}$$

The resulting estimator requires measured rotor speed as well as measured stator current as input, as indicated in the simplified block diagram in Fig. 3.7. The estimator, referred to as the *current model* has good properties at low frequencies but is sensitive to parameter errors at high frequencies (Jansen et al, 1994a).

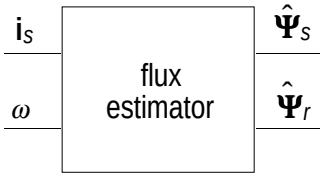

Fig. 3.7 Block diagram showing inputs and outputs of the current model.

Estimator C - Open Loop Simulation

To solve the drift problem of estimator A, the stator current can be estimated instead of measured. If $\mathbf{i}_r = 0$, equations (2.3) and (2.5) suggest the following observer,

$$\hat{\Psi}_{sx} = \int \left(u_{sx} - R_{se}\hat{i}_{sx} \right) dt \tag{3.8}$$

$$\hat{i}_{sx} = \frac{\hat{\Psi}_{sx}}{L_{Me}} \tag{3.9}$$

shown in Fig. 3.8.

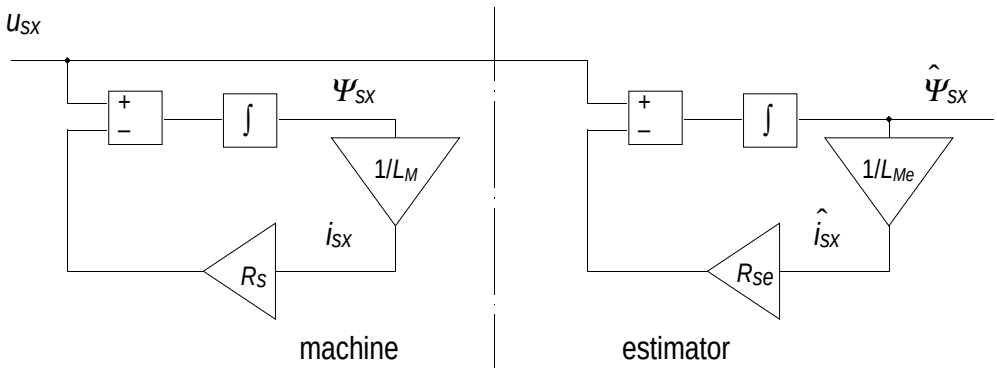

Fig. 3.8 Block diagram of estimator C.

This estimator is basically an open loop simulation model of the machine since it does not feed back any measurements.

Fig. 3.9 shows that the drift in Fig. 3.2 is no longer present. However, there is a steady state error in the estimated flux due to the error in the resistance.

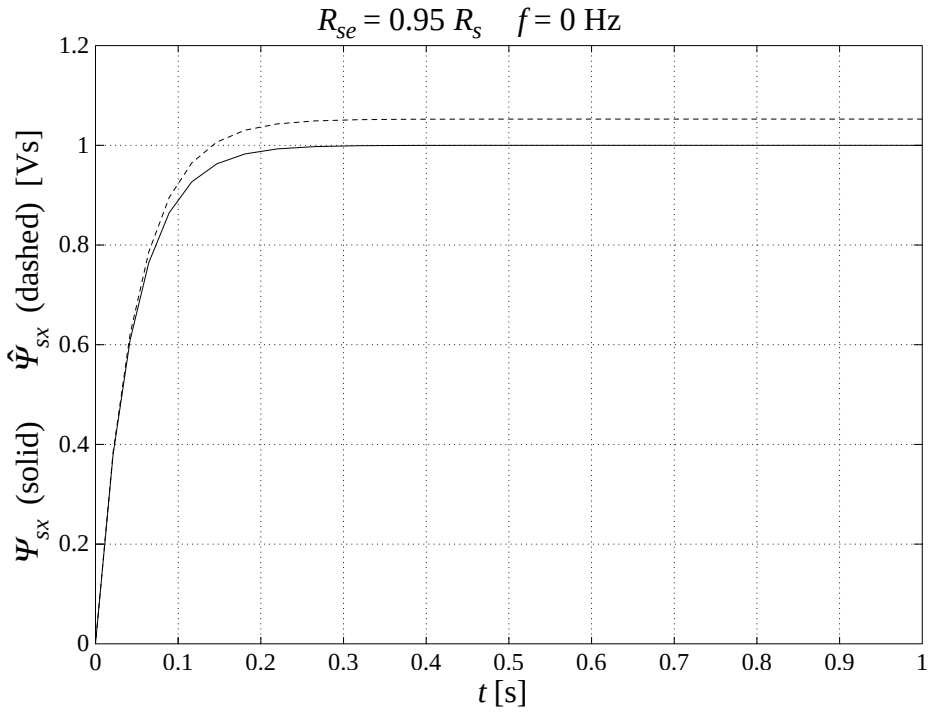

Fig. 3.9 Simulation of estimator C, starting from zero. R_{se} = 0.95 R_s, f = 0 Hz (u_{sx} is constant).

An error in the magnetizing inductance parameter also leads to a steady state error in the estimated flux.

Estimator D - Identity Observer

Various ways have been tried to combine the estimators described to get an estimator with good properties in the entire frequency range (Jönsson, 1991). As estimator A has good high frequency properties, while estimator B has good low frequency properties, Jansen et al (1994a) describes a way of combining them into an estimator with good properties at low and high frequencies. A low pass filter selects estimator B at low frequencies and estimator A at high frequencies. This estimator will be further described in Chapter 4.

Estimator A with ”current correction” to eliminate drift is described in different papers (Bausch et al, 1994 and Pohjalainen et al, 1994).

A straightforward way of combining estimator A, B and C is to use observer theory. The structure used for example by Kalman filters can be used for the induction machine. In matrix notation, an observer for the system

$$\frac{dx}{dt} = Ax + Bu \tag{3.10}$$

$$y = Cu \tag{3.11}$$

where x is the state to be estimated, u is the input and y is the output of the system is described by

$$\frac{d\hat{x}}{dt} = A_e\hat{x} + B_e u + K\left(y - C_e\hat{x}\right) \tag{3.12}$$

where K is the observer gain (Åström, 1976). Note that A_e, B_e and C_e are chosen model parameters. In a Kalman filter, exact model parameters are assumed, $A = A_e$, $B = B_e$ and $C = C_e$. This observer is also referred to as an *identity observer* as it tracks the entire state vector contrary to a *reduced observer* which tracks only a subset of the state vector (Luenberger, 1979).

The example with zero rotor current is used to illustrate this structure for the induction machine flux observer. Estimating only the real axis, we have

$$\begin{aligned} x &= \Psi_{sx} \\ \hat{x} &= \hat{\Psi}_{sx} \\ y &= i_{sx} \\ u &= u_{sx} \\ A_e &= -\frac{R_{se}}{L_{Me}} \\ B_e &= 1 \\ C_e &= \frac{1}{L_{Me}} \end{aligned}$$

The observer takes the form

$$\frac{d\hat{\Psi}_{sx}}{dt} = u_{sx} - \frac{R_{se}}{L_{Me}}\hat{\Psi}_{sx} + K\left(i_{sx} - \frac{1}{L_{Me}}\hat{\Psi}_{sx}\right) \tag{3.13}$$

The selection of the gain can be a difficult task. One way is pole placement (Verghese et al, 1988, Umeno et al, 1990 and Hori et al, 1987). Unfortunately, in the complete observer where the rotor current differs from zero, the poles depend on the speed if the observer gain is constant.

Another way is Linear Quadratic Gaussian (LQG) design, where the obtained gain minimizes the estimation error if the noise is Gaussian distributed (Menander et al, 1991). In the induction machine case, parameter errors and unknown load torque are worse obstacles than noisy measurements, limiting the usefulness of this method.

The unit of the gain parameter K is Ω. Equation (3.13) can be rearranged into equation (3.14) with a new gain parameter, k, which is dimensionless. This will give better physical insight into the observer, making it easier to tune. To get the dimensionless gain parameter, equation (3.13) can be rewritten as

$$\frac{d\hat{\Psi}_{sx}}{dt} = u_{sx} - \frac{R_{se}}{L_{Me}}\hat{\Psi}_{sx} + k\,R_{se}\left(i_{sx} - \hat{i}_{sx}\right) \tag{3.14}$$

where

$$k = \frac{K}{R_{se}} \tag{3.15}$$

and

$$\hat{i}_{sx} = C_e\hat{\Psi}_{sx} = \frac{1}{L_{Me}}\hat{\Psi}_{sx} \tag{3.16}$$

This is shown as a block diagram in Fig. 3.10.

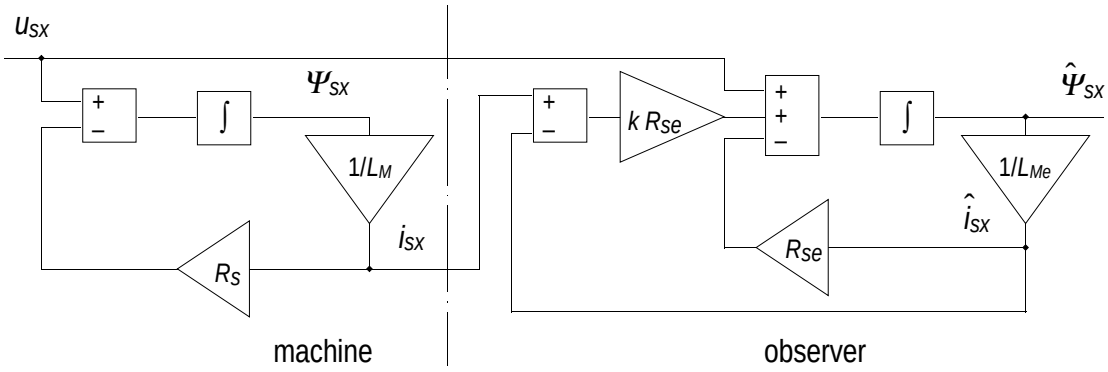

Fig. 3.10 Block diagram of estimator D.

A rearrangement of this diagram gives a much better understanding of the observer, shown in Fig. 3.11,

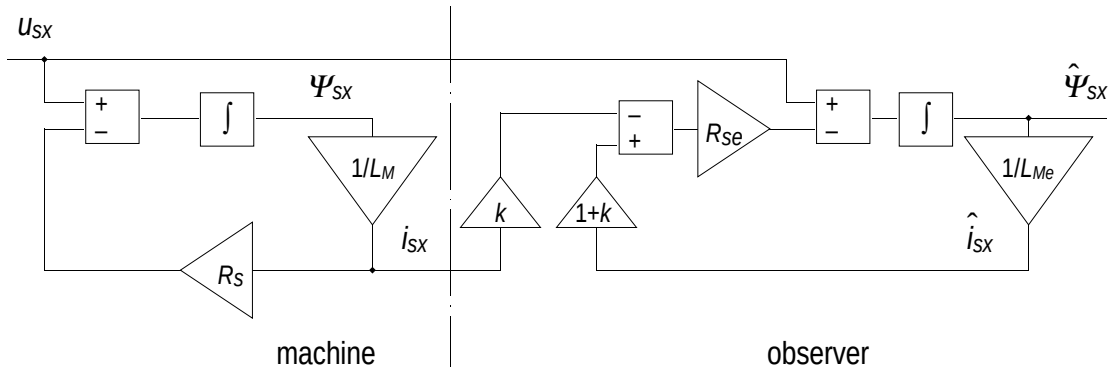

Fig. 3.11 A rearranged block diagram of estimator D.

Equations (3.14) and (3.16) can be rearranged to better describe the diagram in Fig. 3.11.

$$\begin{aligned}\frac{d\hat{\Psi}_{sx}}{dt} &= u_{sx} - R_{se}\left(\frac{\hat{\Psi}_{sx}}{L_{Me}}(1+k) - k\,i_{sx}\right) \\ &= u_{sx} - R_{se}\left((1+k)\,\hat{i}_{sx} - k\,i_{sx}\right)\end{aligned} \tag{3.17}$$

The observer is a combination of estimator A shown in Fig. 3.1 and estimator C shown in Fig. 3.8. In estimator C, $\hat{i}_{sx}$ is fed directly to R_{se}, while an extra part, $k\,\hat{i}_{sx}$ is added here. As a compensation, a corresponding part of the measured current, $k\,i_{sx}$, is subtracted. This means that the measured current acts as a correction for errors in the estimated current. In Fig. 3.12 it is seen how an observer gain $k=1$ reduces the steady state error of estimator C. The integrator drift of estimator A seen in Fig. 3.2 is also eliminated.

The observer pole is the root of the first order characteristic equation,

$$\begin{aligned}\left[\left(A_e - KC_e\right) - s\right] = 0 \Leftrightarrow \\ \left[\left(-\frac{R_{se}}{L_{Me}} - kR_{se}\frac{1}{L_{Me}}\right) - s\right] = 0 \Leftrightarrow \\ s = -\frac{R_{se}}{L_{Me}}(1+k)\end{aligned} \tag{3.18}$$

If $k=-1$, the observer turns into estimator A, and if $k=0$, the observer turns into estimator C. An increasing k results in a faster observer, while

the observer becomes unstable if $k < -1$. This can be seen in Fig. 3.13, which shows a plot in the s-plane of the observer poles.

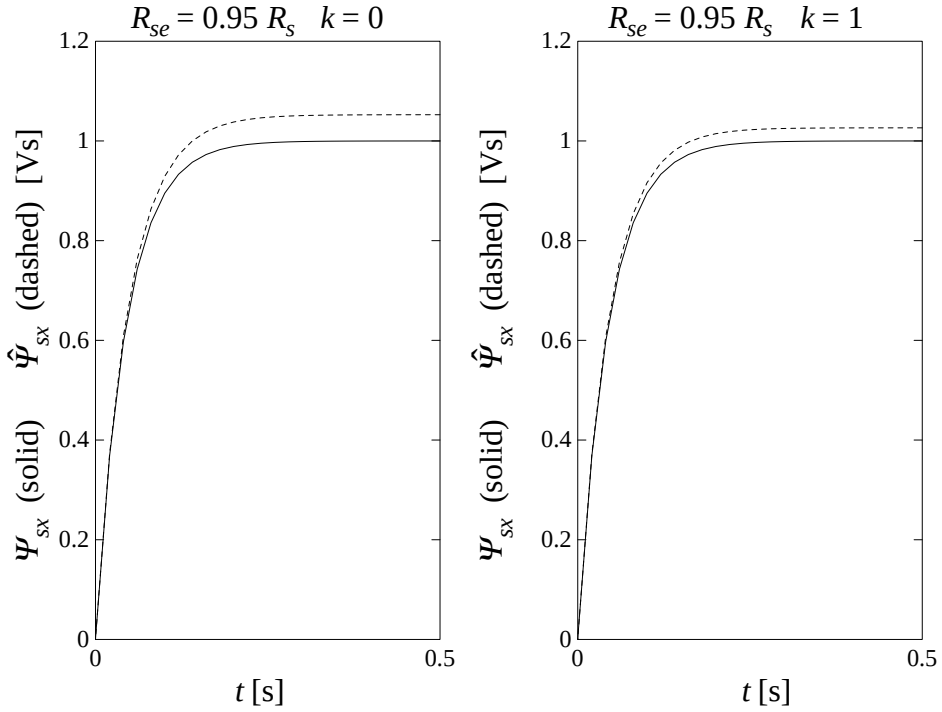

Fig. 3.12 Simulations of estimator D comparing different observer gains. The left diagram shows a simulation with $k = 0$, giving identical result as estimator C, shown in Fig. 3.9. In the right diagram the gain is $k = 1$.

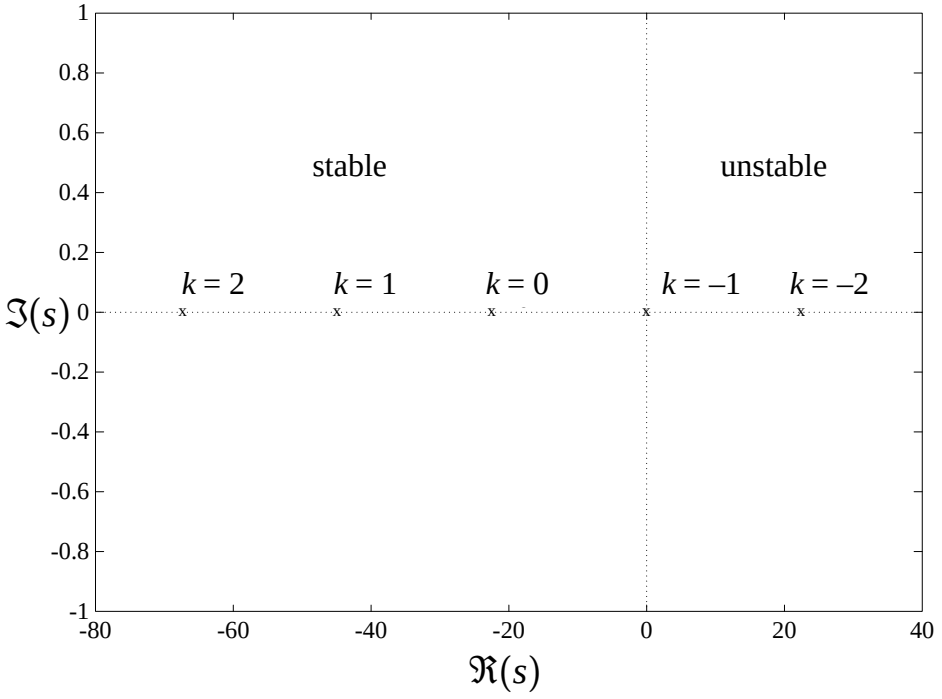

Fig. 3.13 Observer poles at different observer gains k.

An observer is unstable if the real part of a pole is greater than zero. Note that the pole of estimator A ($k = -1$) is in the origin, indicating that the estimator is not asymptotically stable.

Fig. 3.14 shows how the settling time as well as steady state error is decreasing at increasing gain. The flux of the machine is constant, $\Psi_{sx} = 1$, while the observer starts from zero.

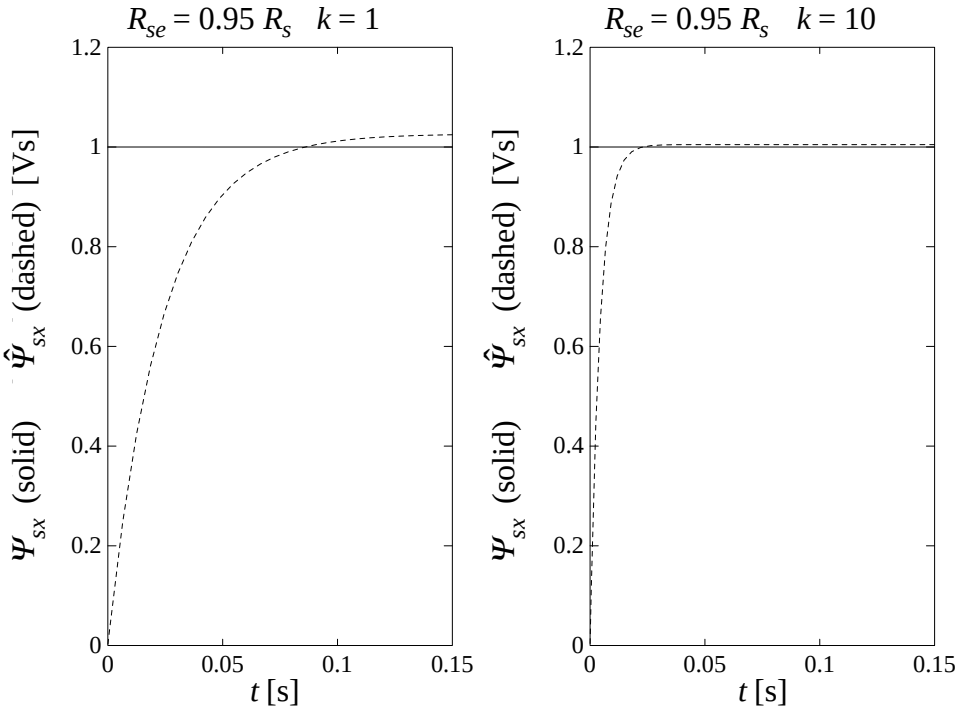

Fig. 3.14 Simulation of estimator D showing how the settling time and steady state error are reduced if the observer gain k is increased.

To summarize, a large observer gain k results in a faster, more stable observer that is less sensitive to errors in R_{se}. The sensitivity to L_{Me} is unchanged.

Unfortunately, as k is increased, the sensitivity to noise is increased as well. Fig. 3.15 shows the estimated current $\hat{i}_{sx}$ of equation (3.16) at different observer gains. The estimated current is more noisy at $k = 10$ than at $k = 1$. However, note that there is much less noise in the estimated current, both at $k = 10$ and at $k = 1$, than in the measured current. The observer automatically filters the measured current.

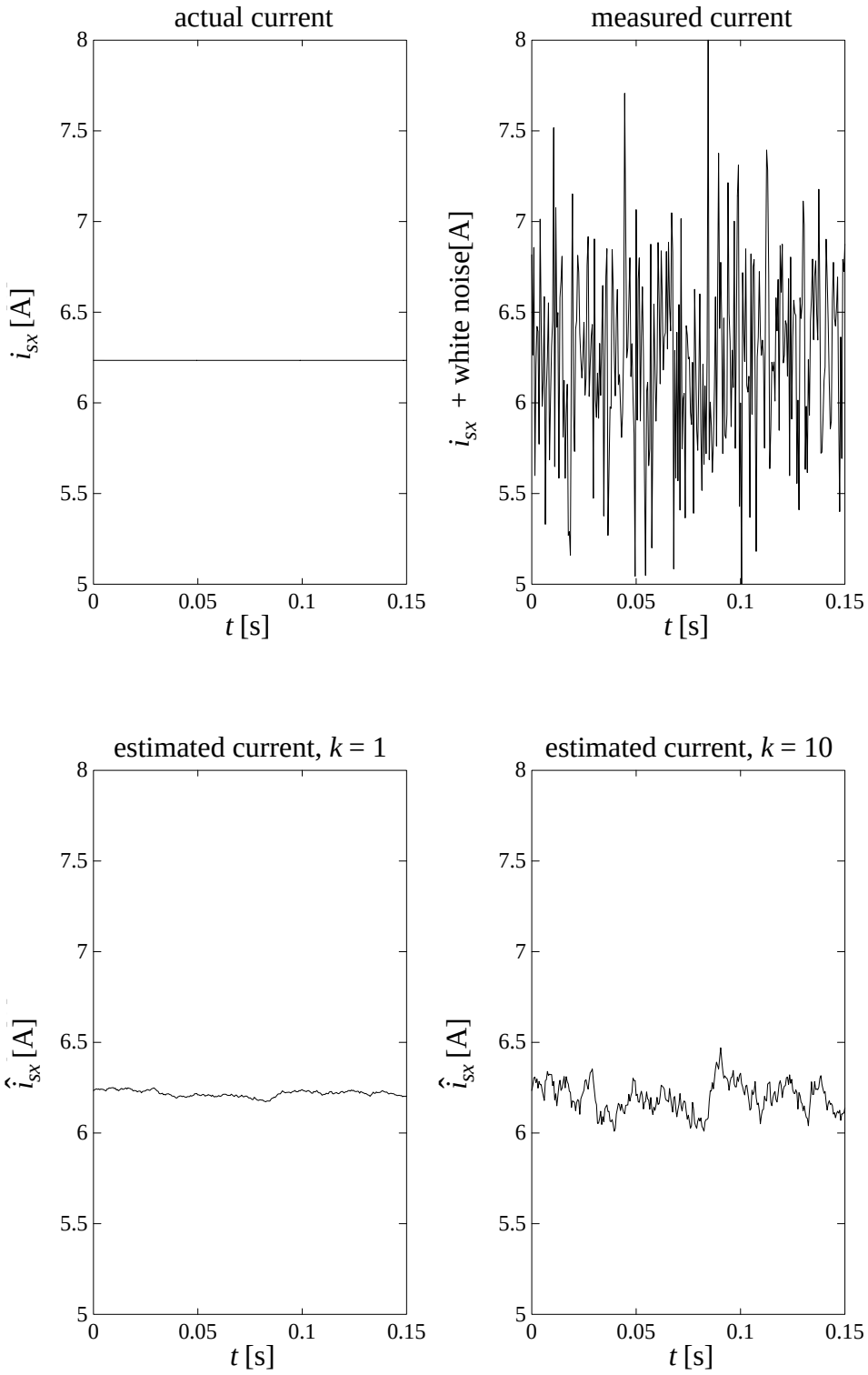

Fig. 3.15 Simulation of estimator D with noisy current measurement, showing that the noise sensitivity is increased with increasing gain k.

Mechanical Models of Estimators

In Chapter 2, a mechanical model of the simplified induction machine, assuming zero rotor current was derived. In a similar manner, mechanical

models of estimators will be studied. Appendix B gives a brief introduction to electrical and mechanical equivalents.

Some people prefer equations and alphanumeric information, and find mechanical models of no use. However, most people have a built in sense for how a mechanical system is affected when forces are applied in different ways. The mechanical models give a feeling of what is actually happening either in the machine or in the observer.

Mechanical Model A

A mechanical model of estimator A is shown in Fig. 3.16 (cf. Fig. 2.3). The inputs to the estimator are the velocity at point *a* and the force at point *b*. The distance $\hat{x}$ between point *b* and a fixed point *o* is the estimated quantity.

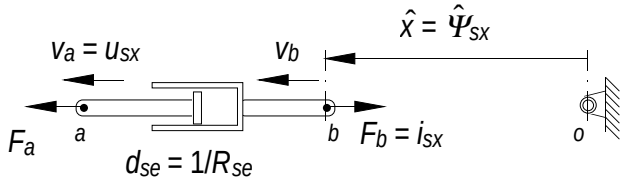

Fig. 3.16 Mechanical model of estimator A.

The mechanical system is described by

$$F_a = F_b = F_{damper} = d_{se}\left(v_a - v_b\right) \tag{3.19}$$

$$v_b = \frac{d\hat{x}}{dt} \tag{3.20}$$

resulting in

$$\frac{d\hat{x}}{dt} = v_a - \frac{1}{d_{se}} F_b \tag{3.21}$$

With the substitutions in Fig. 3.16, we have

$$\frac{d\hat{\Psi}_{sx}}{dt} = u_{sx} - R_{se} i_{sx} \tag{3.22}$$

which is equation (3.2) in differential form.

If the stator resistance is not perfectly matched with the resistance of the machine of which we measure the current and voltage, point *b* will drift

either to the left or to the right at low frequencies. This was also the case for estimator A, shown in Fig. 3.2. At high frequencies on the other hand, when point *a* is rapidly oscillating from left to right, the estimator will produce a more accurate estimate of the flux.

Mechanical Model B

A mechanical model of estimator B is just a spring shown in Fig. 3.17 (cf. Fig. 2.3).

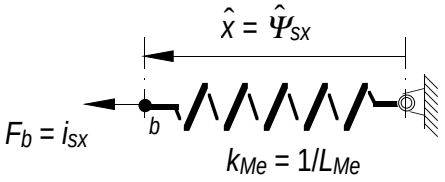

Fig. 3.17 Mechanical model of estimator B.

The estimated flux is

$$\hat{\Psi}_{sx} = \hat{x} = \frac{F_b}{k_{Me}} = L_{Me} i_{sx} \tag{3.23}$$

Like in Fig. 3.6, this estimator will not result in any drift, but an error in the inductance parameter gives the same error in the estimated flux.

Mechanical Model C

Estimator C uses both the viscous damper and the spring, shown in Fig. 3.18. This is the same structure as the mechanical model of the machine in Fig. 2.3,

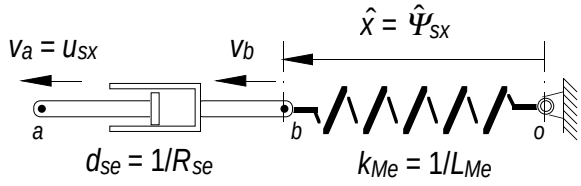

Fig. 3.18 Mechanical model of estimator C.

described by

$$\frac{d\hat{x}}{dt} = v_a - \frac{k_{Me}}{d_{se}} \hat{x} \tag{3.24}$$

which is equations (3.8) and (3.9) combined.

This model gives errors in the estimated flux if there is an error in the resistance or inductance parameters, like in Fig. 3.9.

Mechanical Model D

Just like the block diagram of estimator D, the observer, can be arranged in different ways, shown in Fig. 3.10 and Fig. 3.11, a mechanical model of this observer can be arranged in several ways. The base is a spring representing the magnetizing inductance, a damper representing the stator resistance, and some kind of variable gearing representing the variable gain *k*. One arrangement is shown in Fig. 3.19 where the gearing is a winch with drums of different diameters on the same axis. The diameters (or radii) of the drums are functions of *k*, and the mass of the drums is supposed to be negligible.

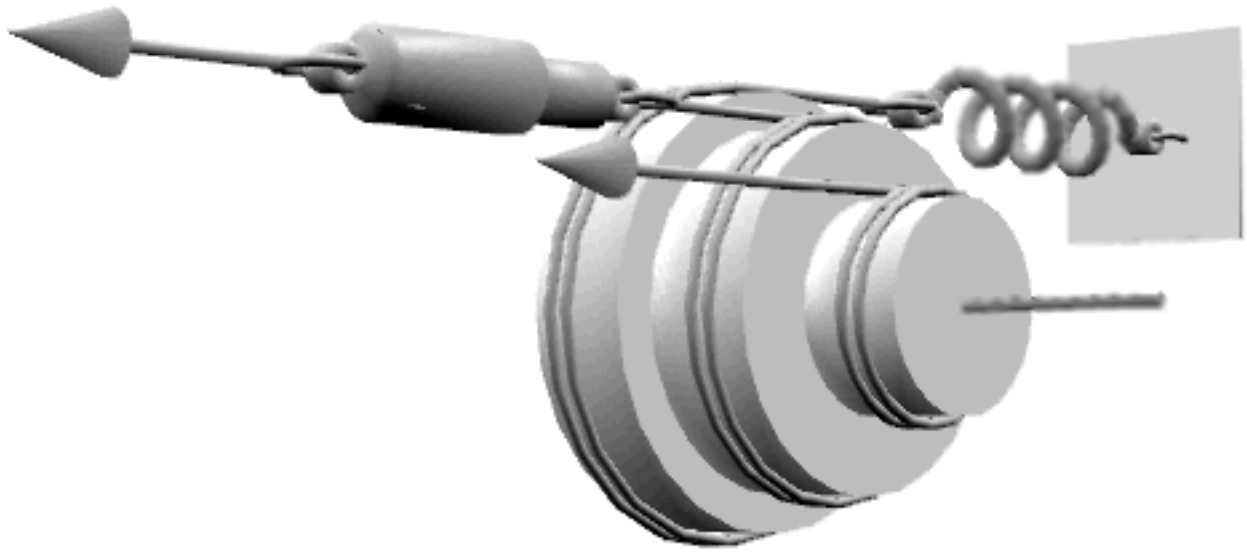

Fig. 3.19 Mechanical model of estimator D.

The stator resistance damper is attached to a wire wrapped around a drum of radius 1, the magnetizing inductance spring is attached on radius r_m while the radius of the current drum is r_i, shown in Fig. 3.20.

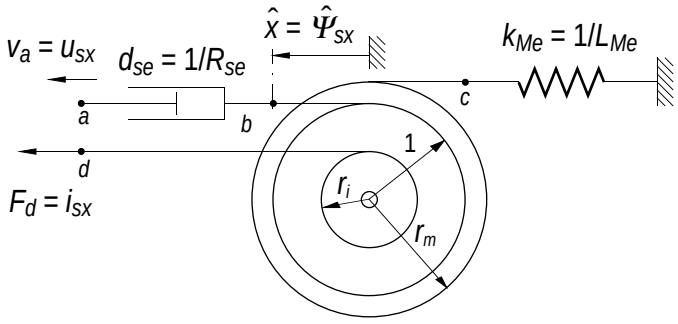

Fig. 3.20 Mechanical model of estimator D, $k = 0.5$.

The position of point *b* is the estimated flux. The following set of equations describes this mechanical system:

$$\begin{aligned} \frac{d\hat{x}}{dt} &= v_b \\ F_a = F_b &= d_{se}\left(v_a - v_b\right) \\ F_c &= k_{Me} r_m \hat{x} \\ F_b \cdot 1 + F_d r_i &= F_c r_m \end{aligned} \tag{3.25}$$

giving

$$\begin{aligned} \frac{d\hat{x}}{dt} &= v_a - \frac{1}{d_{se}} F_b \\ &= v_a - \frac{1}{d_{se}}\left(F_c r_m - F_d r_i\right) \\ &= v_a + r_i \frac{1}{d_{se}} F_d - \frac{k_{Me}}{d_{se}} \hat{x}\, r_m^2 \end{aligned} \tag{3.26}$$

Substituting the mechanical quantities with their electrical counterparts results in equation (3.27),

$$\frac{d\hat{\Psi}_{sx}}{dt} = u_{sx} + r_i R_{se} i_{sx} - \frac{R_{se}}{L_{Me}} \hat{\Psi}_{sx} r_m^2 \tag{3.27}$$

which is equal to equation (3.17) if

$$r_i = k \tag{3.28}$$

and

$$r_m = \sqrt{1 + k} \tag{3.29}$$

Fig. 3.21 shows this observer at different values of the gain *k*.

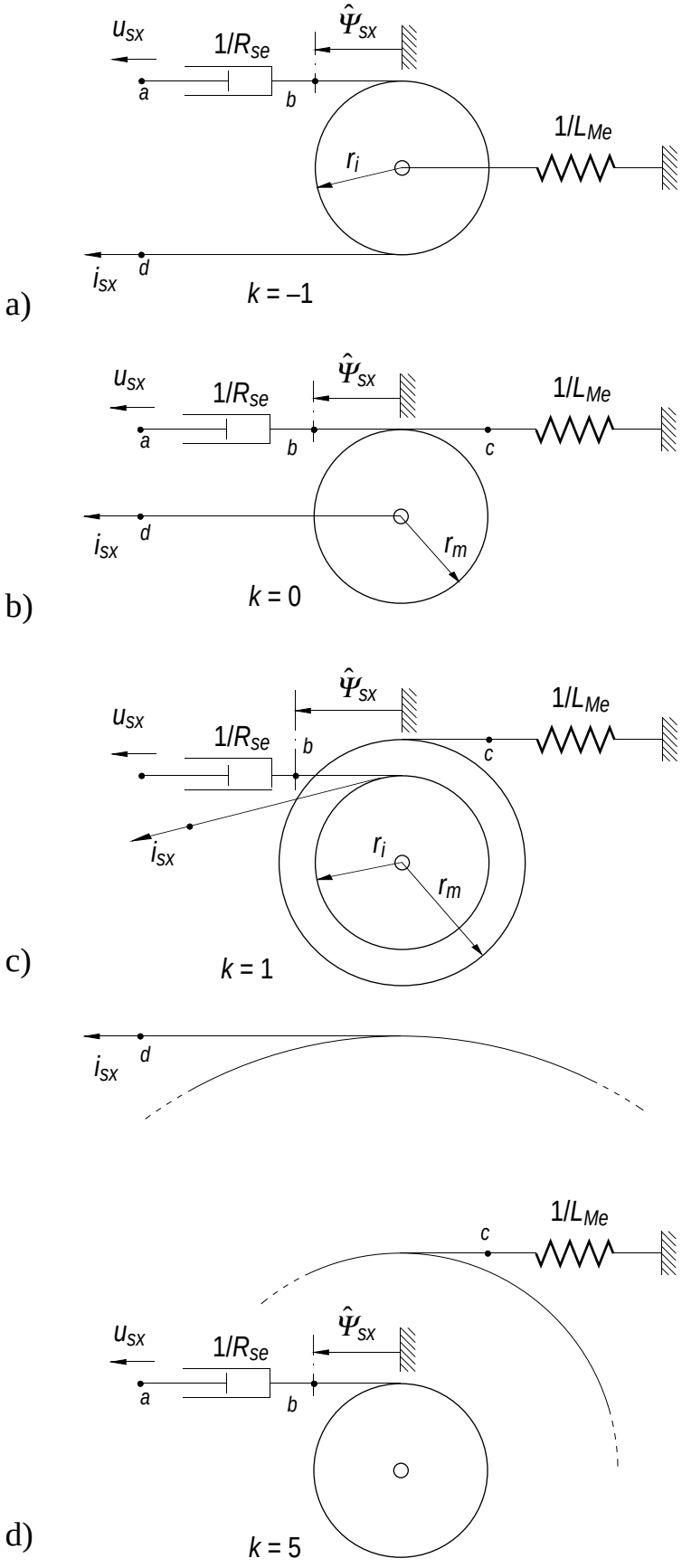

Fig. 3.21 Mechanical model of estimator D, showing how the diameters of the drums are changing when k is changing. a) $k = -1$, $r_i = -1$, $r_m = 0$ b) $k = 0$, $r_i = 0$, $r_m = 1$ c) $k = 1$, $r_i = 1$, $r_m = 1.41$ d) $k = 5$, $r_i = 5$, $r_m = 2.4$

In Fig. 3.21 a), the gain is $k = -1$ corresponding to estimator A. The radius of the magnetizing inductance drum r_m is zero, and we have the mechanical observer shown in Fig. 3.16, with point *b* drifting either to the left or right at low frequencies if the resistance parameter is not perfectly matched with the true resistance.

In Fig. 3.21 b), the gain is $k = 0$. Now the radius of the current drum is zero, and we have estimator C, which does not use the measured current.

As *k* is increased, the radius of the current drum $r_i = k$ is increased, and the influence of the measured current is increased. In Fig. 3.21 c), $k = 1$, which gives a good balance of the trust put into measured current and measured voltage. However, good balance is a relative measure, and noise in measurements and estimator parameter errors are factors that must be regarded in an actual application.

As *k* is further increased, the influence of the measured voltage and the stator resistance parameter errors is decreased, as the levers for the current and for the magnetizing inductance both are becoming dominant. This is seen in Fig. 3.21 d). Neither the equations, the block diagram of the observer nor this mechanical model will tell at a first glance what is happening at a large gain.

A second mechanical model shown in Fig. 3.22 can be derived which clearly illustrates the behaviour when *k* is large. The drawback of the second model is that it will not work at $k = -1$. The ends of the viscous damper representing stator resistance are attached to wires wrapped around two drums of radius r_s, the radius of the current drum is r_i, while the radius of both the magnetizing inductance drum and the stator voltage drum is equal to 1.

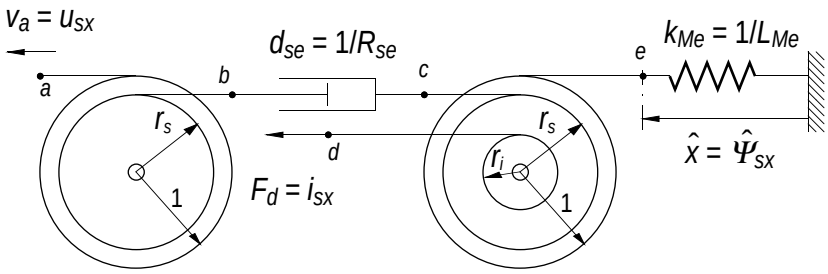

Fig. 3.22 Alternative mechanical model of estimator D, $k = 0.5$.

The equations for the mechanical system are

$$\begin{aligned} \frac{d\hat{x}}{dt} &= v_e \\ v_b &= v_a r_s \\ v_c &= v_e r_s \\ F_b = F_c &= d_{se}\left(v_b - v_c\right) \\ F_e &= k_{Me}\hat{x} \\ F_c r_s + F_d r_i &= F_e \cdot 1 \end{aligned} \tag{3.30}$$

giving

$$\frac{d\hat{x}}{dt} = v_a + \frac{r_i}{r_s^2}\frac{1}{d_{se}}F_d - \frac{k_{Me}}{d_{se}}\hat{x}\frac{1}{r_s^2} \tag{3.31}$$

This equation turns into equation (3.32) when the mechanical quantities are replaced by electrical quantities,

$$\frac{d\hat{\Psi}_{sx}}{dt} = u_{sx} + \frac{r_i}{r_s^2}R_{se}i_{sx} - \frac{R_{se}}{L_{Me}}\hat{\Psi}_{sx}\frac{1}{r_s^2} \tag{3.32}$$

This is equivalent to equation (3.17) if

$$r_s = \frac{1}{\sqrt{1+k}} \tag{3.33}$$

and

$$r_i = \frac{k}{1+k} \tag{3.34}$$

As k is increased, the radii of the viscous damper drums r_s go towards zero, and the radius of the current drum goes towards 1. It is seen that the stator voltage and stator resistance no longer have much influence on the estimated flux, while the stator current force is acting directly on the magnetizing inductance spring. This means that when k is increased, the observer will behave more and more like estimator B shown in Fig. 3.17. Fig. 3.23 shows the observer at $k = 5$.

It is important to notice that there are no extra simplifications involved in these mechanical models. The equations describing the mechanical systems are both identical to the observer equation (3.17).

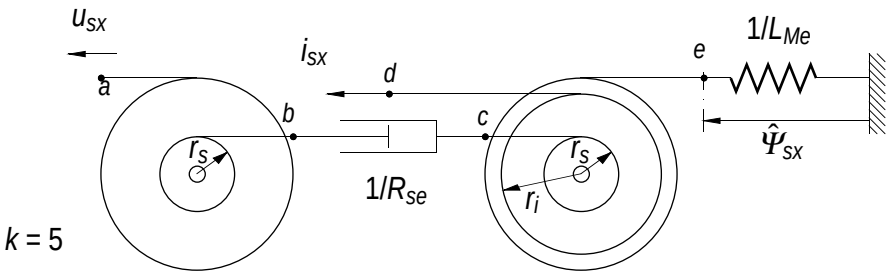

Fig. 3.23 Alternative mechanical model of estimator D, $k = 5$.

As summarized in Table 3.1, the estimators A, B and C are all special cases of estimator D.

k	estimator
–1	A
∞	B
0	C

Table 3.1 Relation between estimator D and estimators A, B and C.

The general observations on the observers assuming zero rotor current are valid also for the complete observer where the rotor current no longer is assumed to be zero. With this basic knowledge of a flux observer, the complete flux observer can now be studied.

4

Flux Observer Models

All the characteristics of the observers in Chapter 3, like noise sensitivity and parameter sensitivity, are valid also for a complete observer. However, new problems such as non-linearities arise when the rotor current no longer is assumed to be zero.

In this chapter it is assumed that the rotor speed ω is measured. In Chapter 5, estimators without speed sensors are studied.

An observer for both stator and rotor flux can be obtained in the same way as the simplified observer described by equation (3.13).

Again, the identity observer in equation (3.12) is the starting point for the flux observer. An observer for the induction machine described by equations (2.9)-(2.14), will take the form

$$\frac{d\hat{x}}{dt} = A_e\hat{x} + B_e u + K\left(y - C_e\hat{x}\right) \tag{4.1}$$

where

$$\hat{x} = \hat{\Psi} = \begin{bmatrix} \hat{\boldsymbol{\Psi}}_s \\ \hat{\boldsymbol{\Psi}}_r \end{bmatrix} \tag{4.2}$$

$$y = \mathbf{i}_s \tag{4.3}$$

$$u = \mathbf{u}_s \tag{4.4}$$

$$A_e(\omega) = \begin{bmatrix} -R_{se}\left(\frac{1}{L_{Me}} + \frac{1}{L_{Le}}\right) & \frac{R_{se}}{L_{Le}} \\ \frac{R_{re}}{L_{Le}} & \frac{-R_{re}}{L_{Le}} + jz_p\omega \end{bmatrix} \tag{4.5}$$

$$B_e = \begin{bmatrix} 1 \\ 0 \end{bmatrix} \tag{4.6}$$

$$C_e = \begin{bmatrix} \frac{1}{L_{Me}} + \frac{1}{L_{Le}} & \frac{-1}{L_{Le}} \end{bmatrix} \tag{4.7}$$

$$K = \begin{bmatrix} \mathbf{K}_s \\ \mathbf{K}_r \end{bmatrix} \tag{4.8}$$

A key to make this observer easy to tune, is to make the observer gains dimensionless, which is done with the relation

$$K = R_e\, k \tag{4.9}$$

where

$$k = \begin{bmatrix} \mathbf{k}_s \\ \mathbf{k}_r \end{bmatrix} = \begin{bmatrix} k_{sx} + j\, k_{sy} \\ k_{rx} + j\, k_{ry} \end{bmatrix} \tag{4.10}$$

and

$$R_e = \begin{bmatrix} R_{se} & 0 \\ 0 & R_{re} \end{bmatrix} \tag{4.11}$$

The observer in matrix notation takes the form

$$\frac{d\hat{\Psi}}{dt} = A_e\, \hat{\Psi} + B_e \mathbf{u}_s + R_e k \left(\mathbf{i}_s - C_e\, \hat{\Psi} \right) \tag{4.12}$$

This equation consists of two complex differential equations, one for the estimated stator flux,

$$\frac{d\hat{\mathbf{\Psi}}_s}{dt} = \mathbf{u}_s - R_{se} \left(\left(1 + \mathbf{k}_s \right) \hat{\mathbf{i}}_s - \mathbf{k}_s\, \mathbf{i}_s \right) \tag{4.13}$$

and one for the estimated rotor flux

$$\frac{d\hat{\mathbf{\Psi}}_r}{dt} = j z_p\, \omega\, \hat{\mathbf{\Psi}}_r - R_{re}\, \hat{\mathbf{i}}_r \tag{4.14}$$

where

$$\hat{\mathbf{i}}_s = \frac{\hat{\mathbf{\Psi}}_s}{L_{Me}} - \frac{\hat{\mathbf{\Psi}}_r - \hat{\mathbf{\Psi}}_s}{L_{Le}} \tag{4.15}$$

$$\hat{\mathbf{i}}_r = \mathbf{k}_r\left(\hat{\mathbf{i}}_s - \mathbf{i}_s\right) + \frac{\hat{\boldsymbol{\Psi}}_r - \hat{\boldsymbol{\Psi}}_s}{L_{Le}} \tag{4.16}$$

The equations are shown as a block diagram in Fig. 4.1 a). Splitting (4.13) and (4.14) in real and imaginary parts results in four differential equations, shown in Fig. 4.1 b).

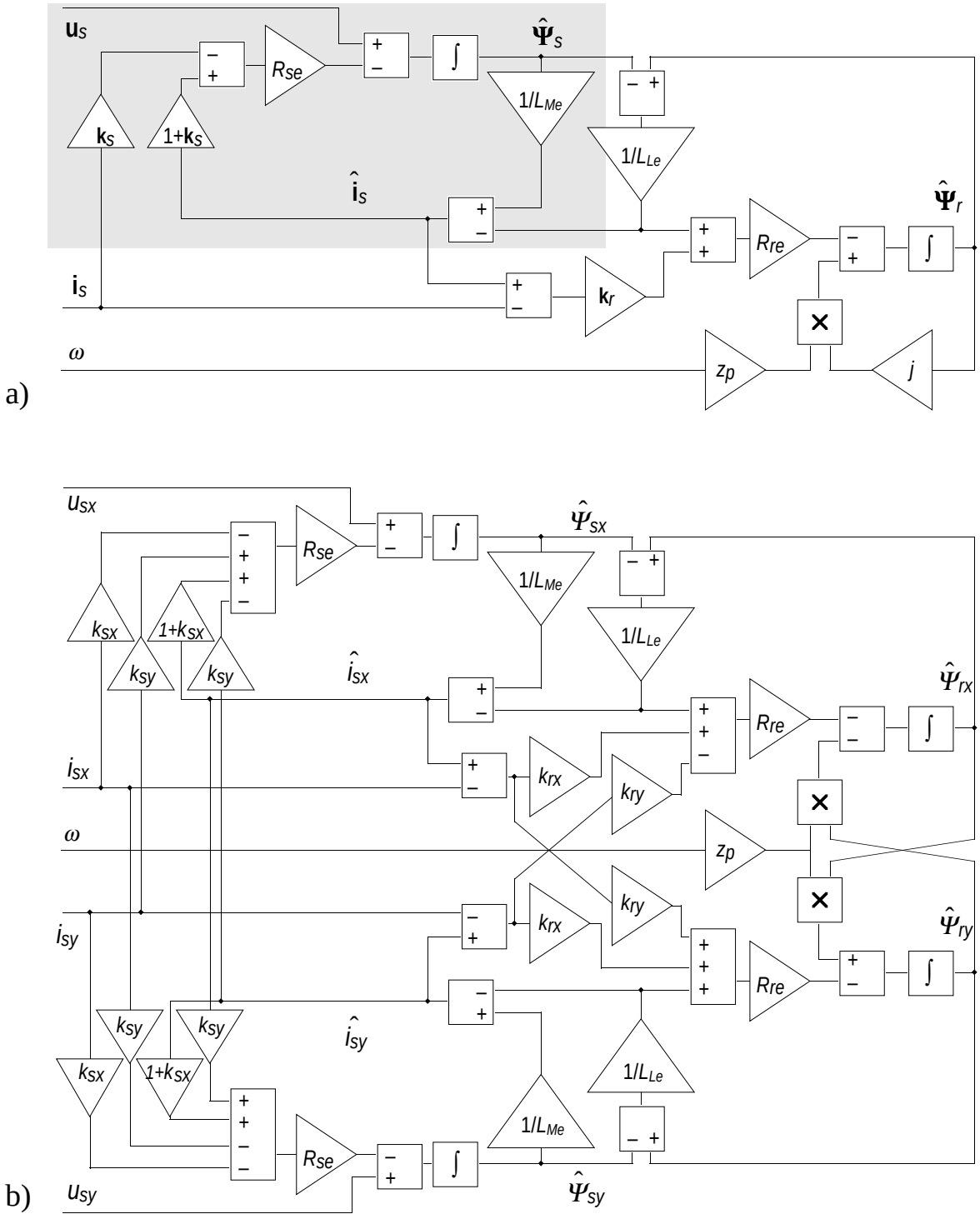

Fig. 4.1 Block diagram of flux observer a) complex representation b) real valued representation.

The upper left corner (shaded) is basically the same as the block diagram of the observer in Fig. 3.11, where the rotor current is assumed to be zero.

Settling Time

One major difference between the simplified observer of Chapter 3, where the rotor current was zero, and the complete observer, is that the rotor speed ω appears in the equations of the complete observer. First, this makes the observer a non-linear system if ω is varying. Second, the rotor speed must be measured or estimated in order to get an accurate flux estimate. Speed estimation will be discussed in Chapter 5. In this chapter, it is assumed that the speed is measured perfectly.

The non-linearities affect the settling time of the observer. An observer with zero gain will be used as a first example to demonstrate how the settling time varies with ω. Fig. 4.2 shows a simulation of the error in the estimate of stator flux amplitude. The amplitude of the actual stator flux is constant during the simulation, while the observer starts from zero.

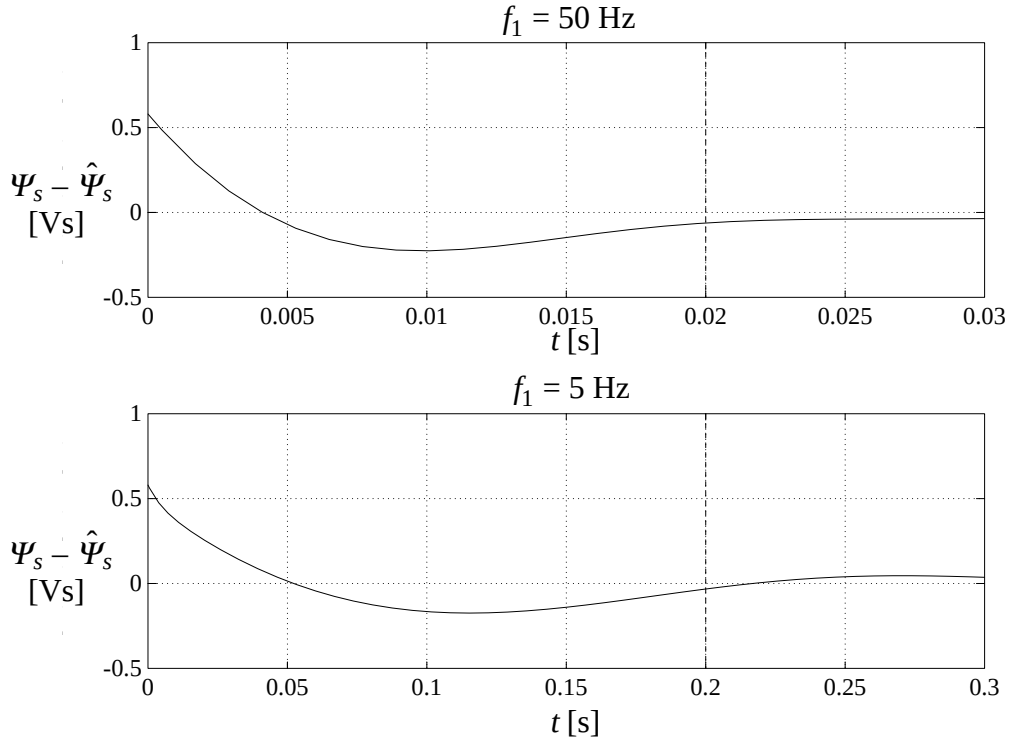

Fig. 4.2 Settling time at 50 Hz and 5 Hz for observer with zero gain.

The motor is running at rated torque and at a stator frequency of 50 Hz in the upper diagram and 5 Hz in the lower one. Note the different time scales in the two diagrams. The vertical lines at 0.02 seconds and 0.2 seconds

respectively, correspond to the time instants when the stator flux has completed one turn.

The diagrams show a very important property: *The observer with gain k = 0 is ten times faster at 50 Hz than at 5 Hz*. However, if the settling time is measured in *stator flux revolutions* instead of *seconds*, the observer is almost *equally fast* at both frequencies. It takes about one revolution for errors in the estimates to reach zero in both cases.

The settling time can be reduced with an appropriate selection of the gain parameters. In Fig. 4.3, the same observer gain *k* is used at 50 Hz and 5 Hz. The response is faster than in Fig. 4.2, but it is still approximately 10 times faster at 50 Hz than at 5 Hz.

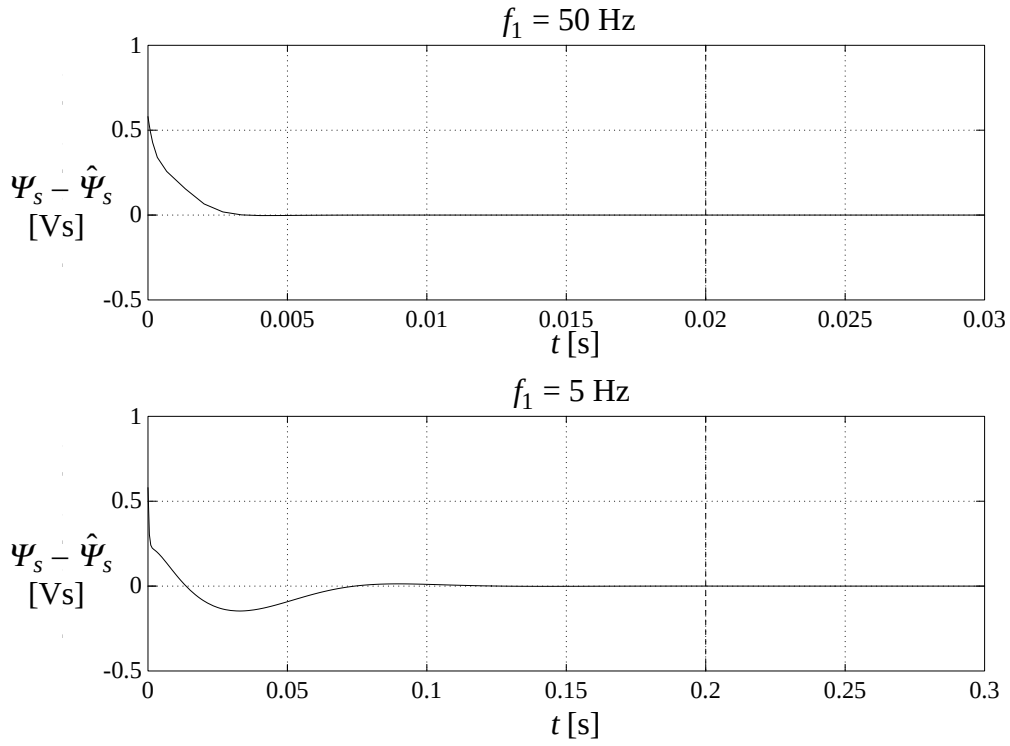

Fig. 4.3 Settling time at 50 Hz and 5 Hz. The same gain $k = [1.3 - 51j \quad -30 + 85j]^{\mathrm{T}}$ is used at both frequencies.

Pole placement (Åström et al, 1984) is a technique that can be used to set the settling time of the observer. The observer poles are the eigenvalues of the matrix $(A_e - R_e k C_e)$ in equation (4.12). If the two complex poles of a complex 2×2 matrix are denoted $\mathbf{p}_1$ and $\mathbf{p}_2$ the characteristic polynomial of the observer can be written

$$P(\mathbf{s}) = \mathbf{s}^2 + \mathbf{c}_1\mathbf{s} + \mathbf{c}_2 = \mathbf{s}^2 - (\mathbf{p}_1 + \mathbf{p}_2)\mathbf{s} + \mathbf{p}_1\mathbf{p}_2 \qquad (4.17)$$

The required observer gain for desired observer poles is given by

$$\begin{aligned} k &= R_e^{-1} P(A_e) W_o^{-1} \begin{bmatrix} 0 \\ 1 \end{bmatrix} \\ &= R_e^{-1} \left(A_e^2 - (\mathbf{p}_1 + \mathbf{p}_2) A_e + \mathbf{p}_1 \mathbf{p}_2 I \right) W_o^{-1} \begin{bmatrix} 0 \\ 1 \end{bmatrix} \end{aligned} \tag{4.18}$$

where W_o is the observability matrix,

$$W_o = \begin{bmatrix} C_e \\ C_e A_e \end{bmatrix} \tag{4.19}$$

Equation (4.18) is evaluated in Appendix E. Unfortunately, the expressions are too complicated to be of much practical use. Note that the two poles do not have to be conjugates, as the 2×2 matrix is complex.

As matrix A_e is varying with rotor speed ω, the observer gain must vary with speed if the poles are held constant. Fig. 4.4 shows a simulation at 50 Hz and 5 Hz, with the same poles at both frequencies. This means that different gain parameters *k* are used at the two frequencies.

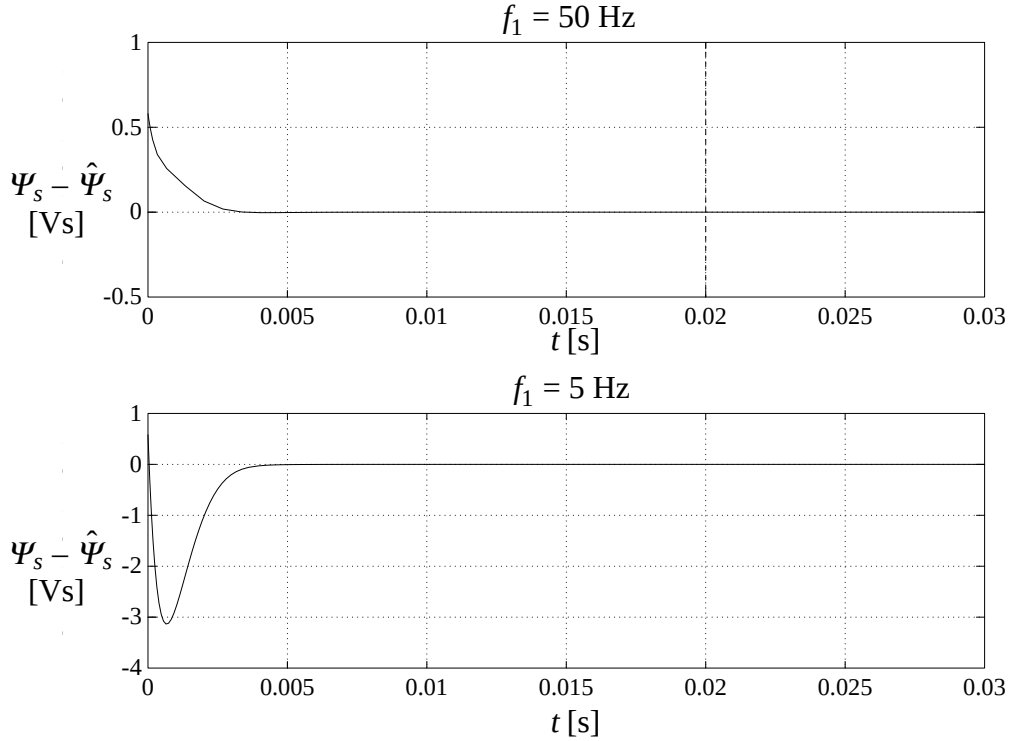

Fig. 4.4 Settling time at 50 Hz and 5 Hz. The poles are placed in –1500 when the observer is operating both at 50 Hz and 5 Hz. The gain is $k = [1.3 - 51j \quad -30 + 85j]^{\mathrm{T}}$ at 50 Hz and $k = [481 + 579j \quad 793 + 996j]^{\mathrm{T}}$ at 5 Hz.

Note that the same time scale is used in the 50 Hz and 5 Hz diagrams. As the poles are the same for the two cases, we have the same response time. The two curves look different because it is the amplitude error $\Psi_s - \hat{\Psi}_s$ that is shown, not the actual states of the observer.

At a first look, pole placement seems to be a useful technique for manipulating the dynamic behaviour of the observer. However, the price is high for a fast observer at a low frequency. The parameters of the gain vector *k* must be increased between 10 and 400 times in order to make the observer as fast at 5 Hz as it is at 50 Hz. Such a high gain is usually not recommendable due to noise sensitivity. The conclusion is that with pole placement, control of the gain vector is lost, and the gain might increase beyond reasonable limits.

The settling time is not the most critical factor of an observer. Usually, the observer flux tracks the flux of the induction machine, and the situation when there is nominal flux in the machine and the observer flux is zero is a rare case. More important is the sensitivity to errors in parameters, which will be discussed later in this chapter.

Poles in Different Reference Frames

Another problem with pole placement is that the choice of reference frame will affect the location of the poles. Two observers in different reference frames, with identical behaviour, will not have the same poles. Why the poles differ in different reference frames is further evaluated in Appendix G. Until now, both the induction machine and the observer have been described in a stator oriented stationary reference frame. They might as well be described in a rotating reference frame, rotating with the angular frequency ω_k. If the observer's frame is rotating with the same frequency as the frequency of the stator voltage vector,

$$\omega_k = \omega_1 \tag{4.20}$$

the estimated stator and rotor flux vectors will be constant, instead of rotating, when the induction machine is running at constant speed and constant torque. This observer is described by

$$\frac{d\hat{\Psi}^r}{dt} = \left(A_e - j\,\omega_1 I\right)\hat{\Psi}^r + B_e \mathbf{u}_s^r + R_e k\left(\mathbf{i}_s^r - C_e \hat{\Psi}^r\right) \tag{4.21}$$

where the r-superscript denotes vectors in the rotating reference frame[1], and

$$\hat{\boldsymbol{\Psi}}^r = \hat{\boldsymbol{\Psi}}\, \mathrm{e}^{-j\omega_1 t} \quad \Leftrightarrow \quad \hat{\boldsymbol{\Psi}} = \hat{\boldsymbol{\Psi}}^r\, \mathrm{e}^{j\omega_1 t} \tag{4.22}$$

$$\mathbf{u}_s^r = \mathbf{u}_s\, \mathrm{e}^{-j\omega_1 t} \tag{4.23}$$

$$\mathbf{i}_s^r = \mathbf{i}_s\, \mathrm{e}^{-j\omega_1 t} \tag{4.24}$$

If the gain k is the same in the observers of equation (4.12) and equation (4.21), they will have identical behaviour, meaning that $\hat{\boldsymbol{\Psi}}$ of the first observer will be identical to $\hat{\boldsymbol{\Psi}}^r\, \mathrm{e}^{j\omega_1 t}$ of the second observer. However, the poles of the first observer (see Appendix E) are the eigenvalues of $\left(A_e - R_e\, k\, C_e\right)$, while the poles of the second observer are the eigenvalues of $\left(A_e - R_e\, k\, C_e - j\omega_1 I\right)$. Fig. 4.5 shows the poles of both observers.

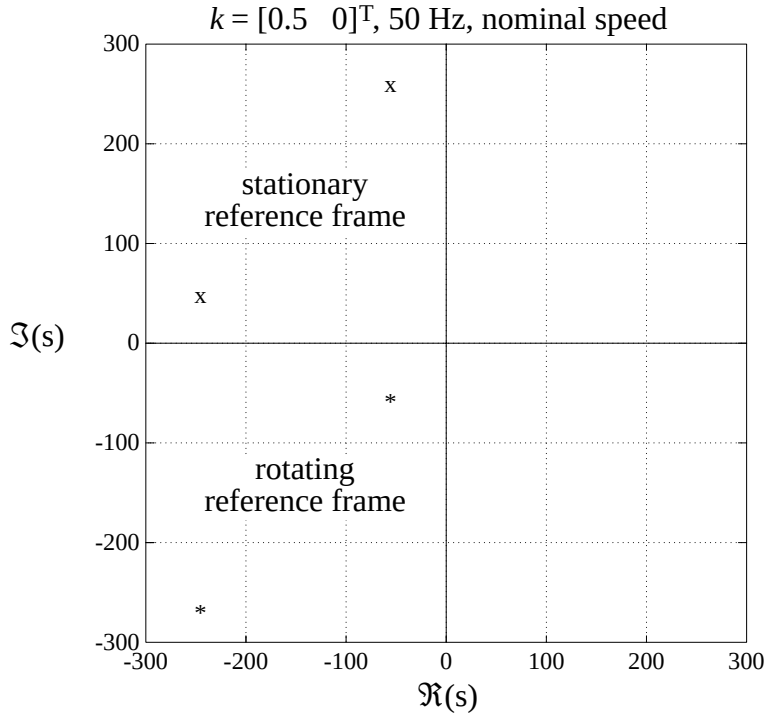

Fig. 4.5 'x' marks the poles of the observer in a stationary reference frame and '*' marks the poles of the observer in a reference frame rotating with angular frequency $\omega_1 = 2\pi f_1 = 2\pi 50 \approx 314\,\mathrm{rad/s}$

[1] the r-superscript is sometimes used in the literature for a rotor oriented reference frame.

Note that the real parts of the poles of both observers are equal, while the difference in the imaginary parts is equal to ω_1. It must also be pointed out that the observer is a non-linear system. Poles in the left half plane guarantee stability only in a linear system. An example of this is given in Appendix G.

Parameter Sensitivity

It is important to have as accurate observer parameters as possible, in order to get accurate estimates. Various methods for parameter identification exist (Zai et al, 1992, Krzeminski, 1991 and Vélez-Reyes et al, 1995), but will not be further discussed here. Instead, the influence of parameter errors will be studied.

The observer structure described by equation (4.12) is sometimes criticized for its parameter sensitivity at low frequencies (Jansen et al, 1994a). This is a misunderstanding due to its similarities to estimator A with poor low frequency properties, but with a proper choice of the gain *k*, this estimator will behave like anything from estimator A to estimator C. With a suitable gain, this observer will work well in its entire frequency range.

It is difficult to derive analytic expressions for the parameter sensitivity. Instead, the flux estimate errors at different frequencies are calculated for a certain motor, and compared with the errors of an observer described by Jansen et al (1994a).

As the flux vectors are rotating, the errors in the stator flux and rotor flux,

$$\tilde{\boldsymbol{\Psi}}_s = \boldsymbol{\Psi}_s - \hat{\boldsymbol{\Psi}}_s \tag{4.25}$$

and

$$\tilde{\boldsymbol{\Psi}}_r = \boldsymbol{\Psi}_r - \hat{\boldsymbol{\Psi}}_r \tag{4.26}$$

will also be rotating vectors. The relative errors in flux magnitude and phase are better measures. Here, the magnitude of the estimated flux related to the actual flux

$$\frac{\left|\hat{\boldsymbol{\Psi}}_s\right|}{\left|\boldsymbol{\Psi}_s\right|} = \frac{\hat{\Psi}_s}{\Psi_s} \tag{4.27}$$

and the error in phase,

$$\arg\left(\hat{\boldsymbol{\Psi}}_s\right) - \arg\left(\boldsymbol{\Psi}_s\right) = \hat{\varphi}_s - \varphi_s \tag{4.28}$$

will be studied.

These measures will be constant if the machine and observer are running with flux of constant magnitude and constant angular velocity. To calculate the steady state[2] flux of the observer, the following relation can be used,

$$\frac{d\hat{\Psi}}{dt} = j\,\omega_1\,\hat{\Psi} \tag{4.29}$$

where

$$\omega_1 = 2\,\pi f_1 \tag{4.30}$$

and f_1 is the frequency of the stator voltage. Equation (4.12) combined with equations (4.29) and (2.10) give

$$j\,\omega_1\,\hat{\Psi} = A_e\,\hat{\Psi} + B_e\mathbf{u}_s + R_e k\left(C\Psi - C_e\,\hat{\Psi}\right) \tag{4.31}$$

or

$$\left(A_e - R_e k C_e - j\,\omega_1 I\right)\hat{\Psi} = -B_e\mathbf{u}_s - R_e k C\,\Psi \tag{4.32}$$

where A_e, B_e and C_e are given by (4.5), (4.6) and (4.7), respectively.

The steady state flux estimate can now be calculated as

$$\hat{\Psi} = -\left(A_e - R_e k C_e - j\,\omega_1 I\right)^{-1}\left(B_e\mathbf{u}_s + R_e k C\,\Psi\right) \tag{4.33}$$

and the steady state flux of the motor is given by

$$\Psi = -\left(A - j\,\omega_1 I\right)^{-1} B\,\mathbf{u}_s \tag{4.34}$$

Parameter Sensitivity Comparison Between Two Observers

The error of the flux estimate in equation (4.33) will be compared to the flux estimate of an observer described by Jansen et al (1994a), shown here as a block diagram in Fig. 4.6. This observer was chosen as reference because of its good properties both at low and high frequencies.

---

[2] The term ”steady state” will be used even though the flux vectors are rotating. The term will be used when the magnitude and the angular velocity of the flux vectors are constant.

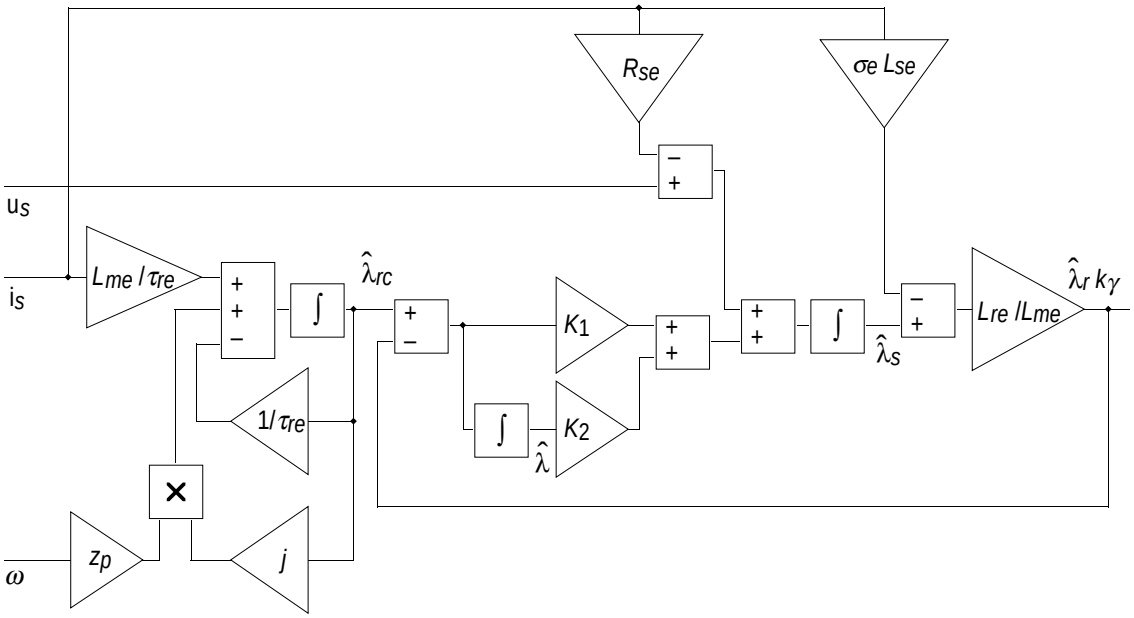

Fig. 4.6 Block diagram of λ-observer.

With the notation used by Jansen et al (1994a), this observer is described by

$$\begin{aligned}
\frac{d\hat{\boldsymbol{\lambda}}_s}{dt} &= -K_1 \frac{L_{re}}{L_{me}} \hat{\boldsymbol{\lambda}}_s + K_1 \hat{\boldsymbol{\lambda}}_{rc} + K_2 \hat{\boldsymbol{\lambda}} + \left(\sigma_e L_{se} \frac{L_{re}}{L_{me}} K_1 - R_{se} \right) \mathbf{i}_s + \mathbf{u}_s \\
\frac{d\hat{\boldsymbol{\lambda}}_{rc}}{dt} &= -\hat{\boldsymbol{\lambda}}_{rc} \left(\frac{1}{\tau_{re}} - j z_p \omega \right) + \frac{1}{\tau_{re}} L_{me} \mathbf{i}_s \\
\frac{d\hat{\boldsymbol{\lambda}}}{dt} &= -\frac{L_{re}}{L_{me}} \hat{\boldsymbol{\lambda}}_s + \hat{\boldsymbol{\lambda}}_{rc} + \sigma_e L_{se} \frac{L_{re}}{L_{me}} \mathbf{i}_s
\end{aligned} \tag{4.35}$$

where $\hat{\boldsymbol{\lambda}}_s$ is the estimated stator flux and $\hat{\boldsymbol{\lambda}}_{rc}$ and $\hat{\boldsymbol{\lambda}}$ are intermediate states. In matrix notation the observer is described by

$$\frac{d\hat{\lambda}}{dt} = A_{\lambda e}\hat{\lambda} + B_{\lambda e}\begin{bmatrix}\mathbf{i}_s \\ \mathbf{u}_s\end{bmatrix}$$

$$= \begin{bmatrix} -K_1\dfrac{L_{re}}{L_{me}} & K_1 & K_2 \\ 0 & -\left(\dfrac{1}{\tau_{re}} - jz_p\omega\right) & 0 \\ -\dfrac{L_{re}}{L_{me}} & 1 & 0 \end{bmatrix}\hat{\lambda} + \begin{bmatrix} \sigma_e L_{se}\dfrac{L_{re}}{L_{me}}K_1 - R_{se} & 1 \\ \dfrac{1}{\tau_{re}}L_{me} & 0 \\ \sigma_e L_{se}\dfrac{L_{re}}{L_{me}} & 0 \end{bmatrix}\begin{bmatrix}\mathbf{i}_s \\ \mathbf{u}_s\end{bmatrix} \tag{4.36}$$

where

$$\hat{\lambda} = \begin{bmatrix}\hat{\boldsymbol{\lambda}}_s \\ \hat{\boldsymbol{\lambda}}_{rc} \\ \hat{\boldsymbol{\lambda}}\end{bmatrix} \tag{4.37}$$

To distinguish between the observers, the observer described by equation (4.12) and Fig. 4.1 will be called the *Ψ-observer*, and the observer described by equation (4.35) and Fig. 4.6 will be called the *λ-observer*. In the US, flux linkage is often denoted λ, while the same quantity in Europe is denoted Ψ.

As a slightly different model of the induction machine is used in the λ-observer (T-model instead of Γ-model), table 2.1 must be used to translate between the models. Equal leakage inductance in stator and rotor is assumed. The stator flux estimate $\hat{\boldsymbol{\lambda}}_s$ can be directly compared to the stator flux estimate $\hat{\boldsymbol{\Psi}}_s$, while a new rotor flux $\hat{\boldsymbol{\lambda}}_r$ must be calculated for comparison with $\hat{\boldsymbol{\Psi}}_r$. The Ψ-observer and the λ-observer can be compared if

$$\hat{\boldsymbol{\lambda}}_r = \frac{1}{k_\gamma}\frac{L_{re}}{L_{me}}\left(\hat{\boldsymbol{\lambda}}_s - \sigma_e L_{se}\mathbf{i}_s\right) \tag{4.38}$$

$$k_\gamma = \sqrt{\frac{L_{Me}}{L_{Me} + L_{Le}}} \tag{4.39}$$

$$L_{me} = k_\gamma L_{Me} = L_{Me}\sqrt{\frac{L_{Me}}{L_{Me} + L_{Le}}} \tag{4.40}$$

$$L_{se} = L_{me} + L_{sle} = L_{Me} \tag{4.41}$$

$$L_{re} = L_{se} \tag{4.42}$$

$$\sigma_e = 1 - \frac{L_{me}^2}{L_{re} L_{se}} \tag{4.43}$$

$$\tau_{re} = \frac{L_{re}}{R_{re} k_\gamma^2} \tag{4.44}$$

$$\hat{\vartheta}_s = \arg\left(\hat{\boldsymbol{\lambda}}_s\right) \tag{4.45}$$

The steady state value of $\hat{\lambda}$ (actually the value when the magnitude and angular velocity of the components are constant) is given by

$$\hat{\lambda} = -\left(A_{\lambda e} - j\omega_1 I\right)^{-1} B_{\lambda e} \begin{bmatrix} \mathbf{i}_s \\ \mathbf{u}_s \end{bmatrix} \tag{4.46}$$

The idea behind this heuristic observer is to combine the good properties of estimators similar to estimator A and estimator C of Chapter 3. The left part of the observer in Fig. 4.6, the *current model*, depends on the measured current and works well at low frequencies. The right part, *the voltage model*, is integrating the measured voltage, with good results at high frequencies. At low frequencies, the estimated flux of the current model is correcting the flux of the voltage model, while at higher frequencies, the influence of the current model is reduced. The break frequency where the observer makes a transition from the current model to the voltage model can be set by the gain parameters K_1 and K_2 in equation (4.35). The parameters can be calculated from the chosen bandwidth of the observer, governed by the real eigenvalues $-\sigma_1$ and $-\sigma_2$. Having selected the bandwidth, the gains are given by

$$K_1 = \frac{L_{me}}{L_{re}}\left(\sigma_1 + \sigma_2\right) \tag{4.47}$$

and

$$K_2 = \frac{L_{me}}{L_{re}} \sigma_1 \sigma_2 \tag{4.48}$$

The λ-observer and Ψ-observer are compared in Fig. 4.7 and Fig. 4.8. The gain of the Ψ-observer is $k = [5 \quad -1]^{\mathrm{T}}$. This gain was chosen empirically, mainly to get a good balance between parameter sensitivity and noise sensitivity.

The eigenvalues of the λ-observer are $-\sigma_1 = -\sigma_2 = -2\pi 20$ rad / s.

Fig. 4.7 shows the error at rated torque when the rotor speed is slowly varied from 1% of the rated speed up to 10 times the rated speed. The solid lines represent the amplitude of the estimated flux of the Ψ-observer related to the actual flux, $\hat{\Psi}_s / \Psi_s$, and its phase error, $\hat{\varphi}_s - \varphi_s$. The dashed lines show the corresponding measures of the λ-observer, $\hat{\lambda}_s / \Psi_s$ and $\hat{\vartheta}_s - \varphi_s$.

It is seen that the errors in estimates of the Ψ-observer are smaller in most cases, except for the case shown in Fig. 4.7 a), where there is an error in R_{se}.

In Fig. 4.8, the two observers are compared again, now at varying slip and load torque. Also in this case, the errors are smaller for the Ψ-observer than for the λ-observer.

If the bandwidth of the λ-observer is increased, the sensitivity to errors in the stator resistance is reduced, because more trust is put into the current model which is completely insensitive to stator resistance error. However, higher bandwidth will accentuate errors due to errors in the other parameters at low frequencies. The bandwidth given by $\sigma_1 = \sigma_2 = 2\pi 20$ rad/s was selected as a good compromise.

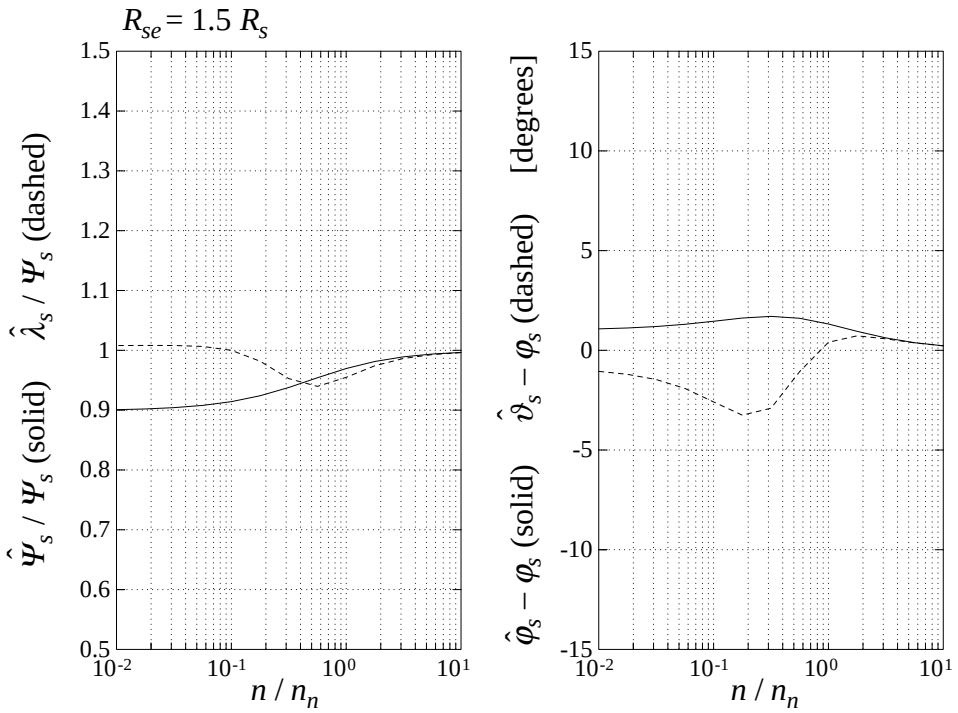
$R_{se} = 1.5\ R_s$
$\hat{\Psi}_s / \Psi_s$ (solid) $\hat{\lambda}_s / \Psi_s$ (dashed)
n / n_n
$\hat{\varphi}_s - \varphi_s$ (solid) $\hat{\vartheta}_s - \varphi_s$ (dashed) [degrees]
n / n_n

a)

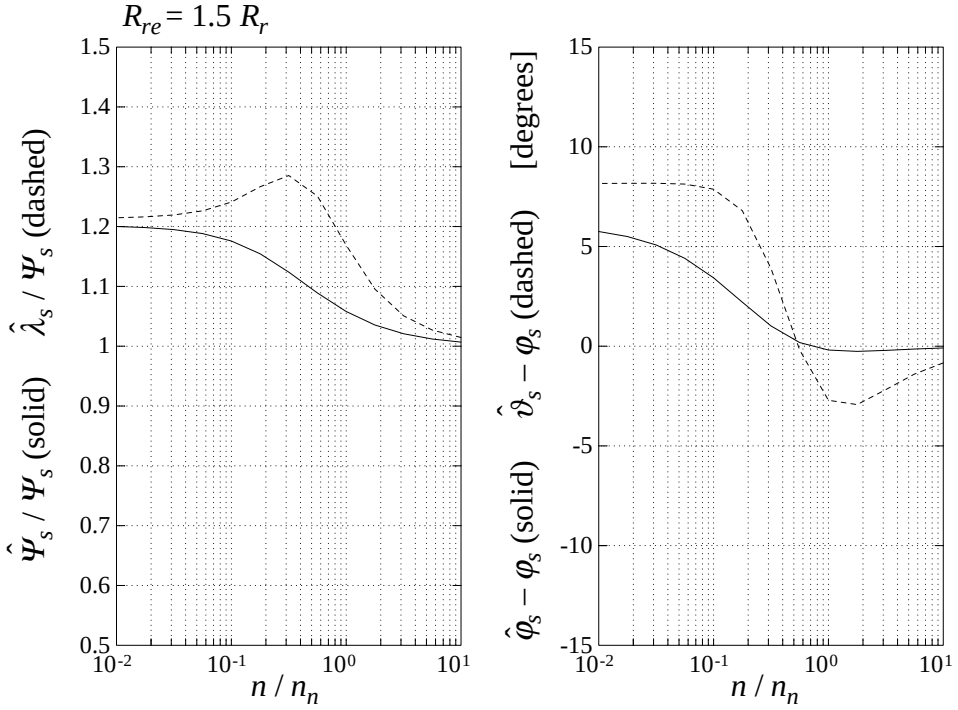
$R_{re} = 1.5\ R_r$
$\hat{\Psi}_s / \Psi_s$ (solid) $\hat{\lambda}_s / \Psi_s$ (dashed)
n / n_n
$\hat{\varphi}_s - \varphi_s$ (solid) $\hat{\vartheta}_s - \varphi_s$ (dashed) [degrees]
n / n_n

b)

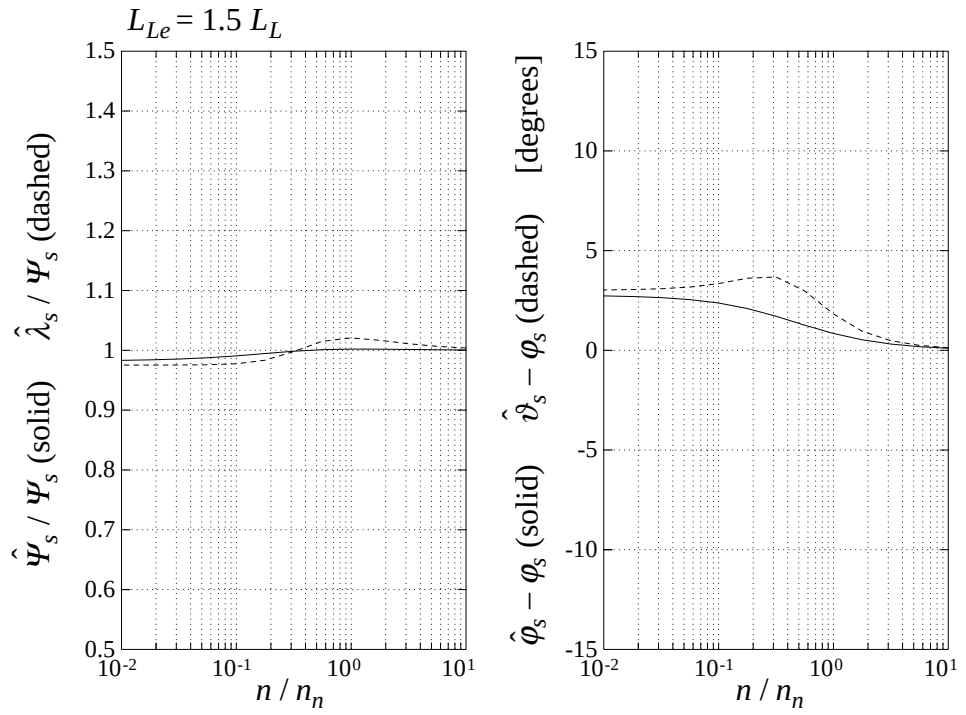

c)

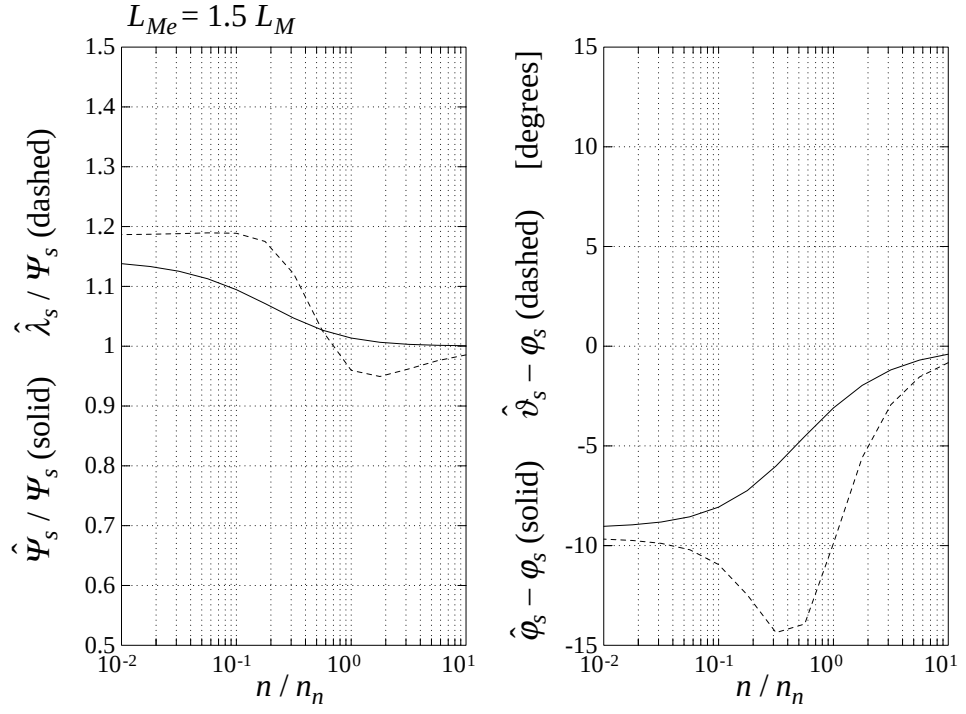

d)

Fig. 4.7 Comparison of parameter sensitivity between Ψ-observer (solid lines) and λ-observer (dashed lines) at rated torque. Ψ-observer gain $k = [5 \quad -1]^T$, λ-observer eigenvalues $-\sigma_1 = -\sigma_2 = -2\pi 20$ rad / s a) R_{se}-error b) R_{re}-error c) L_{Le}-error d) L_{Me}-error

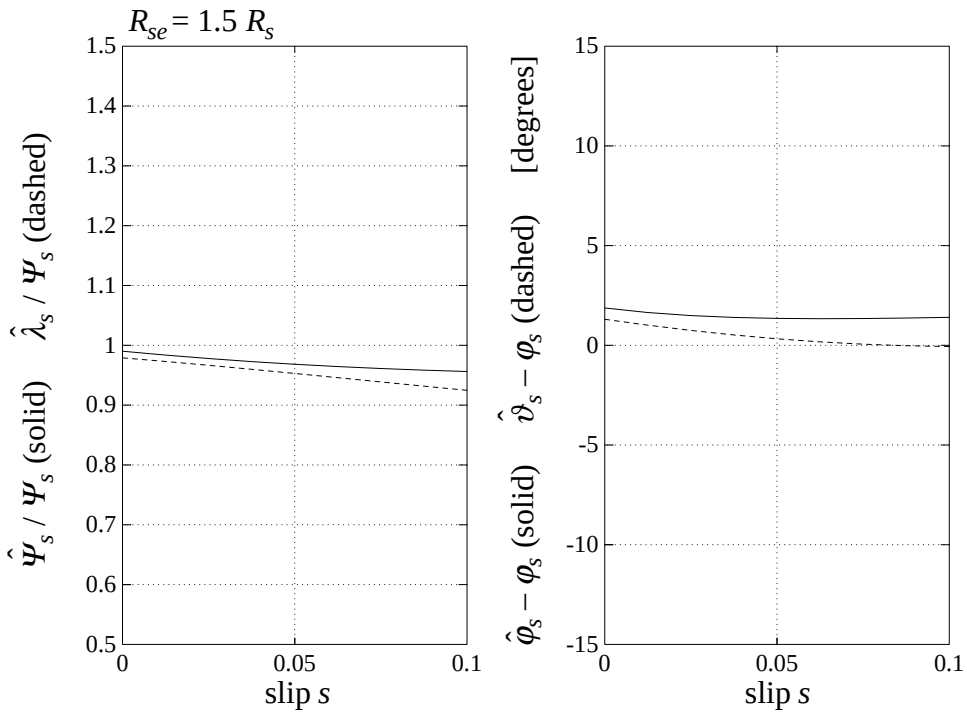
$R_{se} = 1.5\ R_s$
$\hat{\Psi}_s / \Psi_s$ (solid) $\hat{\lambda}_s / \Psi_s$ (dashed)
$\hat{\varphi}_s - \varphi_s$ (solid) $\hat{\vartheta}_s - \varphi_s$ (dashed) [degrees]
slip s
slip s

a)

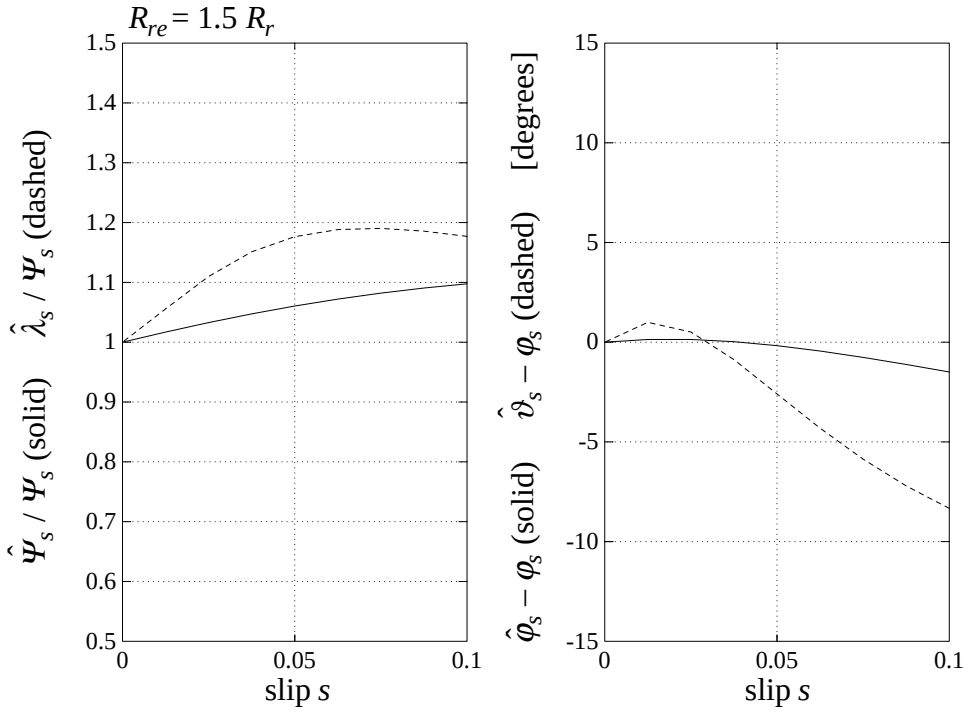
$R_{re} = 1.5\ R_r$
$\hat{\Psi}_s / \Psi_s$ (solid) $\hat{\lambda}_s / \Psi_s$ (dashed)
$\hat{\varphi}_s - \varphi_s$ (solid) $\hat{\vartheta}_s - \varphi_s$ (dashed) [degrees]
slip s
slip s

b)

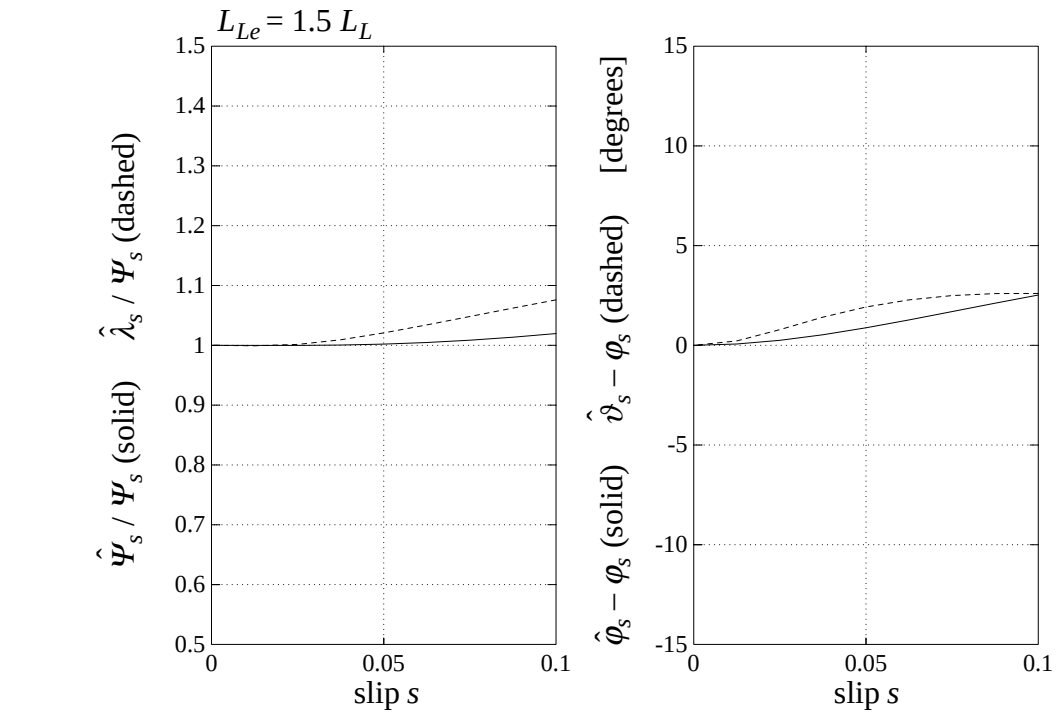

c)

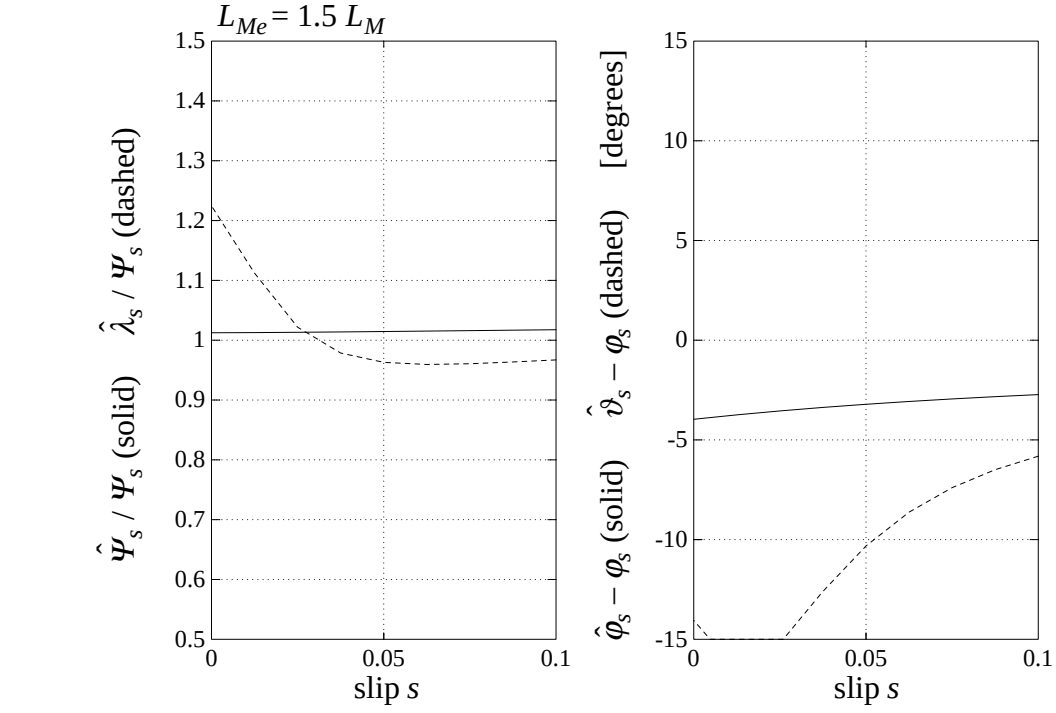

d)

Fig. 4.8 Comparison of parameter sensitivity between Ψ-observer (solid lines) and λ-observer (dashed lines) at varying slip and torque. Ψ-observer gain $k = [5 \quad -1]^T$, λ-observer eigenvalues $-\sigma_1 = -\sigma_2 = -2\pi 20$ rad / s a) R_{se}-error b) R_{re}-error c) L_{Le}-error d) L_{Me}-error

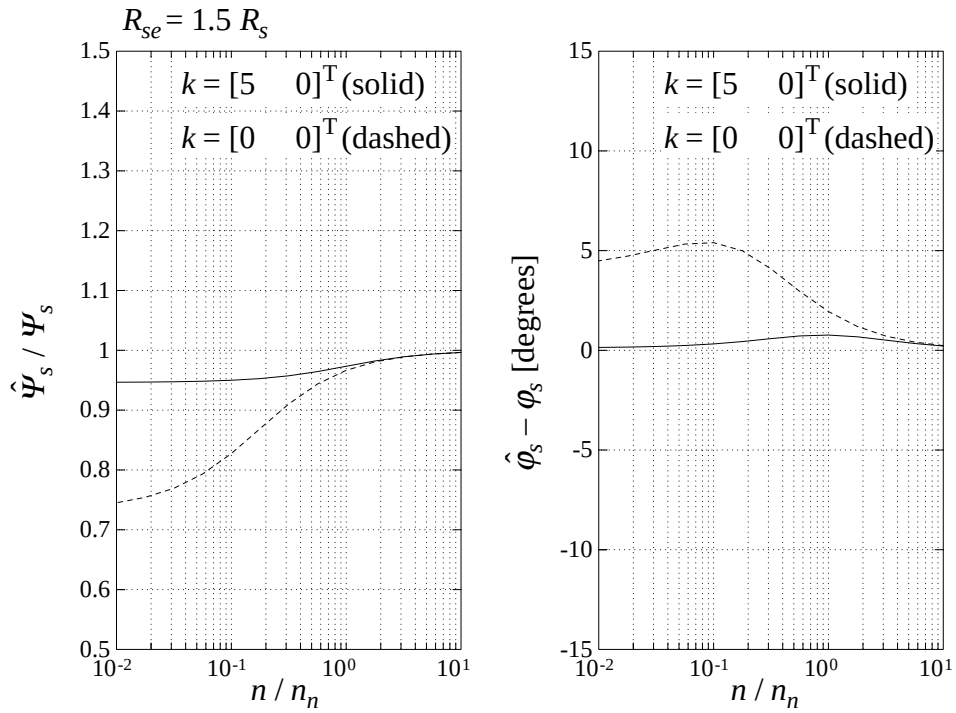
$R_{se} = 1.5\ R_s$
$k = [5 \quad 0]^T$ (solid)
$k = [0 \quad 0]^T$ (dashed)
$\hat{\Psi}_s / \Psi_s$
$\hat{\varphi}_s - \varphi_s$ [degrees]
n / n_n

a)

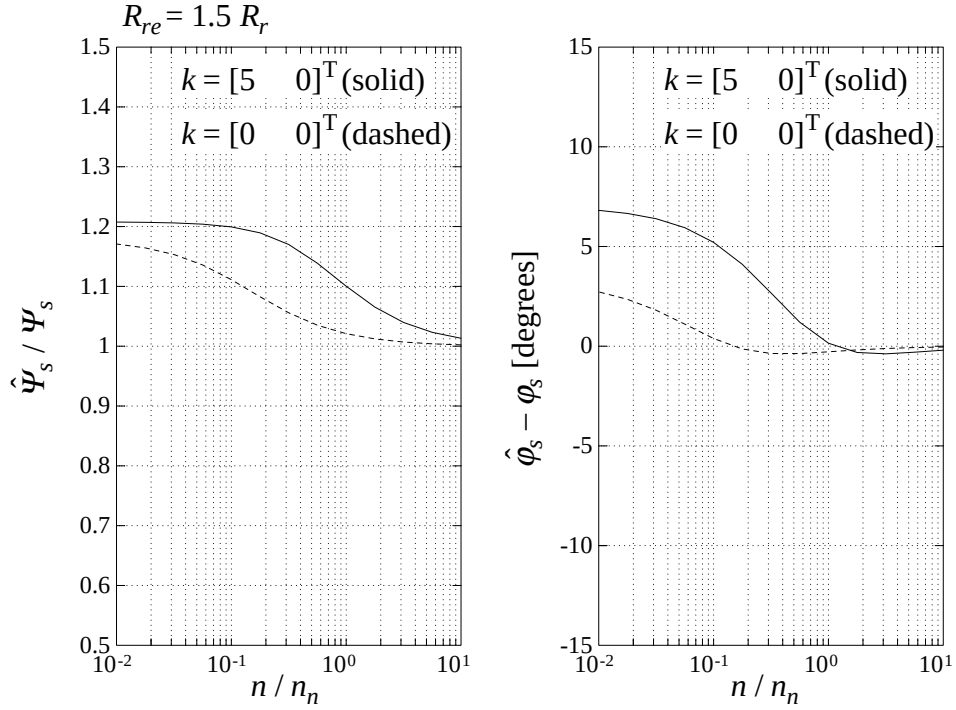
$R_{re} = 1.5\ R_r$
$k = [5 \quad 0]^T$ (solid)
$k = [0 \quad 0]^T$ (dashed)
$\hat{\Psi}_s / \Psi_s$
$\hat{\varphi}_s - \varphi_s$ [degrees]
n / n_n

b)

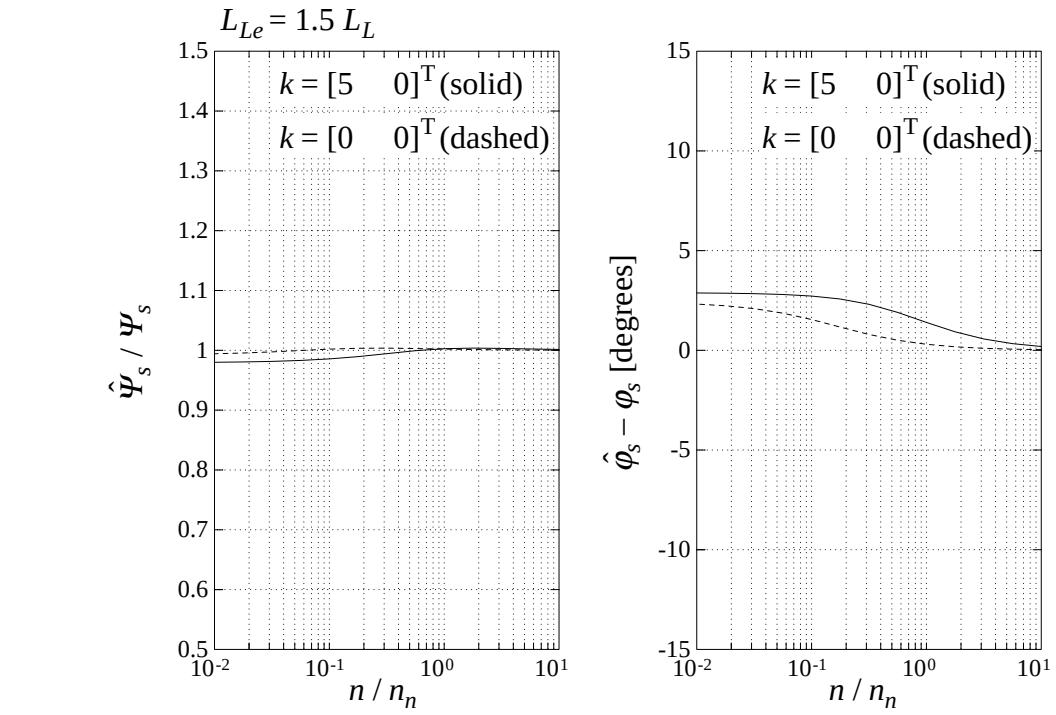

c)

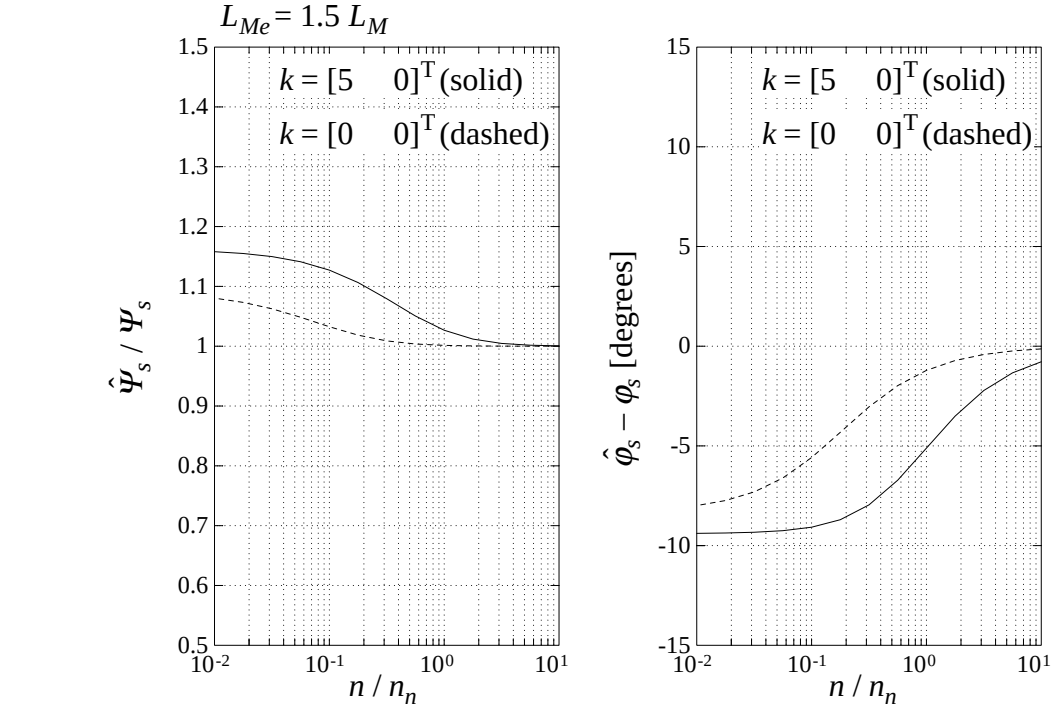

d)

Fig. 4.9 Comparison of parameter sensitivity between Ψ-observers with gain $k = [5 \quad 0]^T$ (solid) and gain $k = [0 \quad 0]^T$ (dashed). a) R_{se}-error b) R_{re}-error c) L_{Le}-error d) L_{Me}-error

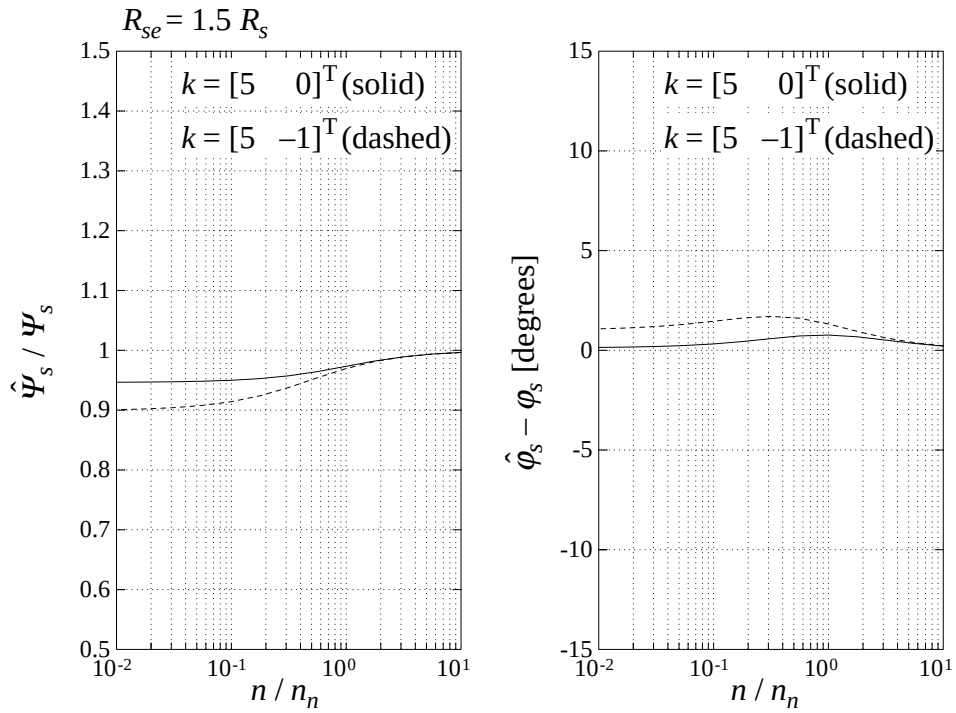
$R_{se} = 1.5\ R_s$
$k = [5 \quad 0]^T$ (solid)
$k = [5 \quad -1]^T$ (dashed)
$\hat{\Psi}_s / \Psi_s$
$\hat{\varphi}_s - \varphi_s$ [degrees]
n / n_n

a)

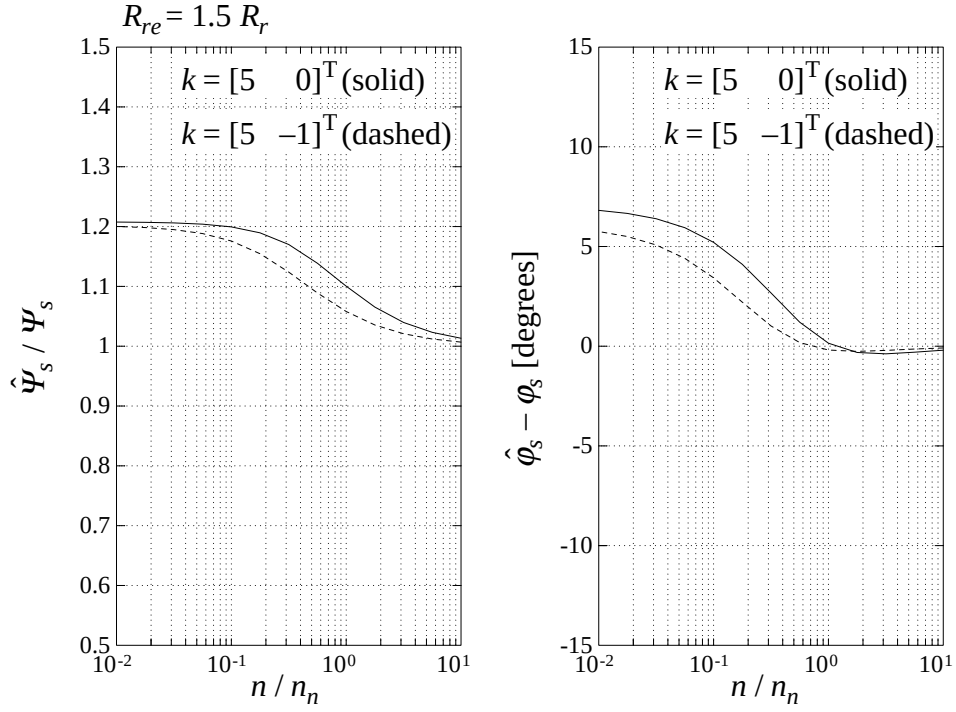
$R_{re} = 1.5\ R_r$
$k = [5 \quad 0]^T$ (solid)
$k = [5 \quad -1]^T$ (dashed)
$\hat{\Psi}_s / \Psi_s$
$\hat{\varphi}_s - \varphi_s$ [degrees]
n / n_n

b)

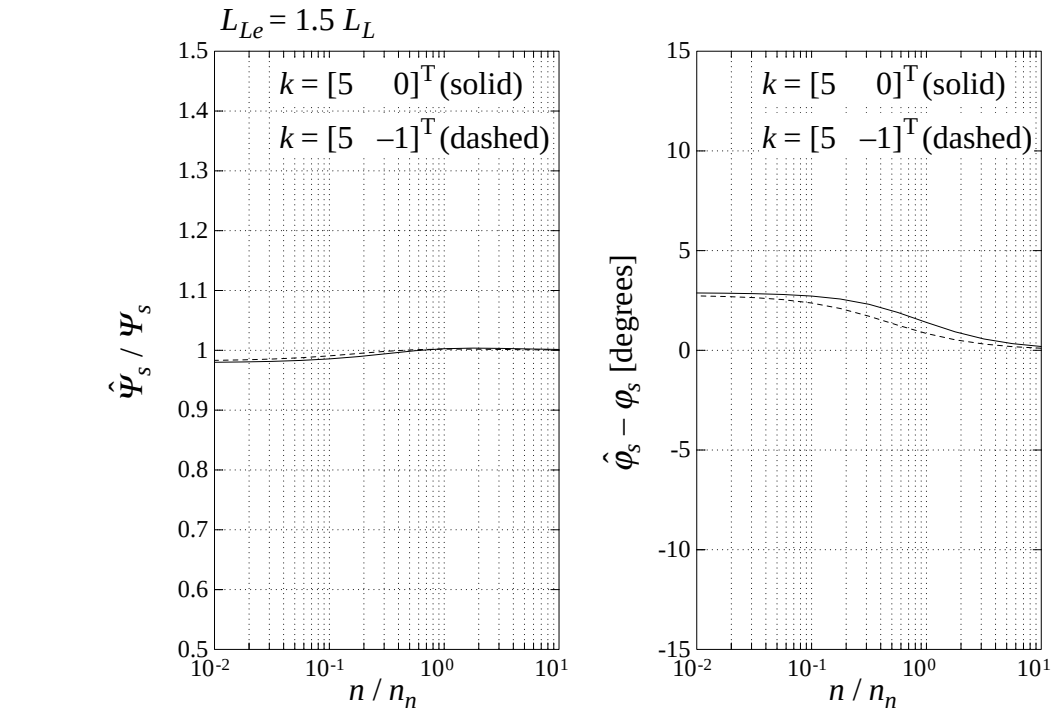

c)

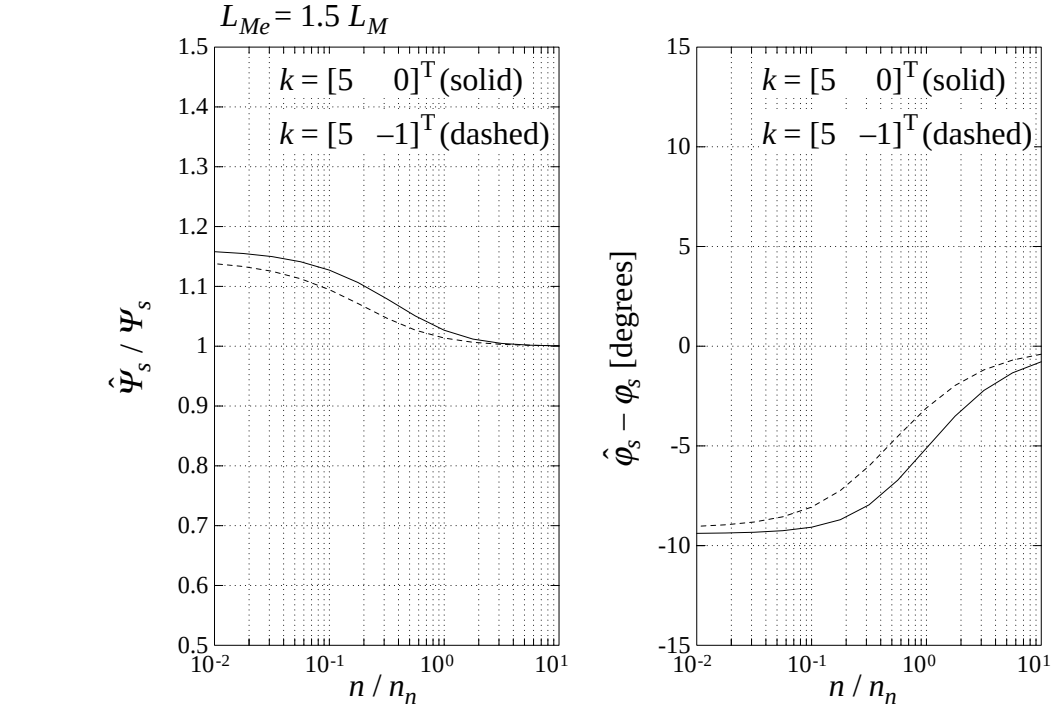

d)

Fig. 4.10 Comparison of parameter sensitivity between Ψ-observers with gain $k = [5 \quad 0]^T$ (solid) and gain $k = [5 \quad -1]^T$ (dashed). a) R_{se}-error b) R_{re}-error c) L_{Le}-error d) L_{Me}-error

Observer Gain Influence on Parameter Sensitivity

The gain vector k of the Ψ-observer will affect the parameter sensitivity in a more direct way than K_1 and K_2 of the λ-observer. At low and high frequencies, the error of the λ-observer is not much affected by K_1 and K_2. At low frequency, the parameter sensitivity is the same as the parameter sensitivity of the current model. At high frequencies, the sensitivity is the same as the sensitivity of the voltage model. The gain k of the Ψ-observer on the other hand, will affect the parameter sensitivity in the entire frequency range. The error of the Ψ-observer in Fig. 4.7 a) can be reduced by increasing the gain of the observer. In Fig. 4.9 and Fig. 4.10, the steady state errors of the Ψ-observer is compared for different selections of the gain. In Fig. 4.9, the solid lines represent a gain of $k_s = 5$ and $k_r = 0$, while the dashed line represent an observer with zero gain.

In Fig. 4.9 it is seen that the error is smaller for $k_{sx} = 5$ than for $k_{sx} = 0$, comparable to the error reduction seen in Fig. 3.12 and Fig. 3.14. The error can be further reduced with $k_{rx} = -1$ instead of $k_{rx} = 0$, seen in Fig. 4.10. However, the effects of k_{rx} are less predictable than the effects of k_{sx} and the observer might be unstable at certain speeds if it is not chosen with great care. As the gain k_{sx} has more influence on the steady state error than k_{rx}, it is recommended to set $k_{rx} = 0$.

The imaginary parts of the observer gain, k_{sy} and k_{ry} should also be zero for stability reasons. Both parameters will have different effects if the rotor speed is positive or negative. If they are chosen so that the observer is stable for clockwise rotation, the observer will be unstable for counter clockwise rotation. If, for some reason k_{sy} and k_{ry}, are given values other than zero, observer gain scheduling must be used, changing the signs of k_{sy} and k_{ry} when the direction of rotation is changed.

Flux Observer Conclusions

The parameter sensitivity of the observer structure shown in Fig. 4.1 can be significantly reduced by selecting an appropriate observer gain. The structure with dimensionless observer gains makes the selection much easier. The gains rather than the poles of the observer should be held constant at varying speed. As a result, the response time of the observer will be slower at lower frequencies. Although the sensitivity to errors in the stator resistance is reduced by using a large value of k_s, the sensitivity to noise is increased. Thus, it is important to have an as accurate parameter R_{se} as possible. This is not a big drawback as the stator resistance is the easiest parameter in the induction machine to measure.

5

Speed Observer Models

In earlier chapters, it was assumed that rotor speed was measured, and the speed signal was used as input to the flux observer. In this chapter, the speed as well as the flux will be estimated instead of measured.

Two basic strategies for speed estimation are found in the literature; one strategy uses the machine model in equations (2.3)-(2.6) together with measured current and voltage (Yang et al, 1993, Schauder, 1992, Tajima et al, 1993 and Jönsson, 1991). The other strategy relies on saliency within the machine. Unfortunately, both strategies are related with limitations.

The difficulty with the first strategy appears at low speeds and low frequencies. Even though it is not directly apparent from the machine model, the measured current and voltage carry no information on the speed if the frequency of the stator voltage is zero as will be shown later. This fact is seldom mentioned in the references. Instead, it is often stated that these methods fail at zero speed, not at zero frequency (Jansen et al, 1993). Extended Kalman filters have been tried to overcome the low frequency problems (von Westerholt et al, 1992b, Henneberger et al, 1991, Kim et al, 1994), but it is obvious that none of these methods will work properly when speed information is not present in the measured signals.

The difficulty with the second strategy is that the rotor of the induction machine is smooth, and the ideal induction machine described by equations (2.3)-(2.6) has no saliency at all. In the actual machine, rotor slotting is present, resulting in current harmonics (Hurst et al, 1994, Beguenane et al, 1994, Haemmerli, 1986 and Veltman, 1994). The FFT analysis required to extract the speed information from the harmonics is time consuming, and the information is reduced at low speed and low frequency for this method as well. A promising method is described by Schroedl (1992) that uses saliency introduced by local saturation of the magnetic flux paths instead. This method has also been reported to fail in the low speed region (Jansen et al, 1994a). To solve the low speed problems, a new method using a modified rotor with a modulation in the width of the slot openings has been presented (Jansen et al, 1994a). The main drawback of this method is that a standard induction machine cannot be used.

The first strategy, using the machine model in equations (2.3)-(2.6), can be implemented with standard induction machines and frequency inverters with moderate additional hardware. Only this strategy will be studied here.

Introduction to Speed Estimation

In this section a simplified mechanical model will illustrate how the rotor speed of the induction machine can be estimated, and also illustrate some related problems.

With some simplifications, the mechanical model in Fig. 5.1 is a model analogous to the torque producing part of the induction machine. In this model, rotational movement is replaced by linear movement and torque is replaced by force. Note that the equilibrium position of the spring is at $\ell = 0$.

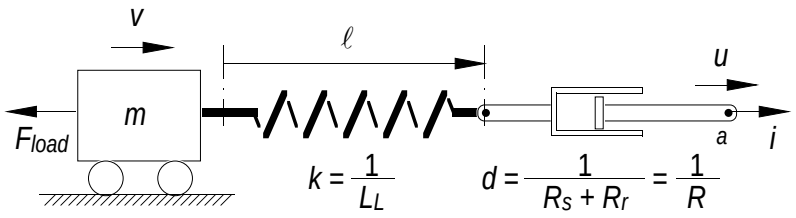

Fig. 5.1 Simplified mechanical model illustrating induction machine speed estimation.

In the mechanical model in Appendix C, Fig. C.2, it is seen that the leakage inductance has the main influence in the tangential direction, the torque producing direction, while the magnetizing inductance can be neglected. The stator and rotor resistance can be considered connected in series. The spring in Fig. 5.1 is representing the leakage inductance L_L and the viscous damper the sum of the stator resistance R_s and rotor resistance R_r. The moment of inertia J is represented by the mass m. Estimating the speed v of the carriage is analogous to estimating the rotor speed ω of an induction machine.

The input to the system u is the speed of point a representing the tangential part of the stator voltage vector. The force i, representing the tangential part of the stator current vector is an output that can be measured. F_{load} is representing the load torque and can not be measured.

According to the laws for a mechanical system described in Appendix B, the system in Fig. 5.1 is described by

$$\frac{d\ell}{dt} = u - \frac{k}{d}\ell - v = u - \frac{R}{L_L}\ell - v \tag{5.1}$$

$$\frac{dv}{dt} = \frac{k}{m}\ell - \frac{F_{load}}{m} = \frac{1}{m\,L_L}\ell - \frac{F_{load}}{m} \tag{5.2}$$

$$i = k\,\ell = \frac{1}{L_L}\ell \tag{5.3}$$

or in matrix notation

$$\frac{dx}{dt} = Ax + Bu + F \tag{5.4}$$

$$y = Cu \tag{5.5}$$

where

$$x = \begin{bmatrix} \ell \\ v \end{bmatrix} \tag{5.6}$$

$$y = i \tag{5.7}$$

$$A = \begin{bmatrix} \dfrac{-R}{L} & -1 \\ \dfrac{1}{m\,L_L} & 0 \end{bmatrix} \tag{5.8}$$

$$B = \begin{bmatrix} 1 \\ 0 \end{bmatrix} \tag{5.9}$$

$$C = [1 / L_L \quad 0] \tag{5.10}$$

$$F = \begin{bmatrix} 0 \\ F_{load} \end{bmatrix} \tag{5.11}$$

If the load force is equal to zero, the velocity *v* of the carriage will be equal to the input *u* at steady state. This is analogous to an induction machine running at synchronous speed. If the load is greater than zero, the velocity *v* will be less than *u*, comparable to a loaded induction machine running with slip. To conclude, estimating the velocity *v* is analogous to estimating the

rotor speed ω of an induction machine with unknown load torque. Deriving a velocity observer for this mechanical system is the first step in deriving an observer for the rotor speed of the induction machine, which will be done later in this chapter.

Velocity Observer, Approach 1

The identity observer structure in equation (3.12) cannot be applied directly to this system because of the unknown input F_{load} in equation (5.2). A first heuristic approach could simply be to integrate the error in an estimate of the force i, resulting in a velocity estimate, where the estimated force is a result of the standard observer structure applied to equation (5.1). We have

$$\frac{d\hat{\ell}}{dt} = u - \frac{R}{L_L}\hat{\ell} - \hat{v} + k_1\left(i - \hat{i}\right) \tag{5.12}$$

$$\hat{i} = \frac{1}{L_L}\hat{\ell} \tag{5.13}$$

$$\frac{d\hat{v}}{dt} = k_2\left(i - \hat{i}\right) \tag{5.14}$$

The velocity estimate $\hat{v}$ will be integrated until the errors in the estimates $i - \hat{i}$ and $\ell - \hat{\ell}$ are zero, giving also the velocity estimate error $v - \hat{v}$ equal to zero at steady state.

If we instead form an observer out of equation (3.12), neglecting the load torque, equations (5.12) and (5.13) remain unchanged, but the velocity estimate equation will be

$$\frac{d\hat{v}}{dt} = \frac{1}{m\,L_L}\hat{\ell} + k_2\left(i - \hat{i}\right) \tag{5.15}$$

As long as the load force F_{load} is zero or varying with zero mean, an observer consisting of equations (5.12), (5.13) and (5.15) is superior to one using equation (5.14) for the velocity estimate. However, the steady state value of the velocity estimate of equation (5.15) will always equal the input u, even when F_{load} is present, resulting in a steady state error in the velocity estimate. The reason is that in the system equation (5.2), the terms $\ell/\left(m\,L_L\right)$ and F_{load}/m will be equal at steady state, and the time derivative of the velocity will be zero. In the observer equation (5.15), there is no term F_{load}/m that can balance $\hat{\ell}/\left(m\,L_L\right)$. Instead, $\hat{\ell}$ will be driven to zero at steady state. If the term $\hat{\ell}/\left(m\,L_L\right)$ simply is deleted, the steady state error

is eliminated, and we are back to the first heuristic approach, equation (5.14).

In conclusion, one term, $\hat{\ell}/(m L_L)$, must be deleted, to get zero error at steady state out of the identity observer originating from equation (3.12), in order to handle the unknown input F_{load}.

Velocity Observer, Approach 2

Another way of handling an unknown input is to augment the state vector (Glad et al, 1981 and von Westerholt et al, 1992b).

$$x = \begin{bmatrix} \ell \\ v \\ F_{load} \end{bmatrix} \tag{5.16}$$

The last row of the system matrix will consist only of zeros, as F_{load} is unknown,

$$A = \begin{bmatrix} \frac{-R}{L} & -1 & 0 \\ \frac{1}{m L_L} & 0 & -\frac{1}{m} \\ 0 & 0 & 0 \end{bmatrix} \tag{5.17}$$

The B and C matrices must be extended with zeros,

$$B = \begin{bmatrix} 1 \\ 0 \\ 0 \end{bmatrix} \tag{5.18}$$

$$C = \begin{bmatrix} 1/L_L & 0 & 0 \end{bmatrix} \tag{5.19}$$

As the unknown force is a state and not an input, the identity observer can be used. Inserting the matrices above into equation (3.12) gives

$$\frac{d\hat{\ell}}{dt} = u - \frac{R}{L_L}\hat{\ell} - \hat{v} + k_1\left(i - \hat{i}\right) \tag{5.20}$$

$$\frac{d\hat{v}}{dt} = \frac{1}{m L_L}\hat{\ell} - \frac{1}{m}\hat{F}_{load} + k_2\left(i - \hat{i}\right) \tag{5.21}$$

$$\frac{d\hat{F}_{load}}{dt} = k_3\left(i - \hat{i}\right) \tag{5.22}$$

$$\hat{i} = \frac{1}{L_L}\hat{\ell} \tag{5.23}$$

The steady state value of this observer is equal to the steady state value of the observer in equations (5.12)-(5.14), that is, no error in the velocity estimates.

The two observers have different dynamic behaviour, making it difficult to say which one is the better. However, the first observer has an advantage in less computational costs.

Speed Calculation through Differentiation

The velocity observers discussed so far are all based on integration. If we look at the complete description of the induction machine, instead of at the simplified model in Fig. 5.1, there is another way of estimating the rotor speed based on differentiation.

The speed of the rotor is present in equation (2.6) which can be used to derive an expression for the speed. Equation (2.6) gives

$$\begin{aligned} jz_p\,\omega &= \frac{\dfrac{d\boldsymbol{\Psi}_r}{dt}}{\boldsymbol{\Psi}_r} + R_r\frac{\mathbf{i}_r}{\boldsymbol{\Psi}_r} = \frac{\boldsymbol{\Psi}_r^*\dfrac{d\boldsymbol{\Psi}_r}{dt}}{\boldsymbol{\Psi}_r^*\boldsymbol{\Psi}_r} + R_r\frac{\boldsymbol{\Psi}_r^*\mathbf{i}_r}{\boldsymbol{\Psi}_r^*\boldsymbol{\Psi}_r} \\ &= \frac{\boldsymbol{\Psi}_r^*\dfrac{d\boldsymbol{\Psi}_r}{dt}}{\left|\boldsymbol{\Psi}_r\right|^2} + R_r\frac{\boldsymbol{\Psi}_r^*\mathbf{i}_r}{\left|\boldsymbol{\Psi}_r\right|^2} \end{aligned} \tag{5.24}$$

As z_p and ω are real, the real part of equation (5.24) must be zero resulting in

$$jz_p\,\omega = \frac{j\Im\left(\boldsymbol{\Psi}_r^*\dfrac{d\boldsymbol{\Psi}_r}{dt}\right)}{\left|\boldsymbol{\Psi}_r\right|^2} + R_r\frac{j\Im\left(\boldsymbol{\Psi}_r^*\mathbf{i}_r\right)}{\left|\boldsymbol{\Psi}_r\right|^2} \tag{5.25}$$

The speed of the rotor can now be calculated,

$$\omega = \frac{1}{z_p}\left(\frac{\Im\left(\boldsymbol{\Psi}_r^* \frac{d\boldsymbol{\Psi}_r}{dt} \right)}{\left|\boldsymbol{\Psi}_r\right|^2} + R_r \frac{\Im\left(\boldsymbol{\Psi}_r^* \mathbf{i}_r \right)}{\left|\boldsymbol{\Psi}_r\right|^2} \right) \tag{5.26}$$

The first term of the right hand side of equation (5.26), the cross product of the rotor flux vector and its time derivative, divided by the square of the length of the vector, is equal to the angular speed ω_e of the rotor flux vector,

$$\omega_e = \frac{\Im\left(\boldsymbol{\Psi}_r^* \frac{d\boldsymbol{\Psi}_r}{dt} \right)}{\left|\boldsymbol{\Psi}_r\right|^2} = \frac{d}{dt}\arg\left(\boldsymbol{\Psi}_r\right) \tag{5.27}$$

The second term includes the motor torque. Combining (2.8), (5.26) and (5.27) gives

$$\omega = \frac{1}{z_p}\left(\omega_e - \frac{2}{3}\frac{R_r}{z_p}\frac{T}{\left|\boldsymbol{\Psi}_r\right|^2} \right) \tag{5.28}$$

At steady state, ω_e is equal to ω_1, meaning that the first term represents the synchronous speed, while the second term represents the slip.

If the stator flux together with all the parameters of the machine are known, the rotor flux can be calculated from equations (2.3) and (2.4),

$$\boldsymbol{\Psi}_r = \boldsymbol{\Psi}_s\left(1 + \frac{L_L}{L_M} \right) - L_L\, \mathbf{i}_s \tag{5.29}$$

It looks simple to calculate the speed of the rotor: when the stator flux is known, calculate the rotor flux from equation (5.29). Then, assuming the speed estimator is implemented as a sampled system, use numerical differentiation to calculate ω_e. Calculate the torque from equation (2.8), and the speed is calculated from (5.28). However, there are problems involved:

- calculation of the stator flux;
- differentiation is sensitive to noise, giving problems when calculating ω_e;

- the slip term is proportional to the rotor resistance. If the rotor resistance, which varies with temperature, is not precisely known, the calculated speed will differ from the actual speed.

The first problem is ”solved” by using one of the flux observers described in Chapter 3 and Chapter 4. The observer in equation (3.1) is often used to calculate the flux (Pohjalainen et al, 1994, Bausch et al, 1994, Takahashi et al, 1989 and Baader et al, 1992). As was shown in Chapter 3, this method cannot be used at low frequencies. Various tricks such as low pass filtering and ”current correction” are used in the mentioned publications to prevent the integrators from saturating at low frequencies. Even though the integrator drift is pointed out in many articles to be the main problem about observers, there are more severe problems than integrator drift at low frequencies as will be discussed later in this chapter.

It was shown in previous chapters that the integrator drift problem is solved by using the flux observer described by equations (4.13) and (4.14). This observer also estimates the rotor flux directly and equation (5.29) is not needed. However, this observer requires the speed as an input. Trying to calculate the rotor speed from equation (5.28) and then feeding it to this observer results in an algebraic loop, making it impossible to use.

Instead, the flux observer together with a new speed observer based on integration rather than differentiation will be studied here. The steady state speed of this observer will be the same as the speed calculated by equation (5.28).

Speed Observer Based on Integration

A speed observer based on the ideas that earlier led to a velocity observer described by equations (5.12)–(5.14) will overcome the problems related to differentiation.

By simply adding a lever to the force error $i - \hat{i}$ in equation (5.14), a torque error is obtained. The lever in the induction machine is the stator flux vector. The torque error is the result of a cross product,

$$\tilde{T} = \Im\left(\left(\mathbf{i}_s - \hat{\mathbf{i}}_s \right)^* \hat{\boldsymbol{\Psi}}_s \right) \tag{5.30}$$

and is analogous to the force error $i - \hat{i}$. In (5.14), the integrated force error resulted in the velocity estimate. Correspondingly, the torque error can be integrated into a rotor speed estimate,

$$\frac{d\hat{\omega}}{dt} = \frac{k_\omega}{J_e}\tilde{T} = \frac{k_\omega}{J_e}\Im\left(\left(\mathbf{i}_s - \hat{\mathbf{i}}_s\right)^* \hat{\mathbf{\Psi}}_s\right) \tag{5.31}$$

where the gain k_ω determines the response time but not the steady state value of the estimated speed. A block diagram of this observer is shown in Fig. 5.2.

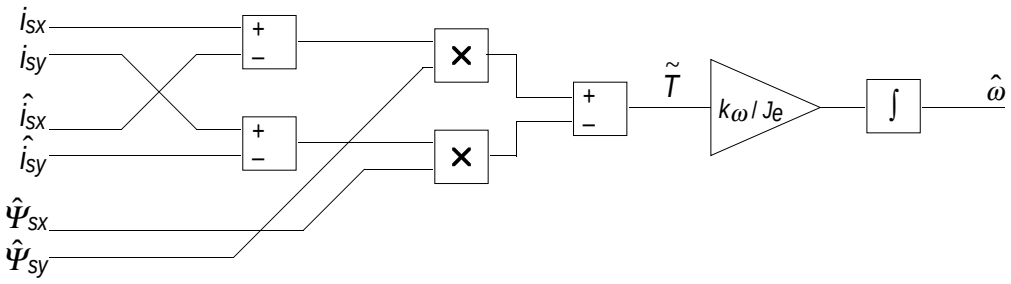

Fig. 5.2 Block diagram of speed observer. i_{sx} is the real part of the stator current, i_{sy} is the imaginary part.

The inputs of this observer are the estimated stator flux and stator current of the flux observer in Fig. 4.1 and the measured stator current. The output $\hat{\omega}$ is connected to the ω-input of the flux observer.

This speed observer is related to speed observers based on *model reference adaptive systems*, MRAS (Tamai et al, 1987, Schauder, 1992 and Tajima et al, 1993). Two models of the induction machine, usually the voltage model (estimator A in Chapter 3) which is speed independent, and the current model (estimator B in Chapter 3), which does depend on the speed, run in parallel. If the speed input to the current model is incorrect, the current model and voltage model will yield different flux estimates. This difference is treated as an error signal, and is adjusting the speed input to the current model until the error is zero. This method has the disadvantage of using the voltage model which does not work at low frequencies due to integrator drift.

The speed observer proposed here use the machine itself as the reference system, and the observer described in Chapter 4 as the adjustable system, solving the integrator drift problems. A similar approach was suggested by Yang et al (1993).

A second velocity observer for the system in Fig. 5.1 was suggested, where a new state, $\hat{F}_{load}$, was introduced. The same approach can be used when designing a rotor speed observer, where the unknown load torque must be introduced as an estimated state. The observer would have the same

structure as the estimator in equations (5.21) and (5.22). This observer is not further investigated here but is mentioned by von Westerholt et al (1992a and 1992b).

Steady State Value of Speed Estimate

The steady state value of the speed observer is more difficult to calculate than that of the flux observer. Calculating the flux meant solving a linear set of equations with two unknown complex variables. Now we have a non-linear set of equations with two unknown complex variables and one unknown real variable. The equations to solve are the two equations (4.31) (with ω replaced by $\hat{\omega}$), and equation (5.31), with the derivative equal to zero. The system matrices A_e, B_e and C_e of equation (4.31) are defined by (4.5)-(4.7).

$$j\omega_1 \hat{\boldsymbol{\Psi}}_s = \mathbf{u}_s - R_{se}(1+\mathbf{k}_s)\left(\hat{\boldsymbol{\Psi}}_s\left(\frac{1}{L_{Me}}+\frac{1}{L_{Le}}\right)-\hat{\boldsymbol{\Psi}}_r\frac{1}{L_{Le}}\right)+R_{se}\mathbf{k}_s\mathbf{i}_s \quad (5.32)$$

$$\begin{aligned} j\omega_1 \hat{\boldsymbol{\Psi}}_r = {} & jz_p\hat{\omega}\hat{\boldsymbol{\Psi}}_r + \frac{R_{re}}{L_{Le}}\left(\hat{\boldsymbol{\Psi}}_s - \hat{\boldsymbol{\Psi}}_r\right) \\ & - R_{re}\mathbf{k}_r\left(\hat{\boldsymbol{\Psi}}_s\left(\frac{1}{L_{Me}}+\frac{1}{L_{Le}}\right)-\hat{\boldsymbol{\Psi}}_r\frac{1}{L_{Le}}-\mathbf{i}_s\right) \end{aligned} \quad (5.33)$$

$$0 = \frac{k_\omega}{J_e}\Im\left(\left(\mathbf{i}_s-\hat{\mathbf{i}}_s\right)^*\hat{\boldsymbol{\Psi}}_s\right) \quad (5.34)$$

The last equation expresses that, at steady state, the estimated stator flux vector is parallel to the error in the estimated current. It follows that

$$\hat{\mathbf{i}}_s - \mathbf{i}_s = \varsigma\hat{\boldsymbol{\Psi}}_s \quad (5.35)$$

where ς is a real valued constant. The estimated stator current can according to equation (4.15) be written

$$\hat{\mathbf{i}}_s = \hat{\boldsymbol{\Psi}}_s\left(\frac{1}{L_{Me}}+\frac{1}{L_{Le}}\right)-\frac{1}{L_{Le}}\hat{\boldsymbol{\Psi}}_r \quad (5.36)$$

Inserting the estimated stator current in equation (5.35) followed by some rearranging gives

$$\hat{\boldsymbol{\Psi}}_r = \varsigma\hat{\boldsymbol{\Psi}}_s - L_{Le}\mathbf{i}_s \quad (5.37)$$

where ς still is a real valued constant, but different from the one in (5.35). We have now introduced an extra unknown variable, but also replaced equation (5.34) by equation (5.37), which can be considered as two equations, one for the real and one for the imaginary part. The steady state value of the speed observer can now be calculated by solving equations (5.32), (5.33) and (5.37). Step one is to express stator and rotor flux estimates as functions of the estimated speed,

$$\hat{\boldsymbol{\Psi}}_s = \mathrm{f}_1\left(\hat{\omega}\right) \tag{5.38}$$

$$\hat{\boldsymbol{\Psi}}_r = \mathrm{f}_2\left(\hat{\omega}\right) \tag{5.39}$$

which is equivalent to solving a linear system of two complex variables. The functions are then inserted into equation (5.37),

$$\mathrm{f}_2\left(\hat{\omega}\right) = \varsigma\,\mathrm{f}_1\left(\hat{\omega}\right) - \hat{L}_L\mathbf{i}_s \tag{5.40}$$

These functions are found in Appendix F. Inserting them in (5.40), and some rearranging gives

$$\varsigma = \frac{\mathbf{n} - \mathbf{m}\hat{\omega}}{\mathbf{h} - \mathbf{p}\hat{\omega}} \tag{5.41}$$

where $\mathbf{n}$, $\mathbf{m}$, $\mathbf{h}$ and $\mathbf{p}$ are explicitly written in Appendix F. As ς is real, equation (5.41) can be solved by setting the imaginary part of the right hand side equal to zero, giving a new equation,

$$\frac{n_x - m_x\hat{\omega}}{h_x - p_x\hat{\omega}} = \frac{n_y - m_y\hat{\omega}}{h_y - p_y\hat{\omega}} \tag{5.42}$$

where index x denotes real parts and index y denotes imaginary parts. This equation has two solutions,

$$\hat{\omega} = \frac{h_y m_x + p_y n_x - h_x m_y - p_x n_y}{2\left(p_y m_x - p_x m_y\right)} + \frac{\sqrt{\left(h_y m_x + p_y n_x - h_x m_y - p_x n_y\right)^2 - 4\left(p_y m_x - p_x m_y\right)\left(h_y n_x - h_x n_y\right)}}{2\left(p_y m_x - p_x m_y\right)} \tag{5.43}$$

and

$$\hat{\omega}_{stat} = \hat{\omega} = \frac{h_y m_x + p_y n_x - h_x m_y - p_x n_y}{2\left(p_y m_x - p_x m_y\right)} - \frac{\sqrt{\left(h_y m_x + p_y n_x - h_x m_y - p_x n_y\right)^2 - 4\left(p_y m_x - p_x m_y\right)\left(h_y n_x - h_x n_y\right)}}{2\left(p_y m_x - p_x m_y\right)} \quad (5.44)$$

The first solution, (5.43), represents an unstable operating point, while the second one, (5.44), represents a stable operating point equal to the steady state value of the speed observer. This is illustrated in Fig. 5.3 which show a graphical solution of equations (5.32)–(5.34). In this example the true speed of the induction machine is 3 rad/s. The operating point is stable if

$$\frac{d\tilde{T}}{d\hat{\omega}} < 0 \quad (5.45)$$

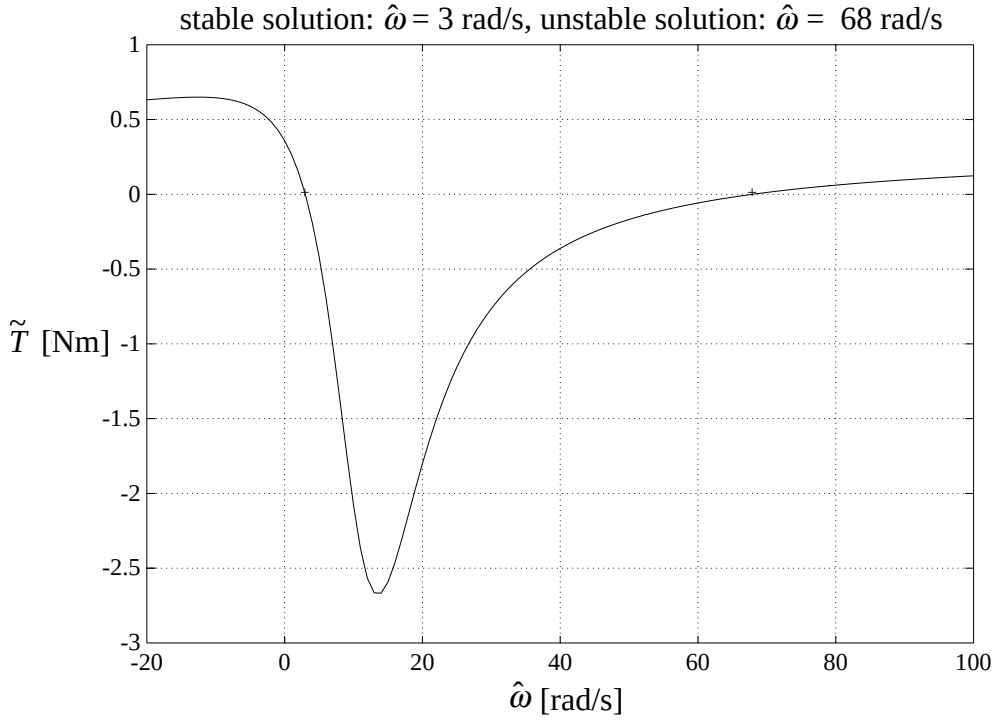

Fig. 5.3 Graphical solution of equations (5.32)–(5.34) showing stable operating point (3 rad/s) and unstable operating point (68 rad/s).

Inserting the expressions for h_y, m_x etc., would lead to an expression about four pages long, and is unfortunately of no help in understanding the speed observer.

If the estimated parameter errors are too large (e.g. $R_{se} > 1.5R_s$), there is a risk that the other solution will be the stable solution.

Just like equation (2.6) can be rearranged into equation (5.26), equation (4.14) can be rearranged into equation (5.46),

$$\hat{\omega} = \frac{1}{z_p}\left(\frac{\Im\left(\hat{\boldsymbol{\Psi}}_r^* \frac{d\hat{\boldsymbol{\Psi}}_r}{dt} \right)}{\left|\hat{\boldsymbol{\Psi}}_r\right|^2} + R_{re} \frac{\Im\left(\hat{\boldsymbol{\Psi}}_r^* \hat{\mathbf{i}}_r \right)}{\left|\hat{\boldsymbol{\Psi}}_r\right|^2} \right) \tag{5.46}$$

At steady state, the first term of the right hand side is equal to ω_1, defined by (4.30) and the steady state speed estimate is equal to

$$\hat{\omega}_{stat} = \frac{1}{z_p}\left(\omega_1 + R_{re} \frac{\Im\left(\hat{\boldsymbol{\Psi}}_r^* \hat{\mathbf{i}}_r \right)}{\left|\hat{\boldsymbol{\Psi}}_r\right|^2} \right) \tag{5.47}$$

This equation says that there is no error in the speed estimate at steady state if the parameters of the observer are correct.

Fig. 5.4 and Fig. 5.5 show the parameter sensitivity of the speed estimate, when the speed observer is connected to the flux observer described in Chapter 4. Fig. 5.4 shows the relative slip error

$$\frac{\tilde{s}}{s} = \frac{s - \hat{s}}{s} \tag{5.48}$$

in a wide speed range at rated torque, while Fig. 5.5 shows the absolute speed error at low speed operation from zero to nominal torque. The same conditions with different gain vectors k of the flux observer are shown. Note that the gain of the speed observer k_ω does not affect the steady state value of the speed estimate.

It is important to notice that a relative slip error of 10% as shown in Fig. 5.4 b) correspond to 0.5% error if the speed error is related to nominal speed,

$$\frac{\tilde{n}}{n_n} = \frac{n - \hat{n}}{n_n} \tag{5.49}$$

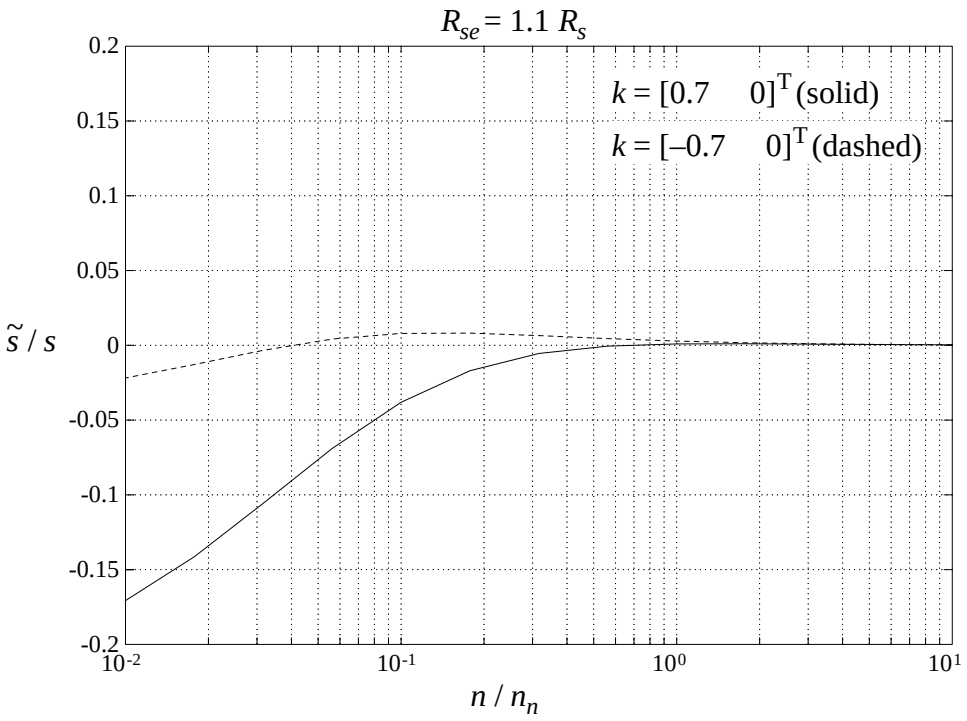
$R_{se} = 1.1\ R_s$
$k = [0.7 \quad 0]^T$ (solid)
$k = [-0.7 \quad 0]^T$ (dashed)
$\tilde{s} / s$
n / n_n
0.2
0.15
0.1
0.05
0
-0.05
-0.1
-0.15
-0.2
10^{-2}
10^{-1}
10^{0}
10^{1}

a)

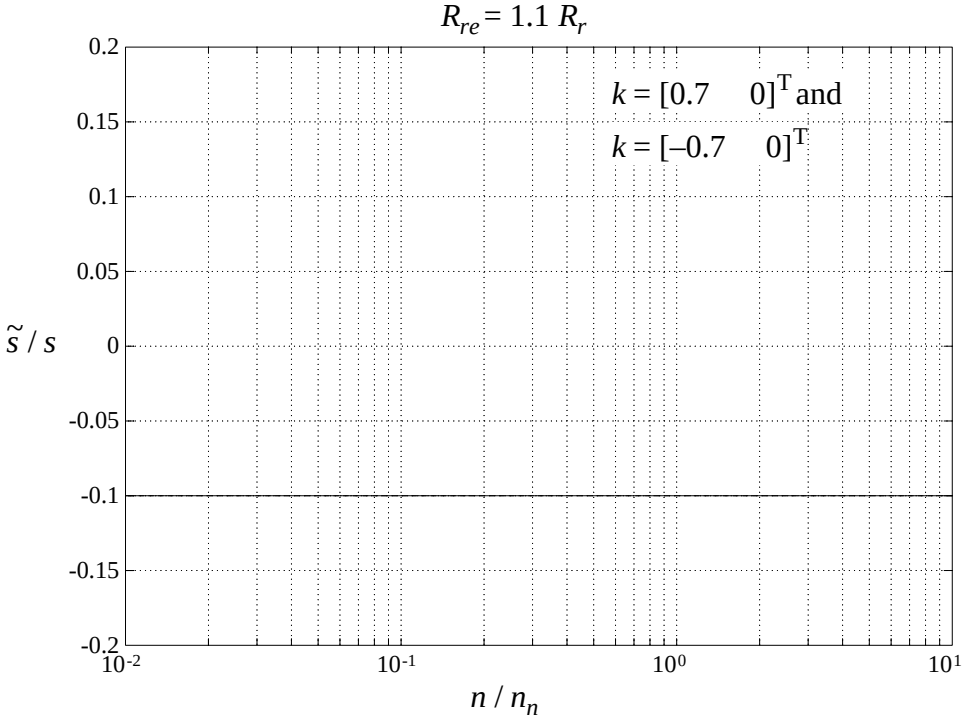
$R_{re} = 1.1\ R_r$
$k = [0.7 \quad 0]^T$ and
$k = [-0.7 \quad 0]^T$
$\tilde{s} / s$
n / n_n
0.2
0.15
0.1
0.05
0
-0.05
-0.1
-0.15
-0.2
10^{-2}
10^{-1}
10^{0}
10^{1}

b)

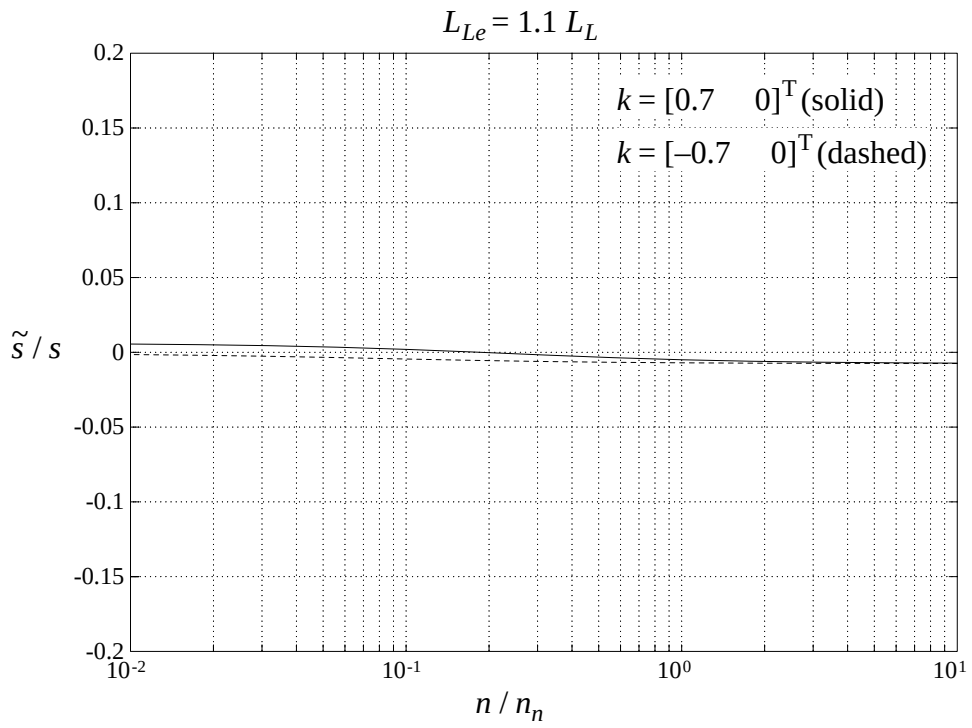

c)

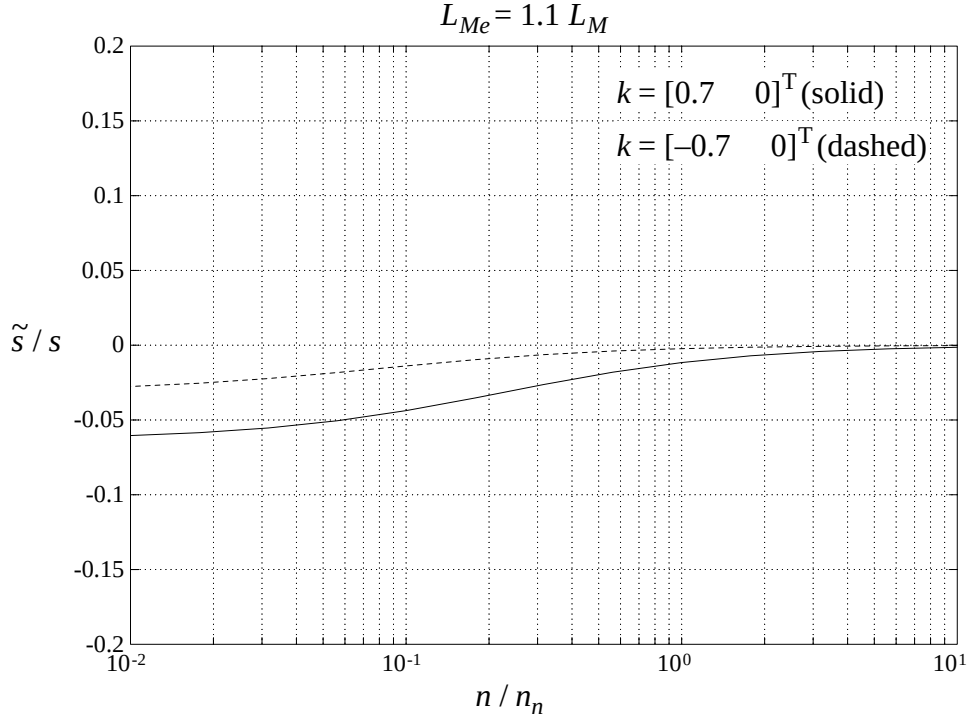

d)

Fig. 5.4 Relative error of estimated slip at rated torque. k = [0.7 0]^T (solid), k = [-0.7 0]^T (dashed) a) R_{se}-error b) R_{re}-error c) L_{Le}-error d) L_{Me}-error

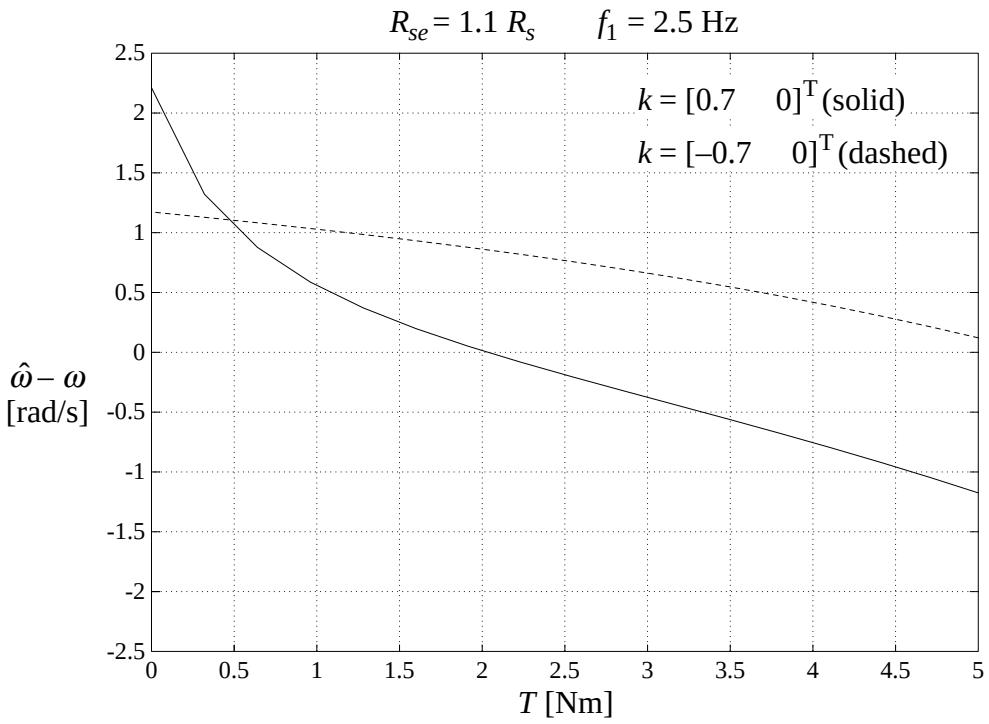
$R_{se} = 1.1\ R_s$ $f_1 = 2.5$ Hz
$k = [0.7 \quad 0]^T$ (solid)
$k = [-0.7 \quad 0]^T$ (dashed)
$\hat{\omega} - \omega$ [rad/s]
T [Nm]

a)

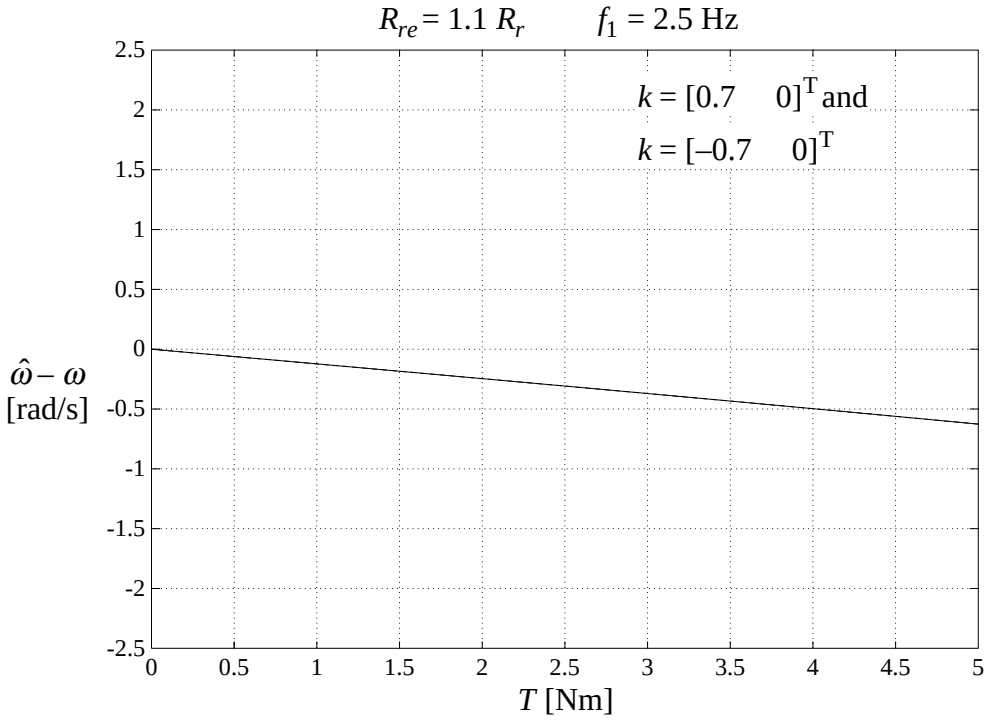
$R_{re} = 1.1\ R_r$ $f_1 = 2.5$ Hz
$k = [0.7 \quad 0]^T$ and
$k = [-0.7 \quad 0]^T$
$\hat{\omega} - \omega$ [rad/s]
T [Nm]

b)

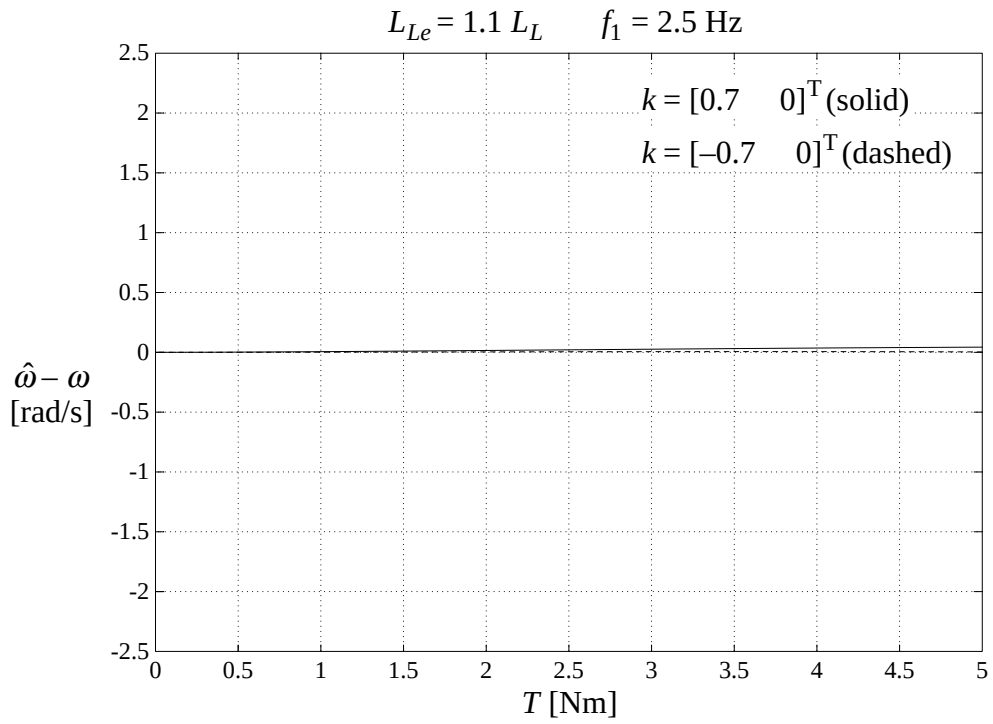

c)

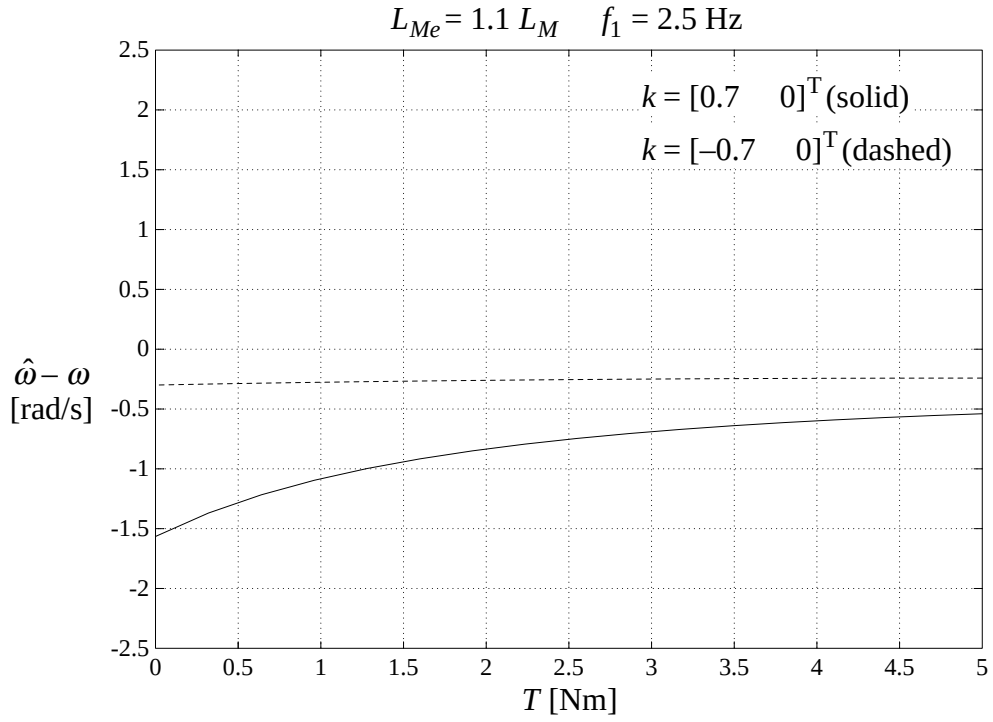

d)

Fig. 5.5 Error of estimated speed at varying slip and torque, k = [0.7 0]^T (solid), k = [-0.7 0]^T (dashed) a) R_{se}-error b) R_{re}-error c) L_{Le}-error d) L_{Me}-error

Note that the error in the speed estimate is smaller at $k = [-0.7 \quad 0]^T$ than at $k = [0.7 \quad 0]^T$. In Chapter 4, the result was the opposite when studying the error in the flux estimates. The explanation to this is that the flux

observer and the speed observer use the same error signal, $\tilde{\mathbf{i}}_s = \mathbf{i}_s - \hat{\mathbf{i}}_s$, to correct the estimated quantities. A large gain vector k in the flux observer will reduce the error in $\tilde{\mathbf{i}}_s$, resulting in less information for the speed observer. Note also that with a gain $k_s < -1$, the flux observer will be unstable as was indicated in Fig. 3.13.

Speed Observer Poles

The flux observer in Chapter 4 is a non-linear system, but can be considered linear if the speed is constant; consequently the poles can be calculated. The linearization of the speed observer, necessary if the poles shall be calculated, is more complicated. If the poles should say anything about local stability, the system must be linearized around an operating point where all derivatives are zero. This is not the case with the observer consisting of the flux observer in Fig. 4.1 and the speed observer in Fig. 5.2; the flux estimates will be rotating vectors. To get all derivatives equal to zero, the observer in a rotating reference frame described by equation (4.21), combined with the speed observer, can be used.

At the operating point, the flux, speed, current and voltage are $\hat{\Psi}_0^r$, $\hat{\omega}_0$, $\mathbf{i}_{s0}^r$ and $\mathbf{u}_{s0}^r$, where

$$\hat{\Psi}^r = \hat{\Psi}_0^r + \delta\hat{\Psi}^r = \begin{bmatrix} \hat{\Psi}_{sx0}^r + j\,\hat{\Psi}_{sy0}^r \\ \\ \hat{\Psi}_{rx0}^r + j\,\hat{\Psi}_{ry0}^r \end{bmatrix} + \begin{bmatrix} \delta\hat{\Psi}_{sx}^r + j\,\delta\hat{\Psi}_{sy}^r \\ \\ \delta\hat{\Psi}_{rx}^r + j\,\delta\hat{\Psi}_{ry}^r \end{bmatrix} \tag{5.50}$$

$$\hat{\omega} = \hat{\omega}_0 + \delta\hat{\omega} \tag{5.51}$$

$$\mathbf{i}_s^r = \mathbf{i}_{s0}^r + \delta\mathbf{i}_s^r \tag{5.52}$$

$$\mathbf{u}_s^r = \mathbf{u}_{s0}^r + \delta\mathbf{u}_s^r \tag{5.53}$$

As the states of the observer are both complex (stator and rotor flux estimates) and real (speed estimate), the linearization is simplified if the real and imaginary parts of the two complex equations are separated, resulting in four equations with real coefficients. This is further discussed in Appendix E.

Inserting equations (5.50)-(5.53) into equations (4.21) and (5.31), and separating real and imaginary parts, gives the following equation,

$$\frac{d}{dt}\begin{bmatrix}\hat{\Psi}_{sx}^r\\ \hat{\Psi}_{rx}^r\\ \hat{\Psi}_{sy}^r\\ \hat{\Psi}_{ry}^r\\ \hat{\omega}\end{bmatrix}=\frac{d}{dt}\begin{bmatrix}\delta\hat{\Psi}_{sx}^r\\ \delta\hat{\Psi}_{rx}^r\\ \delta\hat{\Psi}_{sy}^r\\ \delta\hat{\Psi}_{ry}^r\\ \delta\hat{\omega}\end{bmatrix}$$

$$=M\begin{bmatrix}\delta\hat{\Psi}_{sx}^r\\ \delta\hat{\Psi}_{rx}^r\\ \delta\hat{\Psi}_{sy}^r\\ \delta\hat{\Psi}_{ry}^r\\ \delta\hat{\omega}\end{bmatrix}+\begin{bmatrix}\delta u_{sx}^r\\ 0\\ \delta u_{sy}^r\\ 0\\ 0\end{bmatrix}+N\begin{bmatrix}\delta i_{sx}^r\\ \delta i_{sy}^r\end{bmatrix}$$

$$+\begin{bmatrix}0\\ -z_p\delta\hat{\omega}\,\delta\hat{\Psi}_{ry}^r\\ 0\\ z_p\delta\hat{\omega}\,\delta\hat{\Psi}_{rx}^r\\ \dfrac{k_\omega}{J_e}\left(\dfrac{\delta\hat{\Psi}_{rx}^r\delta\hat{\Psi}_{sy}^r}{L_{Le}}-\dfrac{\delta\hat{\Psi}_{sx}^r\delta\hat{\Psi}_{ry}^r}{L_{Le}}+\delta\hat{\Psi}_{sy}^r\delta i_{sx}^r-\delta\hat{\Psi}_{sx}^r\delta i_{sy}^r\right)\end{bmatrix} \tag{5.54}$$

where M is a 5×5 matrix and N is a 5×2 matrix,

$$M=\left[\begin{array}{cc|c}\Re\left(A_e^r-\hat{R}k\hat{C}\right) & -\Im\left(A_e^r-R_ekC_e\right) & \begin{matrix}0\\0\end{matrix}\\ \hline \Im\left(A_e^r-R_ekC_e\right) & \Re\left(A_e^r-R_ekC_e\right) & \begin{matrix}0\\0\end{matrix}\\ \hline \begin{matrix}0 & 0\end{matrix} & \begin{matrix}0 & 0\end{matrix} & 0\end{array}\right]$$

$$+\frac{k_\omega}{J_e}\begin{bmatrix}0 & 0 & 0 & 0 & 0\\ 0 & 0 & 0 & 0 & -\hat{\Psi}_{ry0}^r\dfrac{J_ez_p}{k_\omega}\\ 0 & 0 & 0 & 0 & 0\\ 0 & 0 & 0 & 0 & \hat{\Psi}_{rx0}^r\dfrac{J_ez_p}{k_\omega}\\ \dfrac{-\hat{\Psi}_{ry0}^r}{L_{Le}}-i_{sy0}^r & \dfrac{\hat{\Psi}_{sy0}^r}{L_{Le}} & \dfrac{\hat{\Psi}_{rx0}^r}{L_{Le}}+i_{sx0}^r & \dfrac{-\hat{\Psi}_{sx0}^r}{L_{Le}} & 0\end{bmatrix} \tag{5.55}$$

$$N = \begin{bmatrix} \Re\left(R_e k\right) & -\Im\left(R_e k\right) \\ \Im\left(R_e k\right) & \Re\left(R_e k\right) \\ \frac{k_\omega}{J_e}\,\hat{\Psi}^r_{sy0} & -\frac{k_\omega}{J_e}\,\hat{\Psi}^r_{sx0} \end{bmatrix} \tag{5.56}$$

and A^r_e is the observer matrix A_e, but adjusted for the rotating reference frame,

$$\begin{aligned} A^r_e &= A_e\left(\hat{\omega}_0\right) - j\,\omega_1 I \\ &= \begin{bmatrix} -R_{se}\left(\frac{1}{L_{Me}} + \frac{1}{L_{Le}}\right) - j\,\omega_1 & \frac{R_{se}}{L_{Le}} \\ \frac{R_{re}}{L_{Le}} & \frac{-R_{re}}{L_{Le}} + jz_p\hat{\omega}_0 - j\,\omega_1 \end{bmatrix} \end{aligned} \tag{5.57}$$

C_e is the same as for the stationary reference frame, defined by equation (4.7).

This observer, still non-linear, is equivalent to the observer of equations (4.21) and (5.31), but if the last term of (5.54), is neglected, we have the following linear approximation,

$$\frac{d}{dt}\begin{bmatrix} \delta\hat{\Psi}^r_{sx} \\ \delta\hat{\Psi}^r_{rx} \\ \delta\hat{\Psi}^r_{sy} \\ \delta\hat{\Psi}^r_{ry} \\ \delta\hat{\omega} \end{bmatrix} \approx M\begin{bmatrix} \delta\hat{\Psi}^r_{sx} \\ \delta\hat{\Psi}^r_{rx} \\ \delta\hat{\Psi}^r_{sy} \\ \delta\hat{\Psi}^r_{ry} \\ \delta\hat{\omega} \end{bmatrix} + \begin{bmatrix} \delta u^r_{sx} \\ 0 \\ \delta u^r_{sy} \\ 0 \\ 0 \end{bmatrix} + N\begin{bmatrix} \delta i^r_{sx} \\ \delta i^r_{sy} \end{bmatrix} \tag{5.58}$$

This linear system can be used for studying local stability.

Poles of Linearized Speed Observer

The poles of the linearized speed observer are the eigenvalues of matrix *M*. If $k_\omega = 0$, the poles will be the same as for the observer in a rotating reference frame discussed in Chapter 4, plus a pole in the origin. Fig. 5.6 shows how the observer poles move when k_ω is increased. As is seen in the figure, a pair of the poles will move to the right half plane if the speed observer gain is increased to much, resulting in an unstable observer.

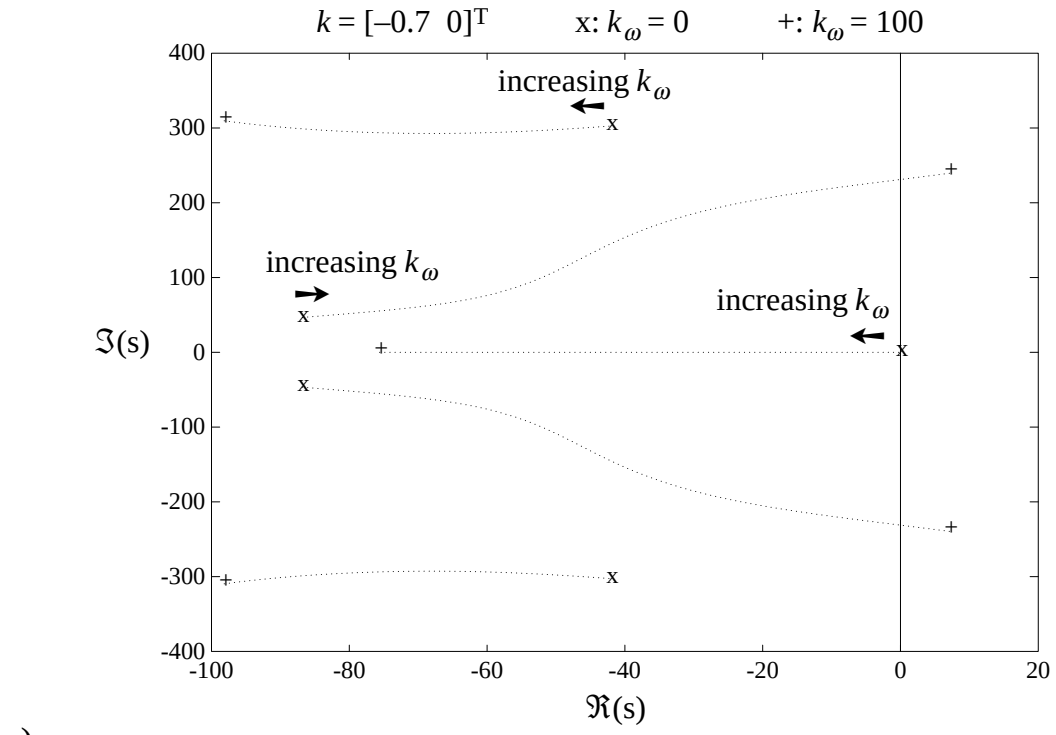

a)

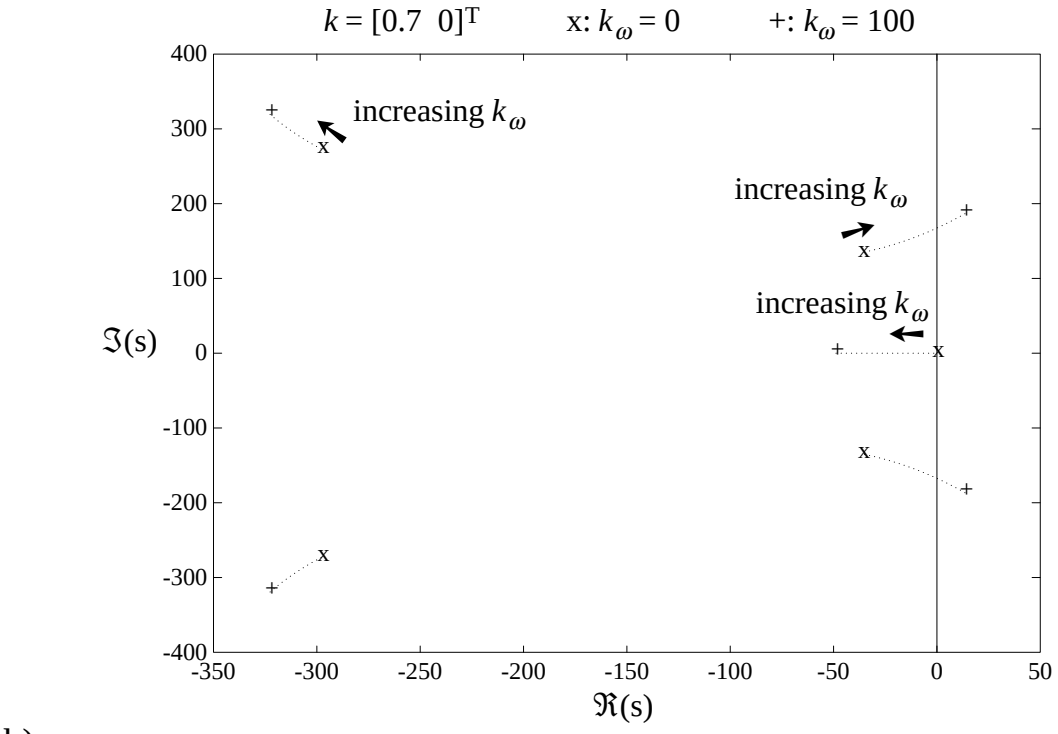

b)

Fig. 5.6 Poles of linearized speed observer as k_ω is varied.

The pole plots also give some information on the settling time of the speed estimate. The speed observer pole, moving from the origin to the left as k_ω is increased, indicates that the settling time of the speed estimate is decreasing as the gain is increasing. This is true to a certain point, but as

the flux and speed observers work hand in hand, all poles must be considered, and while the speed observer pole is moving to the left, a pair of the flux observer poles are moving to the right. If the flux observer becomes too slow, the speed observer will be slower as well.

Sensitivity to Rotor Resistance

A very important property of the speed observer is seen in Fig. 5.4 b); if there is a ten percent error in the estimated rotor resistance, there will be a ten percent error in the estimated slip.

At steady state, it is actually the ratio R_r/s that can be estimated if only voltage and current is measured. This is independent of the structure of the speed observer. As the rotor resistance is varying with temperature, which in turn is varying with load, it is practically impossible to have a correct value of the rotor resistance at all times.

Various parameter adaptation techniques can be used to keep track of the rotor resistance. One way is to measure stator winding temperature, and adjust both rotor and stator resistance according to varying temperature. The rotor temperature differs from the stator temperature, but the performance will still be improved. Other techniques such as superimposing ac components on the current exist (Kubota et al, 1994 and Sugimoto et al, 1987).

Important Problems at Low Frequencies

Integrator drift, noise sensitivity in differentiation, error in rotor resistance, these are all problems often pointed out in articles about speed estimation (Bausch et al, 1994, Schauder, 1992 and Pohjalainen et al, 1994). However, the most important problem, lack of information in the measured signals at low frequencies, is often neglected.

The reason that this fact so often is neglected might be that the equations do not reveal it at a first look. Equation (3.1) gives the stator flux, equation (5.29) gives the rotor flux, and finally equation (5.28) gives the speed. This scheme seems to work at all working condition, at least in theory, if the parameters are perfectly matched.

If the stator frequency f_1 is zero, meaning that the stator voltage vector $\mathbf{u}_s$ is constant, the flux vectors will be constant as well. They can be calculated from equation (2.9) with the left side set to zero, as the derivatives of constant vectors are zero. We have

$$0 = A\,\Psi + B\,\mathbf{u}_s \tag{5.59}$$

giving

$$\Psi = -A^{-1}\,B\,\mathbf{u}_s = \frac{\mathbf{u}_s / R_s}{\dfrac{R_r}{L_M L_L} - j z_p\,\omega\left(\dfrac{1}{L_M} + \dfrac{1}{L_L}\right)} \begin{bmatrix} \dfrac{R_r}{L_L} - j z_p\,\omega \\ R_r / L_L \end{bmatrix} \tag{5.60}$$

The current is given by equation (2.10). The flux calculated by equation (5.60) inserted into equation (2.10) gives

$$\mathbf{i}_s = C\Psi = \frac{\mathbf{u}_s}{R_s} \tag{5.61}$$

The last two relations show why speed estimation based solely on measured voltage and current is impossible at zero frequency: if $f_1 = 0$, the *flux is varying* with varying rotor speed, while the *current is independent* of the speed.

The problem can be illustrated in a second way. At steady state, when all vectors are rotating with constant magnitude and angular velocity, it holds that

$$\frac{d\boldsymbol{\Psi}_s}{dt} = j 2\pi f_1\,\boldsymbol{\Psi}_s \tag{5.62}$$

Inserting (5.62) in equation (2.5) gives

$$\boldsymbol{\Psi}_s = \frac{\mathbf{u}_s - R_s \mathbf{i}_s}{j 2\pi f_1} \tag{5.63}$$

When $f_1 = 0$, the denominator of (5.63) becomes zero, and the stator flux vector cannot be calculated. As the current is independent of the speed when $f_1 = 0$, the measured current carries no information on the speed. As soon as the flux vectors start to rotate, the current will be a function not only of stator voltage $\mathbf{u}_s$, but also a function of speed ω. The current will vary little at low frequencies, making it difficult to separate the speed information from noise and parameter errors. As the frequency is increasing, the variation of the current vector is increasing, and the easier it gets to estimate the speed. Fig. 5.7 shows current vector variation at different frequencies and speeds, all at rated flux, $\Psi_s = 0.6$ Vs.

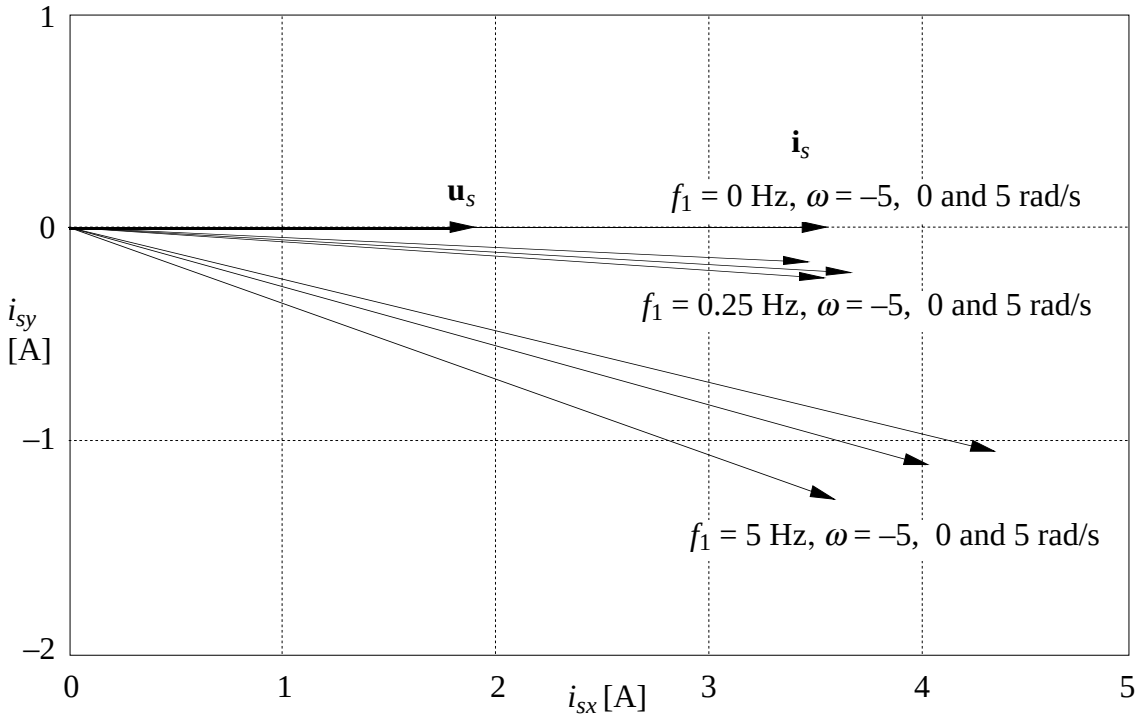

Fig. 5.7 Current vector dependency on rotor speed ω and stator voltage frequency f_1.

Note how the current vectors coincide at all speeds when f_1 = 0 Hz, and that the current and voltage vectors are parallel to each other. At 0.25 Hz, different speeds result in a small variation of the current vector, while the variation is considerable at 5 Hz.

If the induction machine is operating at a point where the frequency is close to zero, there is not much information for the speed observer. Fig. 5.8 shows current vectors at the operating point ω = –1 rad/s and T = 1.6 Nm. The required frequency at rated flux, Ψ = 0.6 Vs, is f_1 = 0.25 Hz. With constant amplitude and frequency of the voltage, the load torque is varied, resulting in a speed variation. At this frequency, the variation of the stator current vector is negligible if ω is varying from –1.5 to –0.5 rad/s. If, however, the flux is reduced to half of its nominal value, a frequency of f_1 = 2.0 Hz is required to produce the same torque at ω = –1 rad/s. At this frequency, the variation of the stator current is increased. This variation gives more information to the speed observer.

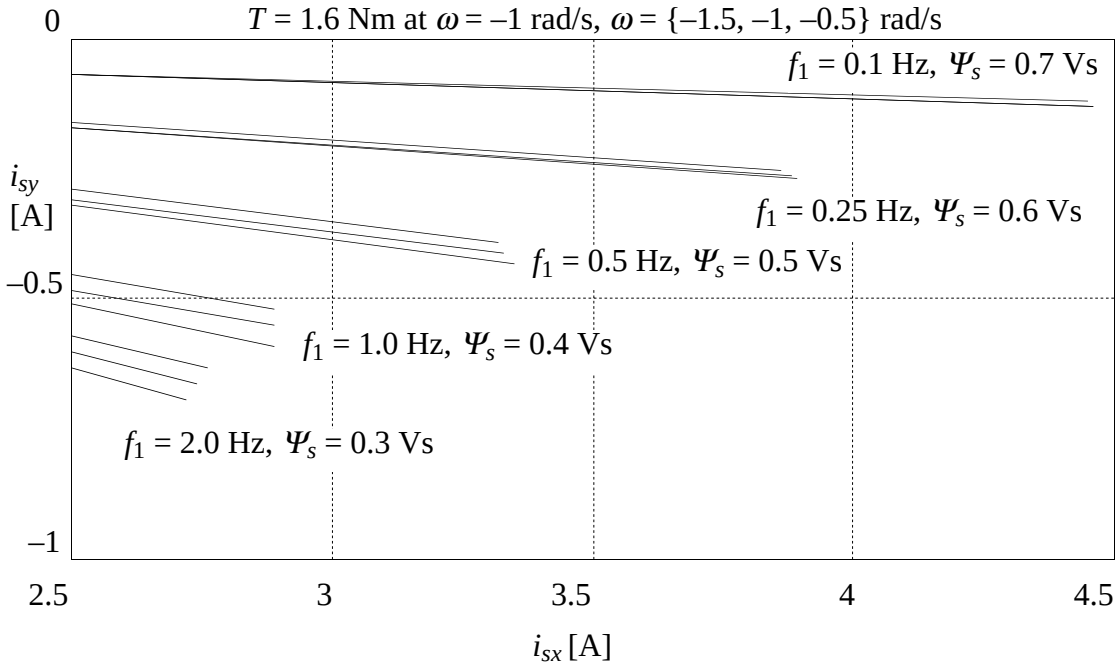

Fig. 5.8 Current vector dependency on rotor speed ω, and flux magnitude Ψ_s. Each group of three vectors shows the current vector at the speeds ω = -1.5, ω = -1 and ω = -0.5 rad/s at the same stator voltage. The middle vector in each group is the current vector at a load torque of 1.6 Nm.

Speed Observer Conclusions

The main problems in estimating speed based on current and voltage measurements is first that current and voltage carries information not on the speed but on the relation R_r/s and second that this information disappears at f_1 = 0 Hz. This means that the lower the frequency, the more difficult it is to estimate speed. To overcome the second problem, the flux can be reduced at operating points with low frequencies, resulting in a higher frequency.

6

Controller Structure

This thesis is focusing on the estimation of flux and rotor speed of the induction machine. The estimated flux and speed serve as inputs to a controller, controlling both speed and flux. The controller is not the main subject here, still a controller is needed for experimental verification of the flux and speed observer properties.

No attempt has been made to look systematically for the ”best” controller. A basic stator flux oriented controller is used. However, rotor flux oriented controllers can also be used, as the observer estimates both stator flux and rotor flux. Further discussions on controllers for induction machines are found in the literature (Leonhard, 1985, Lorenz et al, 1994, Baader et al, 1994, Takahashi et al, 1989 and Habetler et al, 1992).

Controller Overview

The complete control scheme is divided into three PI-controllers, one for the magnitude of the stator flux vector, Ψ_s, one for the torque T, and one for the speed ω. This separation can be done for example if the induction machine vector equations (2.3)-(2.6) are split, not in the real and imaginary axis directions (x and y), but in directions parallel and perpendicular to the stator flux vector. These directions will be referred to as the d- and q-directions. Index d will designate vector components parallel to the stator flux vector, and index q will designate components perpendicular to the stator flux vector. The stator flux component in the d-direction will equal the magnitude of the stator flux vector,

$$\Psi_{sd} = \left|\boldsymbol{\Psi}_s\right| = \Psi_s \tag{6.1}$$

while its component in the q-direction is zero,

$$\Psi_{sq} = 0 \tag{6.2}$$

The first cross product in torque equation (2.8) is actually expressing the product of the magnitude of the stator flux vector, and the component of the stator current vector at right angle to the stator flux, i_{sq},

$$T = \frac{3}{2} z_p \, \Im\left(\boldsymbol{\Psi}_s^* \mathbf{i}_s\right) = \frac{3}{2} z_p \, \Psi_{sd} \, i_{sq} \tag{6.3}$$

Appendix C describes the mechanical equivalent model of the induction machine. Fig. 6.1 shows the springs representing magnetizing inductance and leakage inductance. In Fig. 6.2, the stator resistance drag-pad (a two dimensional viscous damper) is replaced by two dampers, one perpendicular to the stator flux vector shown in a), and one parallel to the stator flux vector shown in b).

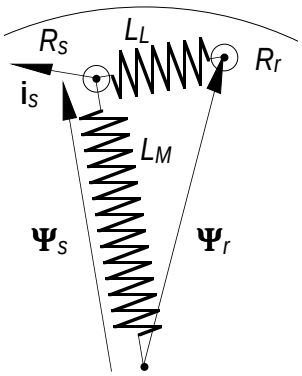

Fig. 6.1 Mechanical model of induction machine. The springs represent magnetizing inductance and leakage inductance.

It is seen in Fig. 6.2 a) that the magnetizing inductance L_M has no influence in the *q*-direction. In Fig. 6.2 b) it is seen that the leakage inductance L_L has little influence in the *d*-direction as the leakage inductance spring is almost at right angle to the *d*-direction.

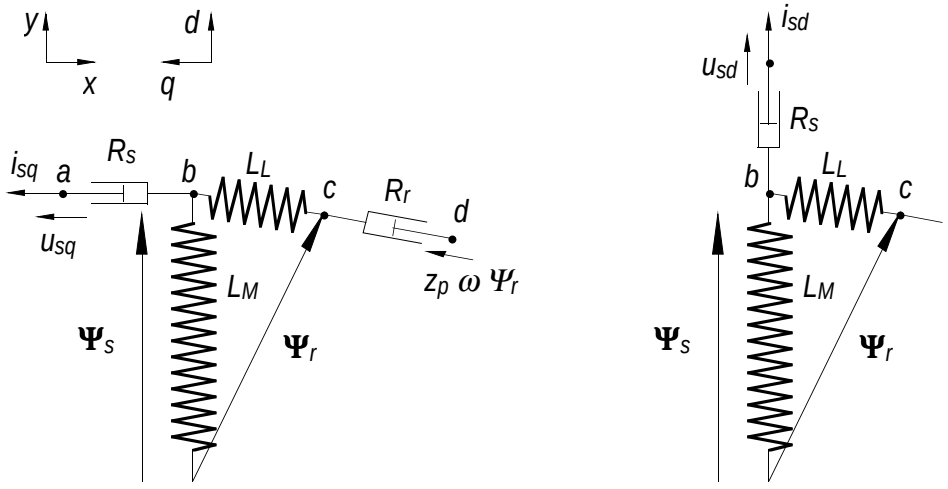

a) b)

Fig. 6.2 d- and q-axis decomposition of mechanical model.

Assuming that the leakage inductance spring and magnetizing inductance spring are at right angles to each other, the *d*-axis and *q*-axis will be decoupled, and we have the following model shown in Fig. 6.3. This assumption is not completely correct. At steady state, the rotor flux vector is perfectly perpendicular to the leakage inductance spring, while the stator flux vector is almost perpendicular.

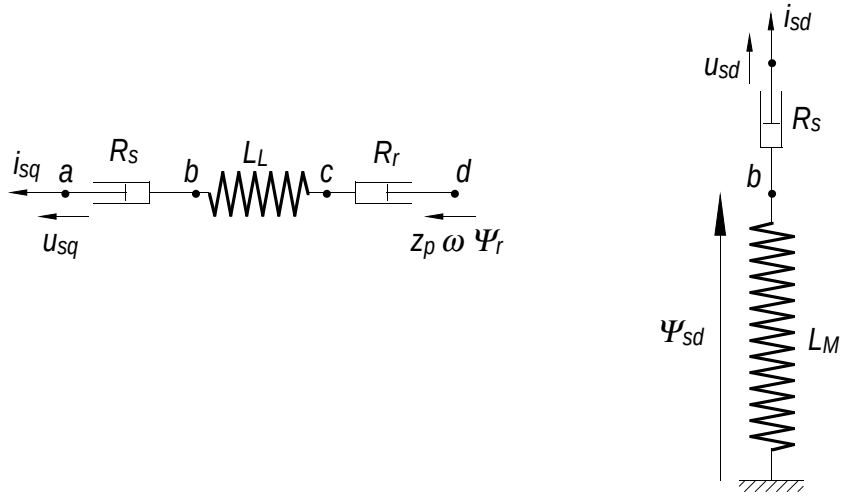

a) b)

Fig. 6.3 approximate dq-decomposition. a) q-axis model b) d-axis model.

The purpose of one controller, *the flux controller*, is to keep the magnitude of the stator flux constant. With constant stator flux magnitude, the torque can be controlled by controlling i_{sq}, which is done by the *torque controller*. Finally, the *speed controller* gives the torque reference, as indicated in Fig. 6.4. There are methods referred to as *direct torque control* (Takahashi et al, 1989, Baader et al, 1992 and Pohjalainen et al, 1994) where the flux and torque controllers are not separated, with reported better dynamic performance than the controller structure described here.

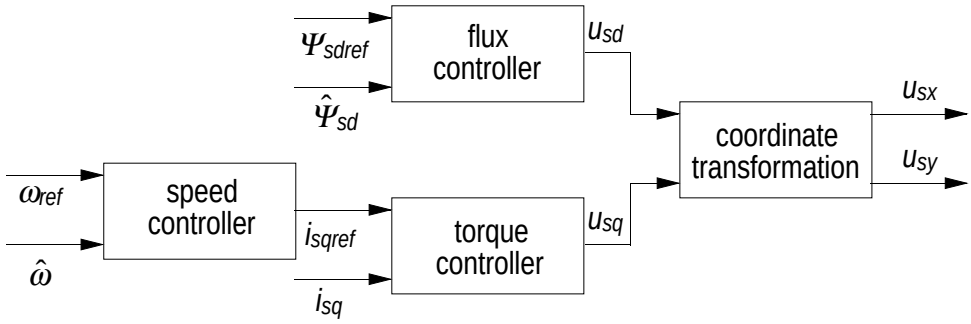

Fig. 6.4 Block diagram of controller structure. Estimated flux and speed are used as controller inputs.

Note that the estimated flux, and not the actual flux is controlled, as the actual flux usually cannot be measured.

Flux Controller

The flux controller is approximately controlling the system in Fig. 6.3 b), described by

$$\frac{d\hat{\Psi}_{sd}}{dt} = u_{sd} - \frac{R_s}{L_M}\hat{\Psi}_{sd} \tag{6.4}$$

or with the Laplace transform

$$\mathbf{s}\hat{\mathbf{\Psi}}_{sd} = \mathbf{u}_{sd} - \frac{R_s}{L_M}\hat{\mathbf{\Psi}}_{sd} \tag{6.5}$$

where $\hat{\mathbf{\Psi}}_{sd}$ is the Laplace transform of $\hat{\Psi}_{sd}$, and $\mathbf{u}_{sd}$ is the Laplace transform of u_{sd}. In the following sections of this chapter, bold typeface will distinguish Laplace transforms from the corresponding time function.

A PI-controller is described by

$$y = k_p\left(e + \frac{1}{T_i}\int e\,dt\right) \tag{6.6}$$

where k_p is the proportional gain, T_i is the integration time, e is the error of the controlled quantity, and y is the controller output. Let u_{sd} be the output of the controller, and let $\Psi_{sdref} - \hat{\Psi}_{sd}$ be the error. With these substitutions together with the Laplace transform, equation (6.6) can be written

$$\mathbf{u}_{sd} = k_p\left(1 + \frac{1}{\mathbf{s}T_i}\right)\left(\mathbf{\Psi}_{sdref} - \hat{\mathbf{\Psi}}_{sd}\right) \tag{6.7}$$

Combining (6.5) and (6.7) gives the transfer function **H**(**s**) of the closed loop system,

$$\hat{\mathbf{\Psi}}_{sd} = \mathbf{H}(\mathbf{s})\mathbf{\Psi}_{sdref} = k_p\frac{\mathbf{s} + \frac{1}{T_i}}{\mathbf{s}^2 + \mathbf{s}\left(\frac{R_s}{L_M} + k_p\right) + \frac{k_p}{T_i}}\mathbf{\Psi}_{sdref} \tag{6.8}$$

with the characteristic polynomial

$$\mathbf{P}(\mathbf{s}) = \mathbf{s}^2 + \mathbf{s}\left(\frac{R_s}{L_M} + k_p\right) + \frac{k_p}{T_i} \tag{6.9}$$

A general polynomial of the second order can be written

$$\mathbf{s}^2 + 2\zeta\,\Omega\,\mathbf{s} + \Omega^2 \tag{6.10}$$

where Ω is the *natural frequency* and ζ is the *relative damping*. The natural frequency of the flux controller system is

$$\Omega = \sqrt{k_p / T_i} \tag{6.11}$$

and the relative damping is

$$\zeta = \left(\frac{R_s}{L_M} + k_p\right)\sqrt{\frac{T_i}{4k_p}} \tag{6.12}$$

Torque Controller

The torque controller structure is similar to the flux controller structure with one exception; the equation describing Fig. 6.3 a) contains one term dependent on the rotor speed ω and the magnitude of the rotor flux Ψ_r (assumed to be constant to avoid non-linearities),

$$\mathbf{s}L_L\,\mathbf{i}_{sq} = \mathbf{u}_{sq} - (R_s + R_r)\mathbf{i}_{sq} - z_p\,\boldsymbol{\omega}\,\Psi_r \tag{6.13}$$

This term can be dealt with by adding a feed forward term y_{ff} to the PI-controller in equation (6.6),

$$y = k_p\left(e + \frac{1}{T_i}\int e\,dt\right) + y_{ff} \tag{6.14}$$

The output of the torque controller is u_{sq} and the error signal is $i_{sqref} - i_{sq}$. The feed forward term should be equal to the rotor speed dependent term, $z_p\,\omega\,\Psi_r$. The Laplace transform of the torque controller is described by

$$\mathbf{u}_{sq} = k_p\left(1 + \frac{1}{\mathbf{s}T_i}\right)\left(\mathbf{i}_{sqref} - \mathbf{i}_{sq}\right) + z_p\,\boldsymbol{\omega}\,\Psi_r \tag{6.15}$$

If the rotor speed ω and rotor flux magnitude Ψ_r are estimated instead of measured, the feed forward term in (6.15) should be replaced by $z_p\,\hat{\boldsymbol{\omega}}\,\hat{\Psi}_r$. Equation (6.13) and (6.15) give the closed loop transfer function,

$$\mathbf{i}_{sq} = \mathbf{H}(\mathbf{s})\mathbf{i}_{sqref} = \frac{k_p}{L_L} \frac{\mathbf{s} + \frac{1}{T_i}}{\mathbf{s}^2 + \mathbf{s}\frac{R_s + R_r + k_p}{L_L} + \frac{k_p}{T_i L_L}} \mathbf{i}_{sqref} \tag{6.16}$$

The natural frequency is

$$\Omega = \sqrt{\frac{k_p}{T_i L_L}} \tag{6.17}$$

and the relative damping is

$$\zeta = \left(R_s + R_r + k_p\right)\sqrt{\frac{T_i}{4 k_p L_L}} \tag{6.18}$$

Speed Controller

The system regulated by the speed controller is described by equation (2.7), with the Laplace transform

$$\mathbf{s}\, J\boldsymbol{\omega} = \mathbf{T} - \mathbf{T}_{load} \tag{6.19}$$

Again, a PI-controller will be used, where T_{ref} is the output and $\omega_{ref} - \omega$ is the error. The Laplace transform of the controller can be written

$$\mathbf{T}_{ref} = k_p\left(1 + \frac{1}{\mathbf{s}T_i}\right)\left(\boldsymbol{\omega}_{ref} - \boldsymbol{\omega}\right) \tag{6.20}$$

Assuming that the torque controller is significantly faster than the speed controller, T_{ref} and T can be considered equal in the speed controller time scale. With

$$\mathbf{T} = \mathbf{T}_{ref} \tag{6.21}$$

equations (6.19) and (6.20) can be combined into

$$\boldsymbol{\omega} = \frac{k_p}{J} \frac{\mathbf{s} + \frac{1}{T_i}}{\mathbf{s}^2 + \mathbf{s}\frac{k_p}{J} + \frac{k_p}{JT_i}} \boldsymbol{\omega}_{ref} - \frac{1}{J} \frac{\mathbf{s}}{\mathbf{s}^2 + \mathbf{s}\frac{k_p}{J} + \frac{k_p}{JT_i}} \mathbf{T}_{load} \tag{6.22}$$

with the natural frequency

$$\Omega = \sqrt{\frac{k_p}{JT_i}} \tag{6.23}$$

and relative damping

$$\zeta = \sqrt{\frac{k_p T_i}{4J}} \tag{6.24}$$

According to Fig. 6.4, the output of the speed controller should be a reference for the current i_{sq} and not the torque reference T_{ref} as in equation (6.20). Equation (6.3) gives the relation between i_{sq} and the torque T. The desired current reference is given by

$$i_{sqref} = \frac{2}{3z_p \Psi_{sdref}} T_{ref} \tag{6.25}$$

If the speed is estimated instead of measured, $\boldsymbol{\omega}$ should be replaced by $\hat{\boldsymbol{\omega}}$ in equations (6.19), (6.20) and (6.22).

Further connections between the controller, the observer, the motor and power electronics are discussed in Chapter 7.

7

Implementation

The flux observer, speed observer, and controller described in earlier chapters have been tested in a laboratory set-up described in this chapter.

General Configuration of Laboratory Set-up

The set-up is shown in Fig. 7.1 and Fig. 7.3. On top of the instrument rack in Fig. 7.1, an induction machine with an incremental encoder is placed, shown in detail in Fig. 7.2. The incremental encoder is used only for comparison of the estimated and actual speed of the induction machine. The ratings and parameters of the induction machine are found in Appendix D.

a) 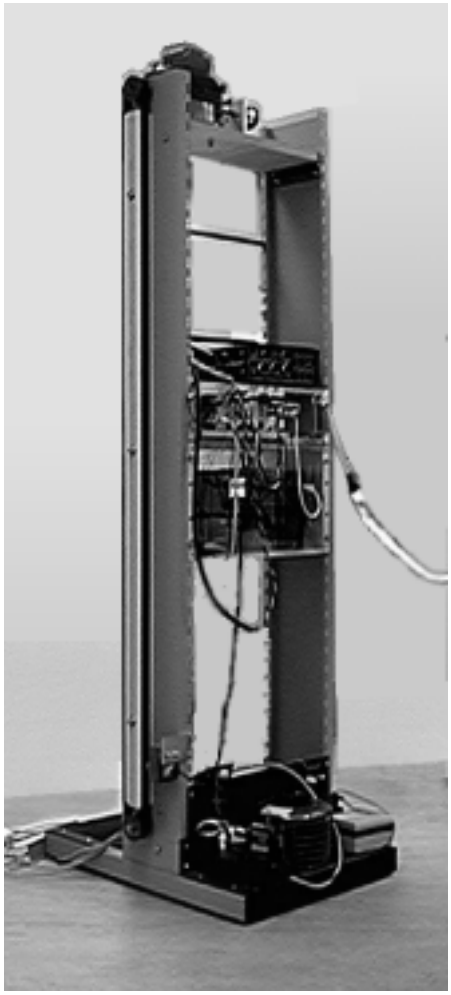 b) 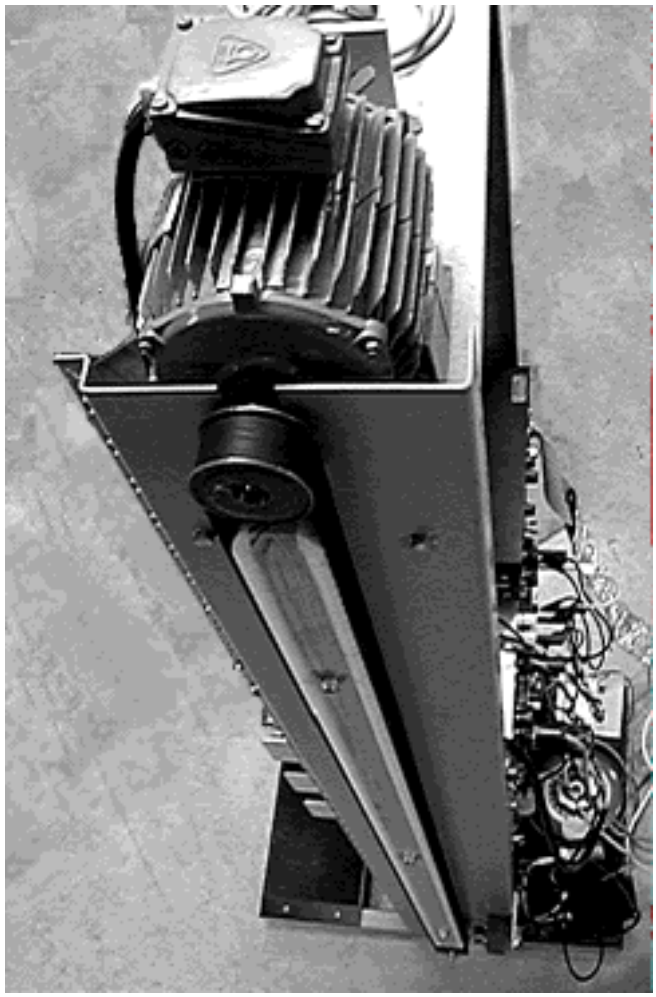

Fig. 7.1 Instrument rack with controlled induction machine at the top and braking DC machine at the bottom. a) side view b) top view

The 0.75 kW machine used in the set-up is in no way representative to all induction machines. The p.u. stator resistance is much higher for such a small machine than for a larger one. However, as a large stator resistance makes flux estimation and speed estimation more difficult at low frequencies, the chosen machine represents a ”near worst case”.

a)

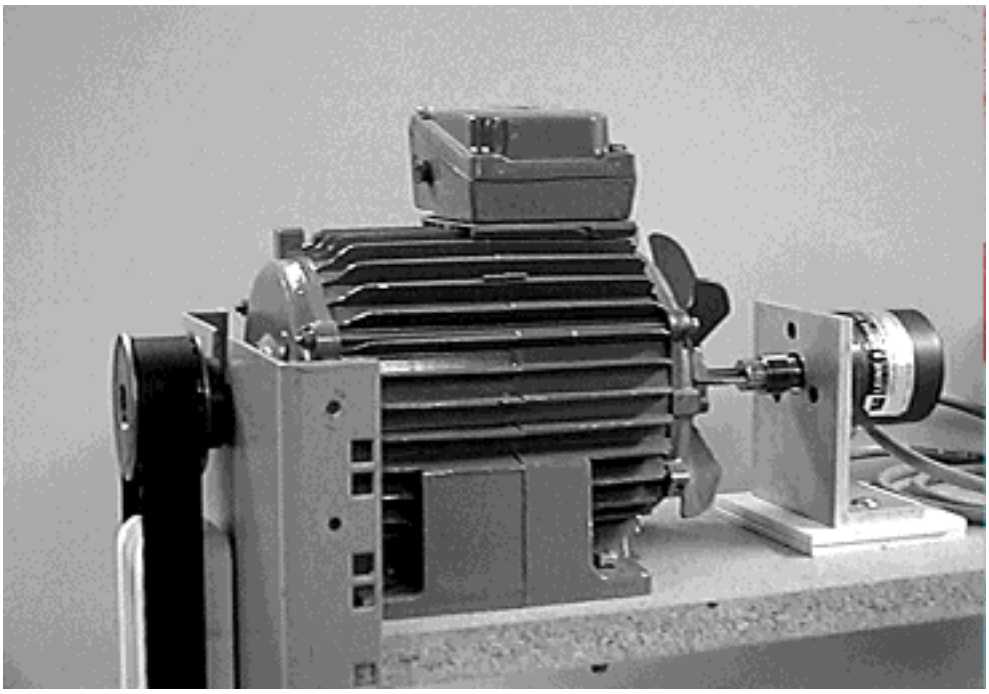

b)

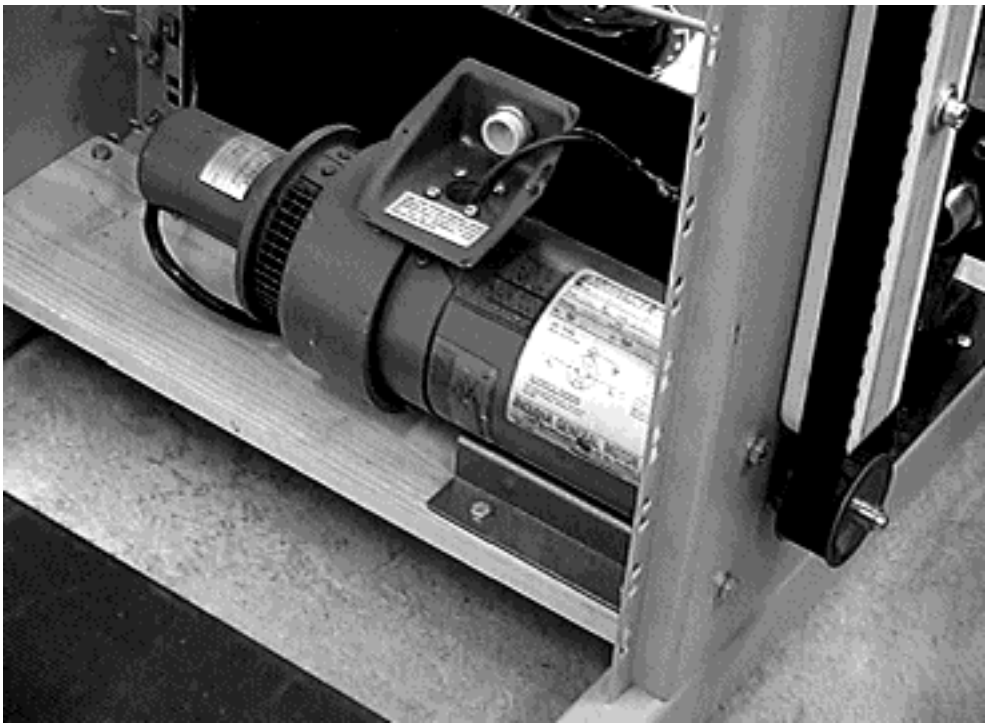

Fig. 7.2 a) induction machine with incremental encoder b) permanent magnet DC machine providing load torque for the induction machine.

A DC machine with torque control providing load torque for the induction machine is placed at the bottom of the rack.

The induction machine and DC machine are connected via a belt drive. An IGBT inverter bridge, current and voltage sensors and computer interface hardware are placed between the two machines. The same set-up has been used for position control experiments (Samuelsson, 1994).

a)

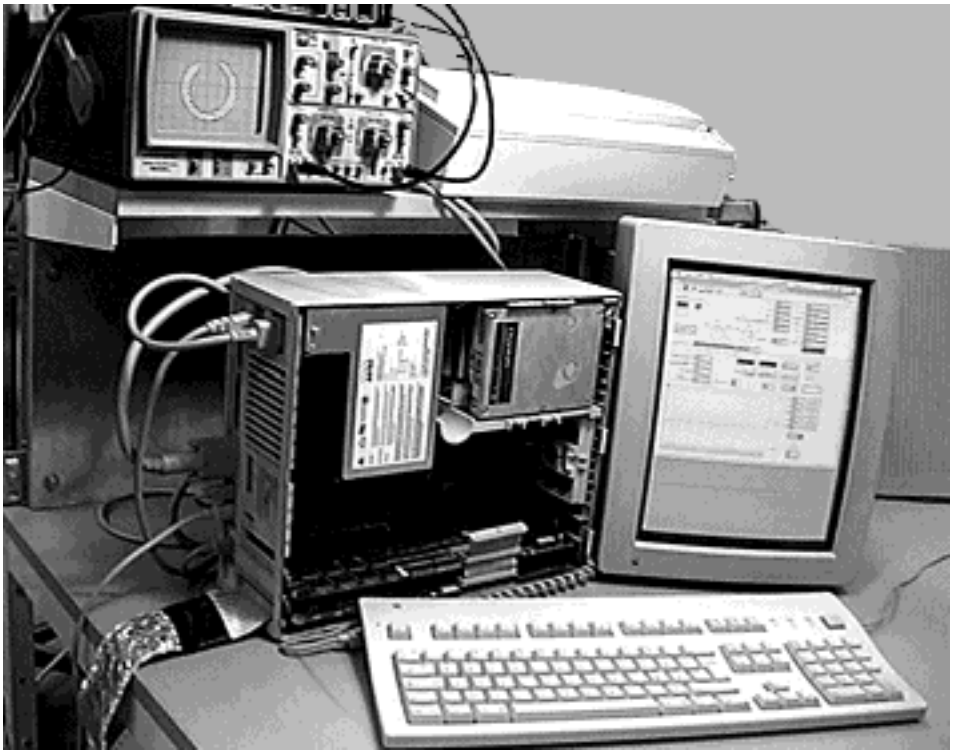

b)

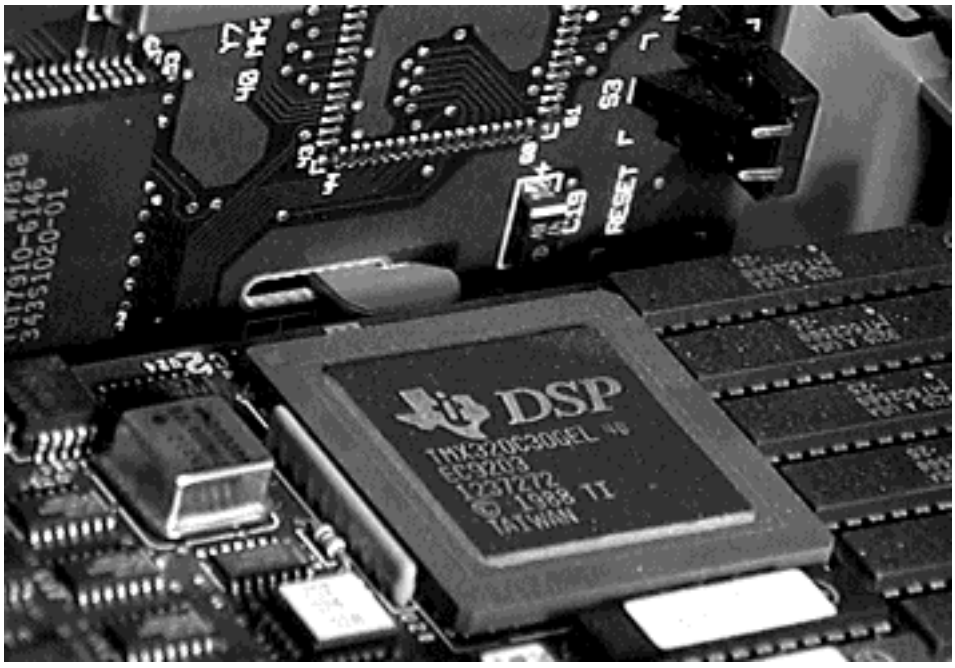

Fig. 7.3 a) Macintosh computer holding the DSP board. b) DSP board.

The rack is connected to computer hardware consisting of a digital signal processor (DSP) board and a multi purpose I/O board, both from National Instruments, placed in a Macintosh IIci computer, shown in Fig. 7.3. The DSP, a TMS320C30 from Texas Instruments is of floating point type, and was chosen because of its ease of use in an experimental environment. In an industrial application, the floating point DSP would be replaced by a less expensive fixed point DSP.

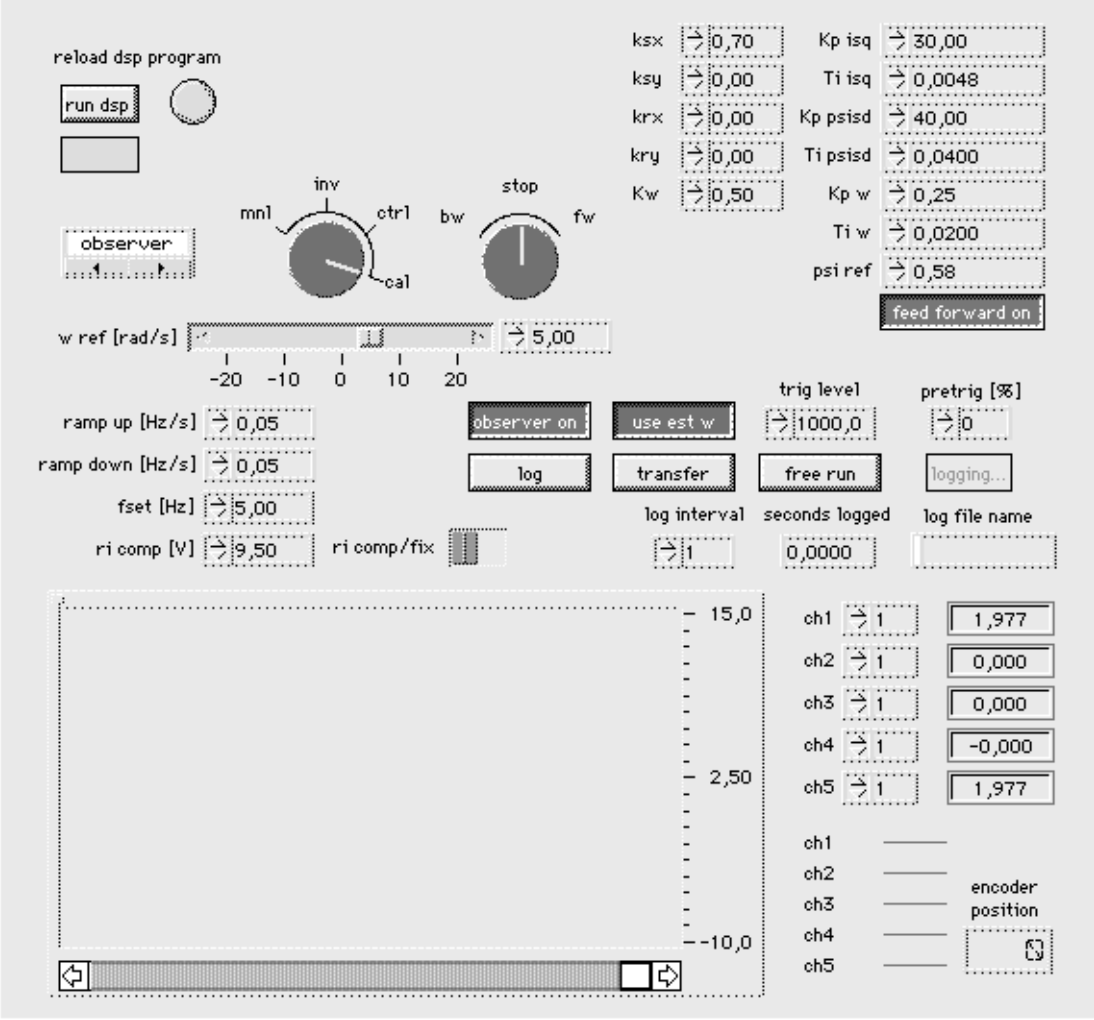

Fig. 7.4 LabVIEW control panel.

The observer and controller calculations are performed by the DSP, while a graphical user interface is running on the Macintosh. The user interface is realized as a *virtual instrument*, developed with the LabVIEW software from National Instruments. The LabVIEW control panel is shown in Fig. 7.4. The user can select inverter (inv) or controller (ctrl) mode. In inverter mode, the induction machine is running in open loop as if it was connected to a standard open loop frequency inverter with features like RI-compensation, ramp times, and set-point frequency (Peterson, 1996). With

the observer running at the same time, the estimated and measured speed can be compared, and the observer can be tuned. In controller mode, the closed loop controller described in Chapter 6 is controlling the induction machine based on the estimated flux and speed. The measured speed instead of estimated speed can also be chosen as controller input.

Excluding the machines, the set-up consists of four logical blocks shown in Fig. 7.5: the control panel, the observer, the controller, and a voltage source inverter.

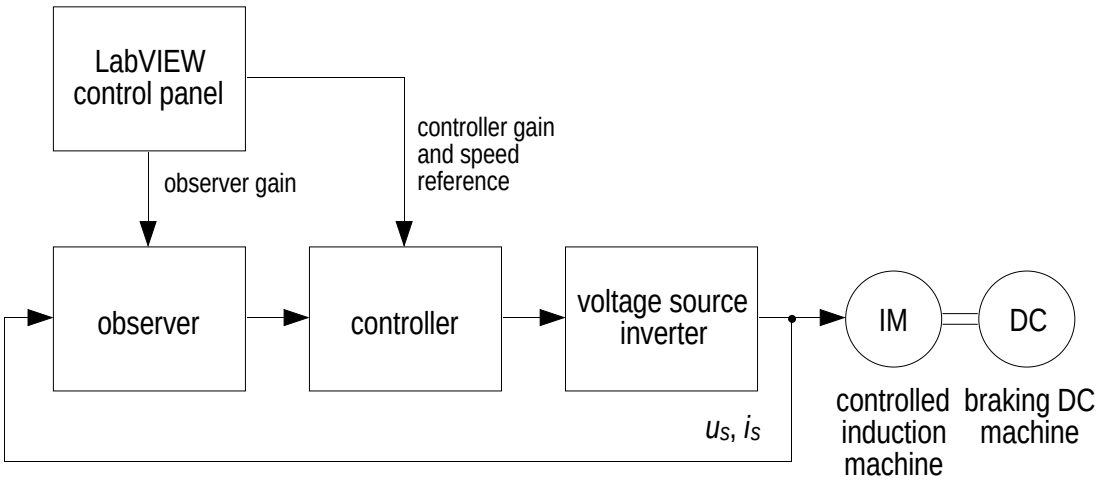

Fig. 7.5 Connections between control panel, observer, controller and inverter.

Voltage Source Inverter Implementation

Diagrams of the voltage source inverter are shown in Fig. 7.6.

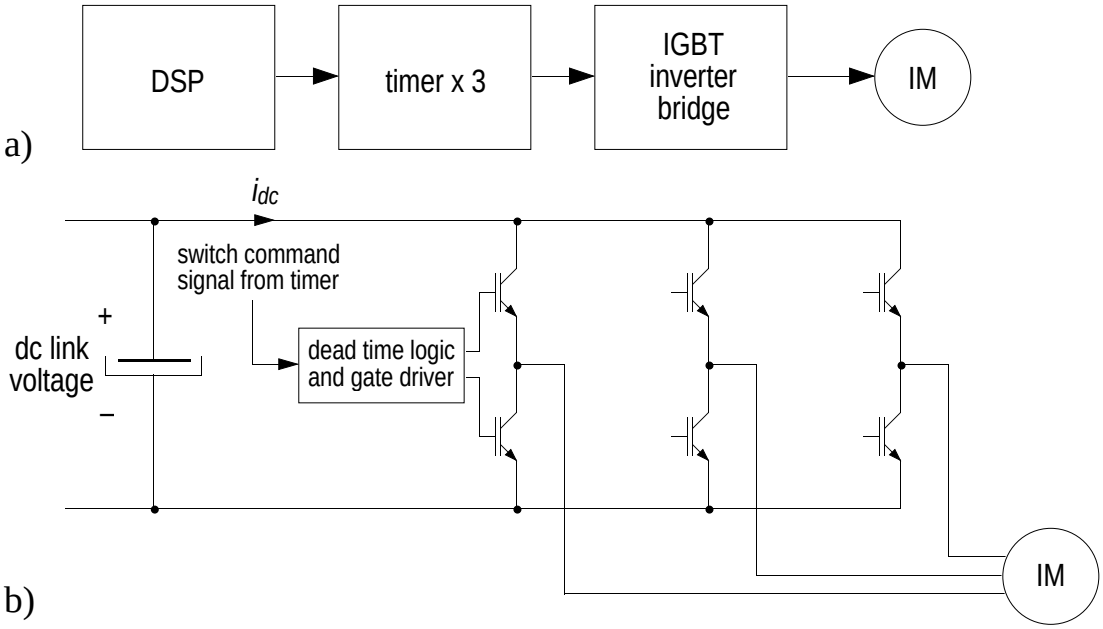

Fig. 7.6 Voltage source inverter. a) block diagram of the inverter b) IGBT inverter bridge. Each leg is controlled by a timer.

The inverter consists of a pulse width modulator and an IGBT inverter bridge supplied by a diode rectifier which is not shown in the figure. The pulse width modulator is realized by three timer circuits together with the DSP. For each sample interval, the DSP loads the timers with appropriate switch patterns for the desired voltage vector, emulating the pulse width modulation method where a triangular wave form is compared with a control voltage (Mohan et al, 1989). Each timer controls one leg of the inverter bridge.

Observer Implementation

The observer can be implemented in several ways. If the DC link voltage of the voltage source inverter is measured, and the states of the switches in the inverter are known, the stator voltage vector $\mathbf{u}_s$ can be calculated. However, this method requires the switches to be ideal if an accurate value should be obtained. Normally there is a delay between the time when one transistor is turned off and the other transistor is turned on in one inverter leg. This delay is usually called the deadtime, and makes the calculated output voltage differ from the true voltage. Resistive voltage drop in the transistors contribute as well to the error in the calculated voltage. To avoid problems due to deadtime and voltage drop, the output voltage of all three phases can be measured. This method gives a new problem; as the output voltage is a switched voltage, it must be filtered before it is A/D-converted and fed to the DSP, introducing time delays in the measured voltage.

These problems are solved if analogue integrators are used instead. Fig. 7.7 shows how the output voltage $\mathbf{u}_s$ of the inverter is fed to an analogue integrator. The output of the integrator is then A/D-converted and fed to the DSP. If Fig. 7.7 is compared with Fig. 4.1, it is seen that only the stator flux integration and one subtraction need to be performed outside the DSP, while all the other observer calculations can be done by the DSP. The input voltage to this combined analogue and digital observer is identical to the voltage seen by the induction machine, and no compensation for deadtime and voltage drop is needed.

The rotor flux integration in equation (4.14) and the speed integration in equation (5.31) are approximated by first order Euler approximations. Instead of Euler approximations of the continuous time system, a discrete-time representation of the system can be calculated (Åström et al, 1984). With periodic sampling time h, the discrete-time representation of the general system in (3.10) is given by

$$x(kh + h) = \Phi x(kh) + \Gamma u(kh) \tag{7.1}$$

where

$$\Phi = e^{Ah} \tag{7.2}$$

and

$$\Gamma = \int_0^h e^{As} ds B \tag{7.3}$$

This is straightforward for a time-invariant system, but as the matrix A for the induction motor is varying with ω, the discrete-time representation must be updated for each sample. Using (7.2) and (7.3) for an on-line update is too time consuming. However, an approximation of (7.2) and (7.3), presented by Böcker et al (1991) makes on-line calculation possible. Still, the Euler approximation was chosen here due to its simplicity. There have been reports on disastrous performance by flux observers using the Euler approximation (Verghese et al, 1988), but it must be noted that all integrators were approximated in those examples. In the set-up described here, the analogue integrators shown in Fig. 7.7 are working continuously, and need not be approximated at all.

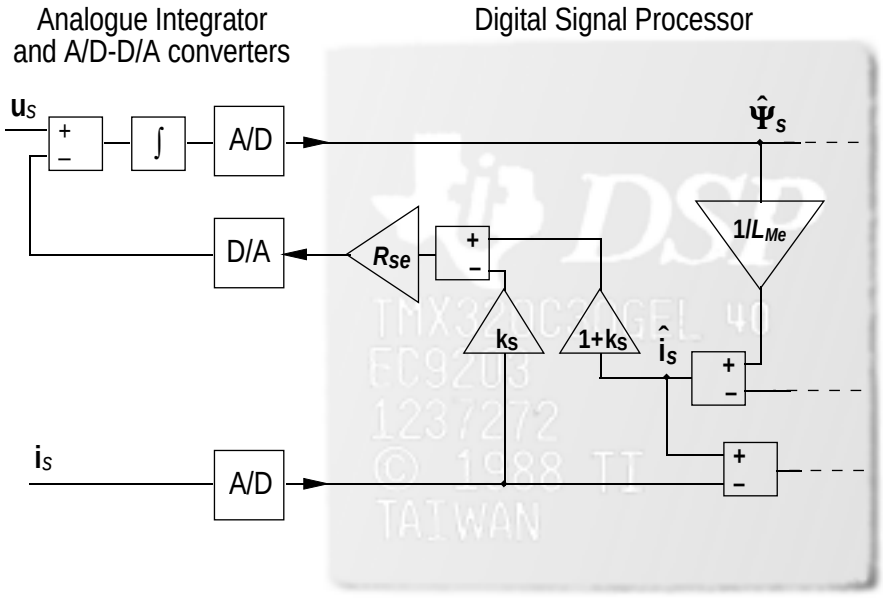

Fig. 7.7 Observer implementation combining analogue and digital integrators.

Controller Implementation

All controller calculations are performed by the DSP, again using first order Euler approximations for the integral parts. The output of the controller is the desired stator voltage vector. Based on this vector, the DSP

calculates an appropriate switch pattern and loads the timers as described above.

DSP programming

The DSP is programmed using the high level C language (Peterson, 1996). To further facilitate high level programming, a real time kernel (Carlsson, 1993) has been developed. Both the controller and the observer run with a sample period of 500 μs. The choice of sample period in this configuration is limited by the relatively slow A/D-converters being used. The calculations can be done in a fraction of this time. As this thesis is focusing on the low frequency region, where flux vectors and other quantities are slowly varying, the sample period of 500 μs is acceptable, even though a shorter sampling period would be preferred.

8

Measurements

To evaluate the performance of the system, a series of measurements has been accomplished. The measurements can be divided into three groups:

- a step change of the load torque at constant speed reference;
- a step change of the speed reference at constant load torque;
- a slow ramp of the speed reference at constant load torque.

As the most critical problems arise at low speed and low frequency, all measurements are done in a speed range of 0–20% of rated speed.

Step Change of Load Torque

Fig. 8.1 shows two cases of a change in load torque at constant speed reference $\omega_{ref} = 0$. The upper diagram shows a step change in the load torque at an observer gain $k = \begin{bmatrix} -0.7 & 0 \end{bmatrix}^T$ while the gain is $k = \begin{bmatrix} 2 & 0 \end{bmatrix}^T$ in the lower diagram. It can be seen that the steady state error is smaller in the upper diagram. In Fig. 5.4 and Fig. 5.5 it was also seen that $k = \begin{bmatrix} -0.7 & 0 \end{bmatrix}^T$ resulted in a small steady state error. It is seen in the upper diagram that there is a slow beat in the speed signal when the load torque is zero. At zero speed and zero torque, the frequency f_1 of the stator voltage should be zero. At zero frequency, there is not enough information for the observer to keep the speed perfectly at zero, as was described in Chapter 5, in the section *Important Problems at Low Frequencies*.

In Fig. 8.2 and Fig. 8.3, the speed reference is 5 rad/s (3.5% of rated speed) and 10 rad/s (7% of rated speed) respectively. In both cases, the stator frequency will differ from zero, and the beat that occurred at zero frequency is no longer present. Again, the steady state error is smaller at $k = \begin{bmatrix} -0.7 & 0 \end{bmatrix}^T$.

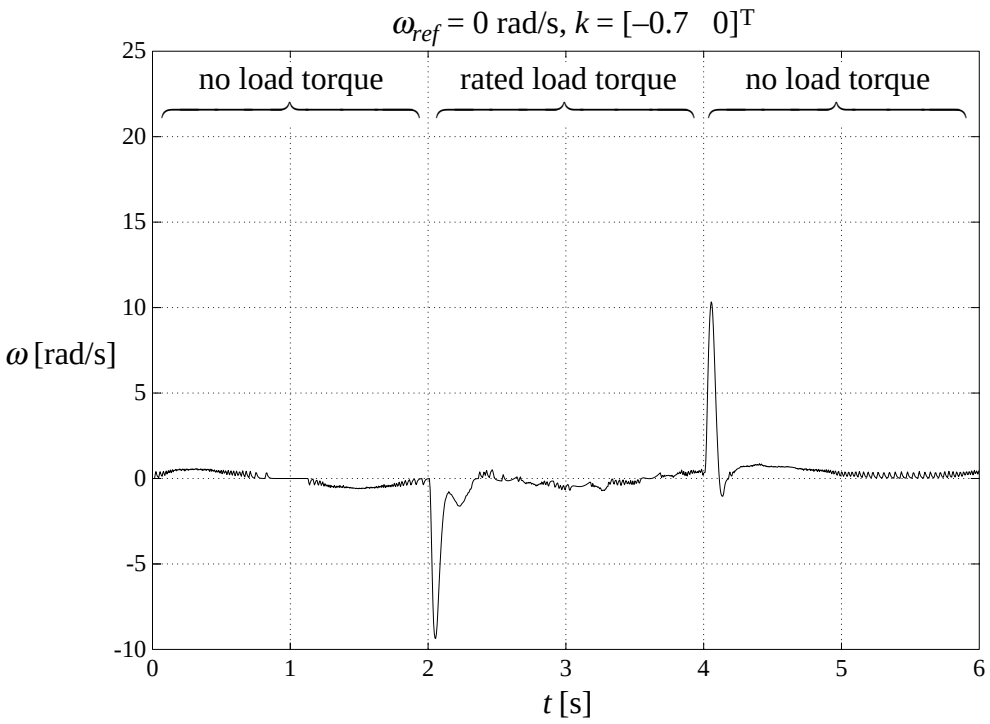

a)

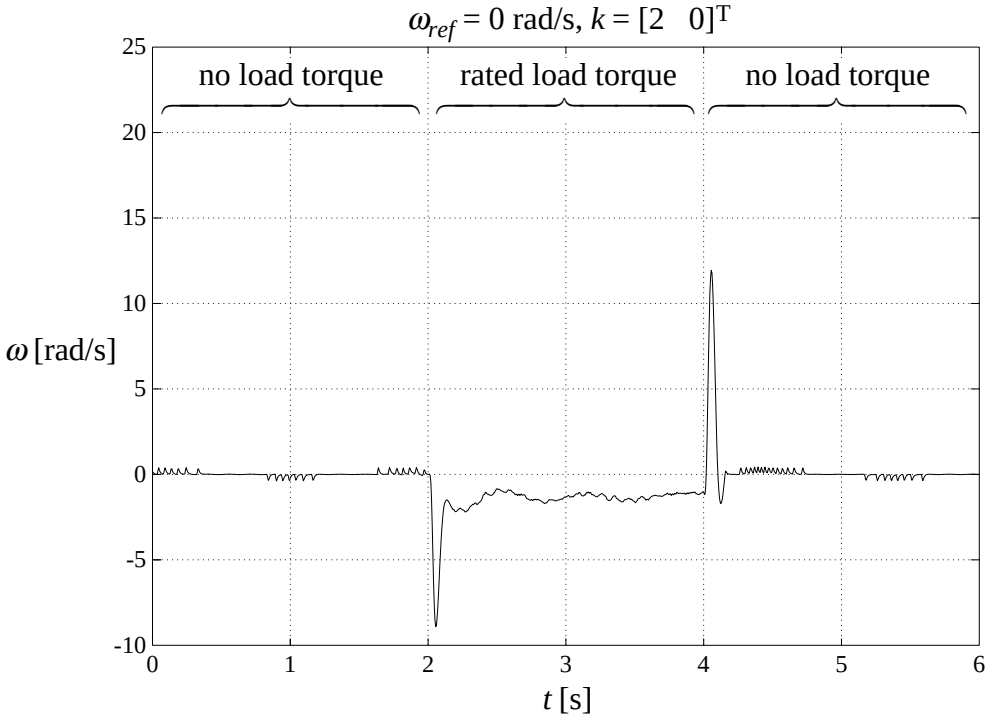

b)

Fig. 8.1 Step change of load torque at constant speed reference $\omega_{ref} = 0$. a) $k = [-0.7 \quad 0]^T$ b) $k = [2 \quad 0]^T$

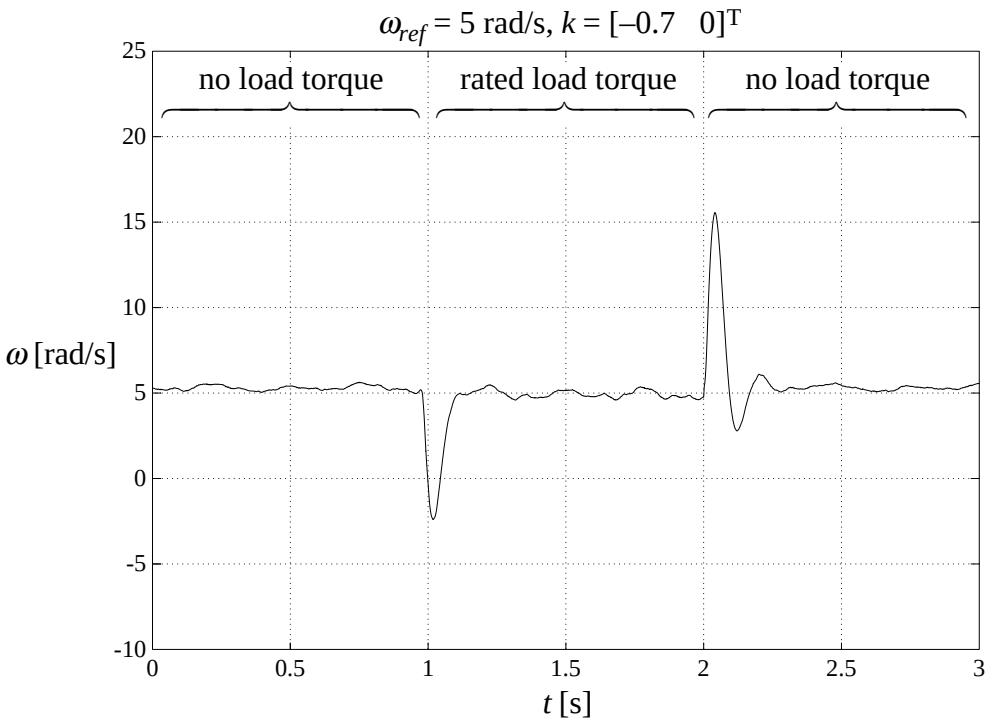

a)

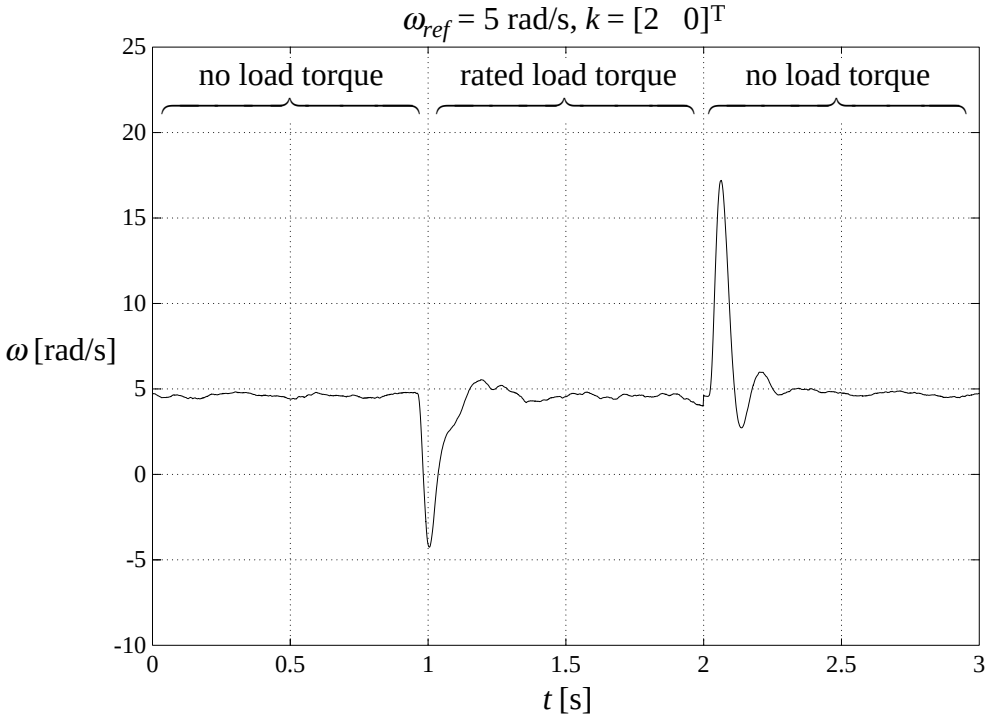

b)

Fig. 8.2 Step change of load torque at constant speed reference ω_{ref} = 5 rad/s (3.5% of rated speed). a) $k = [-0.7 \quad 0]^T$ b) $k = [2 \quad 0]^T$

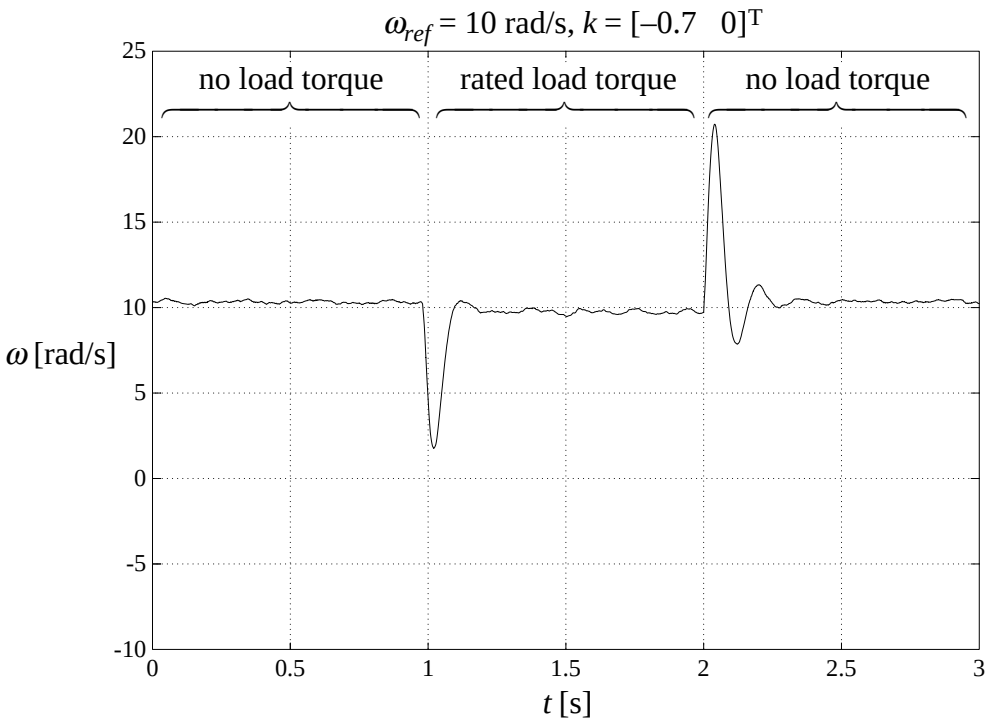

a)

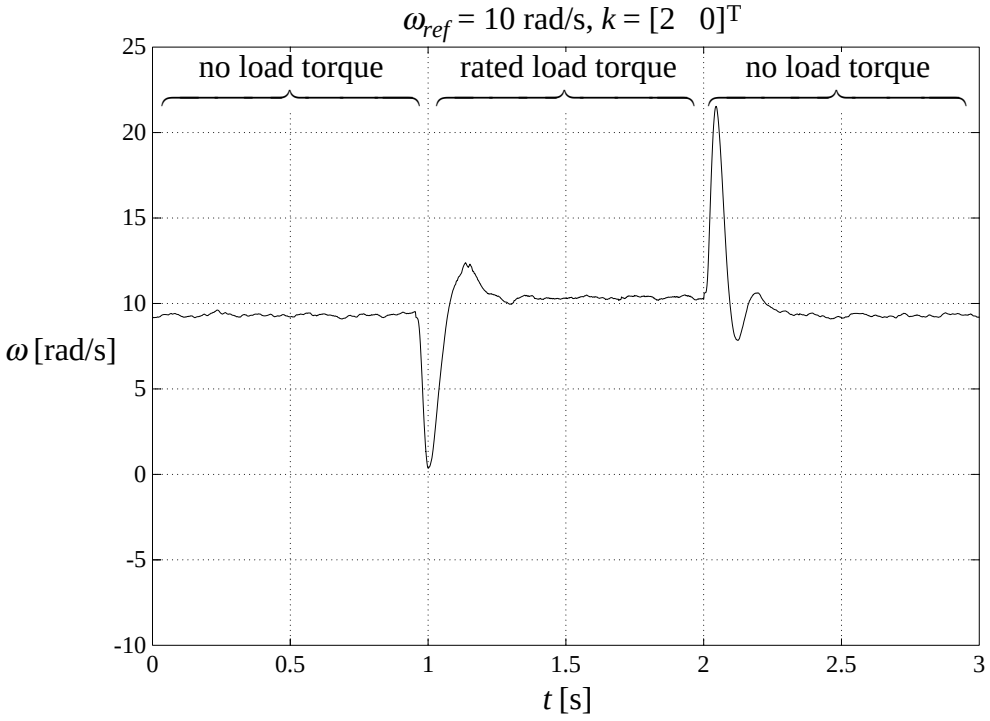

b)

Fig. 8.3 Step change of load torque at constant speed reference ω_{ref} = 10 rad/s (7% of rated speed). a) $k = [-0.7 \quad 0]^T$ b) $k = [2 \quad 0]^T$

Step Change of Speed Reference

In Fig. 8.4 and Fig. 8.5, the load torque is equal to rated torque in the upper diagrams and equal to zero in the lower diagrams.

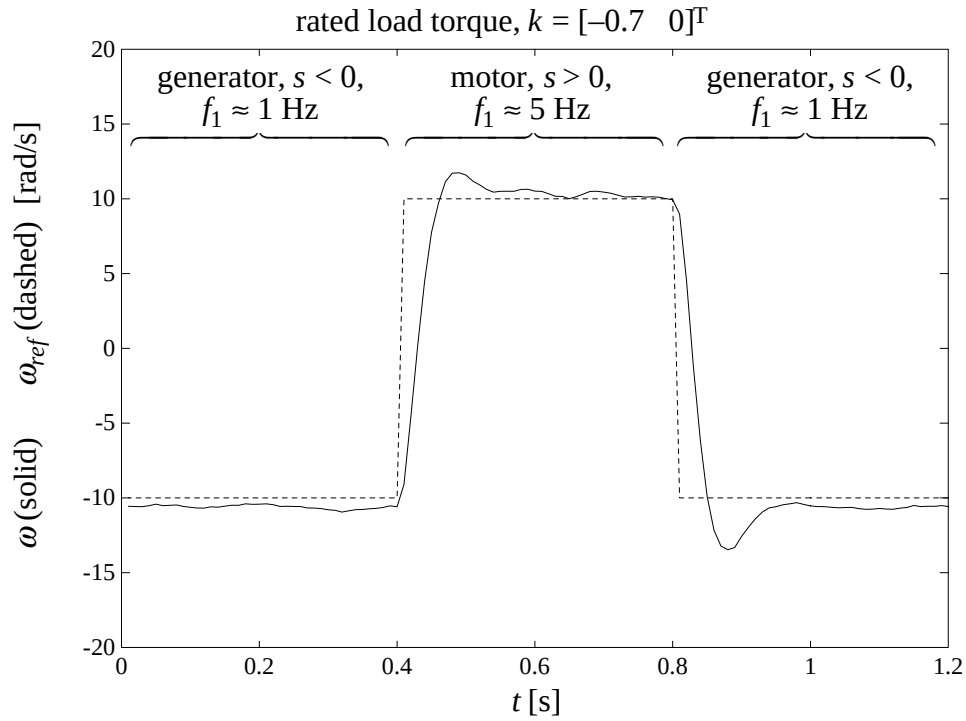

a)

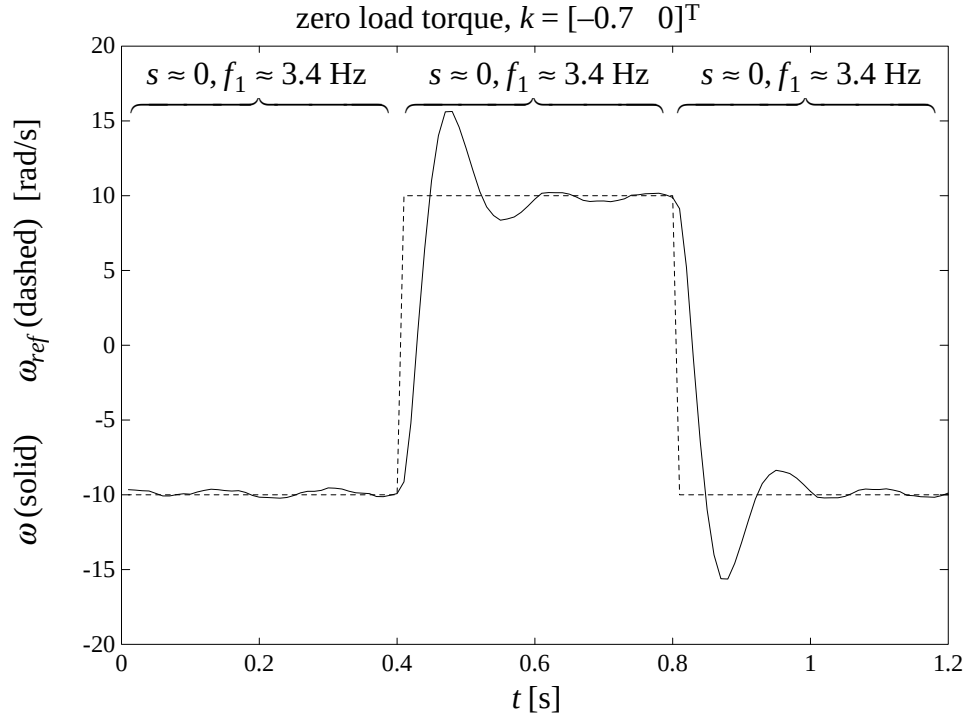

b)

Fig. 8.4 Step change of speed reference from –10 to +10 rad/s (7% of rated speed). a) rated load b) zero load

The speed reference is changed from –10 to +10 rad/s and back to –10 rad/s in Fig. 8.4. At negative speed and positive torque, the slip is negative, and the induction machine is running as a generator. As the diode rectifier supplying the inverter bridge in Fig. 7.6 does not accept a negative current i_{dc}, power cannot be fed from the induction machine to the supply. However, the generated power at $\omega = -10\,\mathrm{rad/s}$ is less than the internal losses in the induction machine. It is seen that the error in the speed is larger at $\omega = -10\,\mathrm{rad/s}$ than at $\omega = +10\,\mathrm{rad/s}$. This is no surprise as the frequency of the stator voltage is lower in generator case (about 1 Hz) than in the motor case (about 5 Hz), and the lower the frequency, the harder it is to estimate the speed. In the lower diagram of Fig. 8.4, the load is zero and the machine is running approximately with zero slip in both directions, giving identical performance at positive and negative speed. The overshoot in the speed is a combination of observer and controller properties. A change of the gain of the controller can reduce the overshoot, but as the speed controller input is the estimated speed and not the actual speed, a perfectly tuned controller would not have perfect performance due to observer dynamics.

Fig. 8.5 shows a step in the speed reference from 0 rad/s to +10 rad/s and back to 0 rad/s, with rated load torque in the upper diagram and zero load torque in the lower. When the speed reference is going from 10 to 0 rad/s at rated load, it takes some time before the speed stabilizes. The reason is that the stator voltage frequency f_1 must fall from about 5 Hz down to 1 Hz. There is an undershoot in the frequency, almost reaching 0 Hz. When the frequency temporarily is close to 0 Hz, there will be an error in the speed. This is further accentuated in the next section, when the speed reference is slowly changed. Comparing the upper diagrams of Fig. 8.4 and Fig. 8.5 shows that $f_1 = 0$ at rated torque at $\omega = 0$ and $\omega = -10\,\mathrm{rad/s}$. However, the stator voltage vector is rotating in different directions in the two cases.

Both diagrams in Fig. 8.6 show a step change of the speed reference at zero load torque, but up to 25 rad/s instead of 10 rad/s as before. The response is comparable to that of Fig. 8.4 and Fig. 8.5.

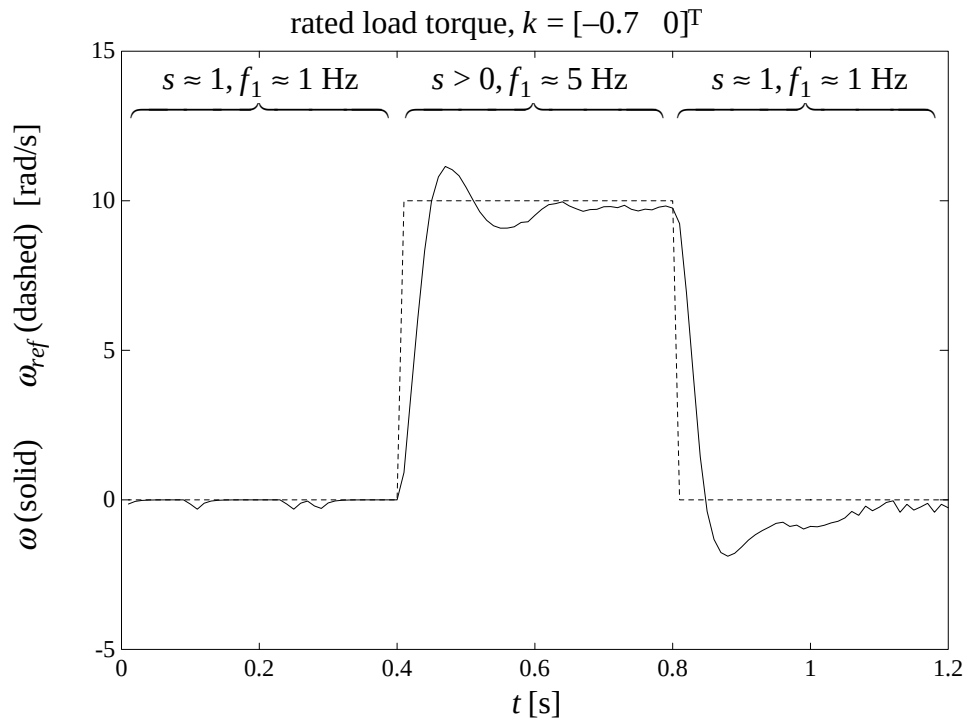

a)

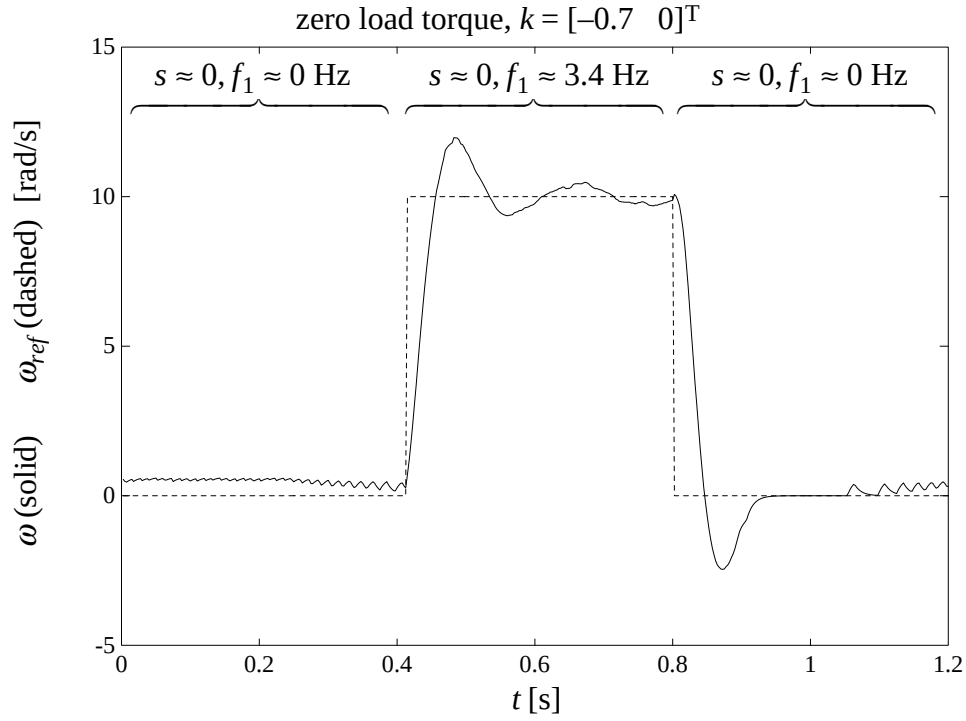

b)

Fig. 8.5 Step change of speed reference from 0 to +10 rad/s (7% of rated speed). a) rated load b) zero load

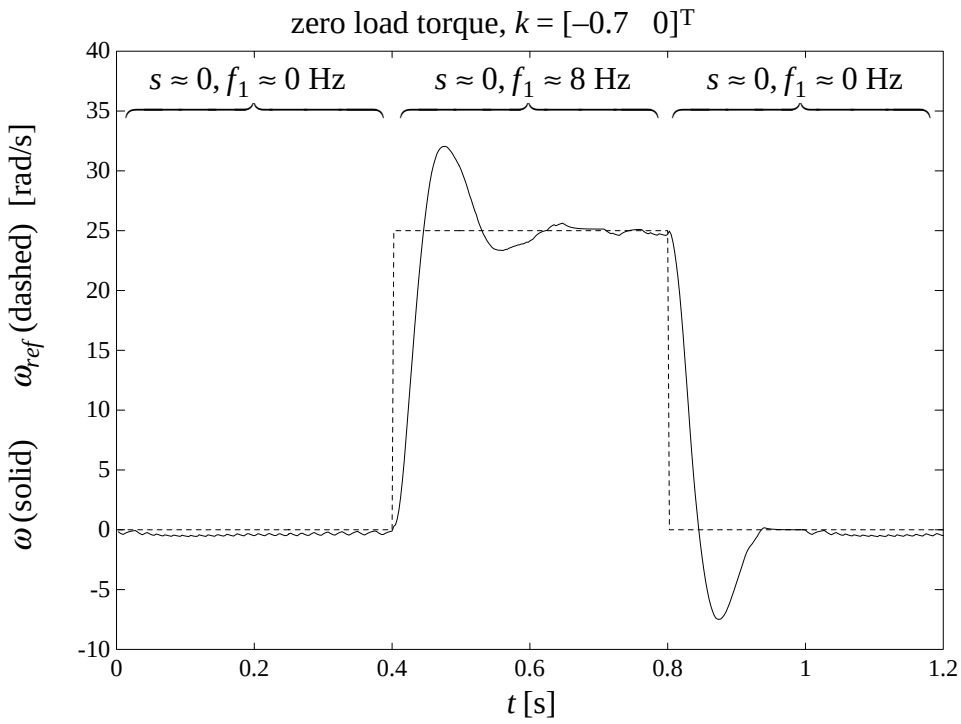

a)

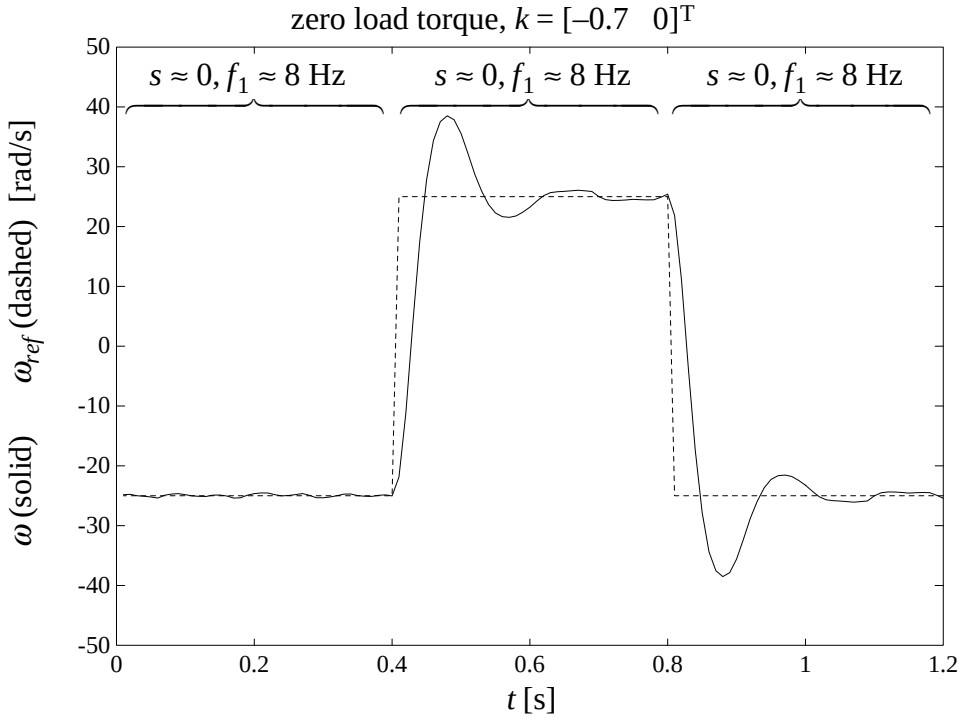

b)

Fig. 8.6 Step change of speed reference at zero load a) 0 to 25 rad/s (17% of rated speed). b) –25 to 25 rad/s.

Slow Ramp of Speed Reference

Fig. 8.7 shows a positive and a negative ramp of the speed reference, between –10 rad/s and +10 rad/s.

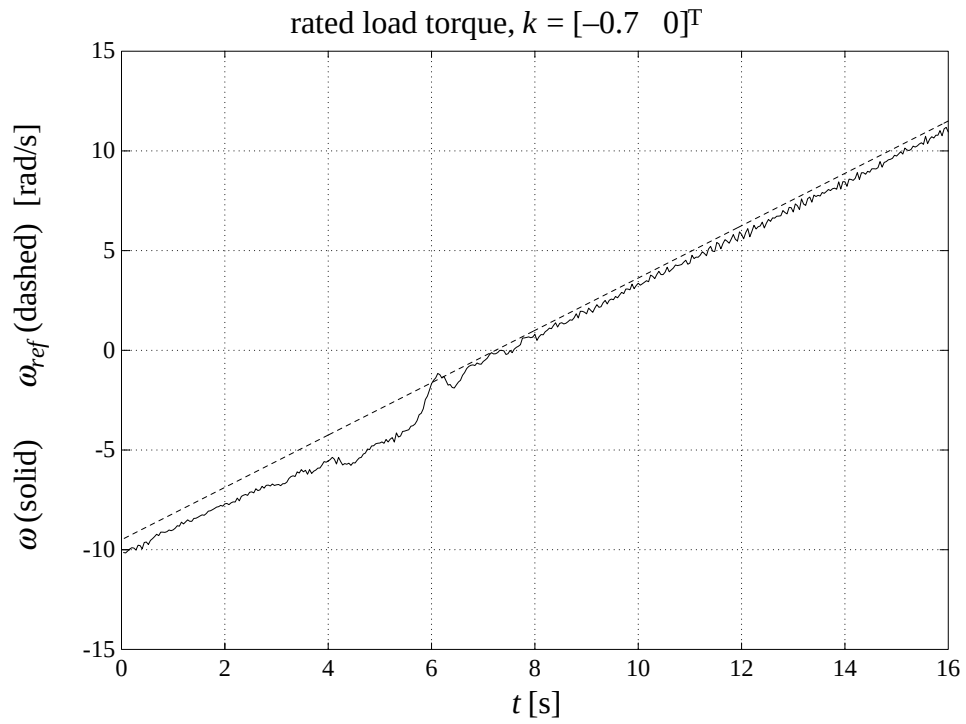

a)

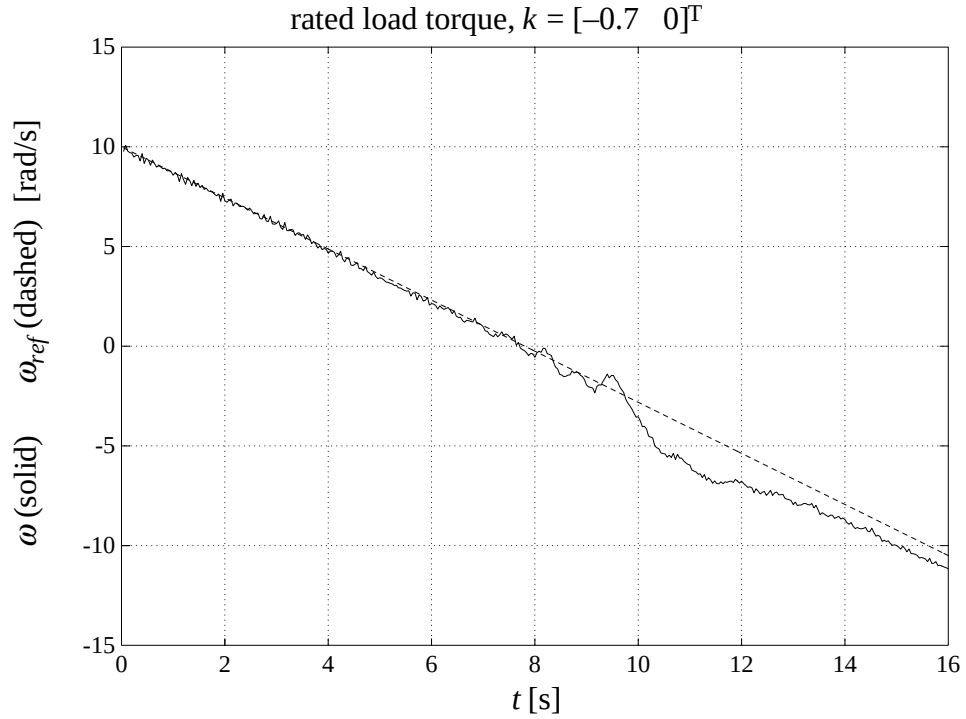

b)

Fig. 8.7 Slow change of ω_{ref} at rated load. a) –10 to +10 rad/s (7% of rated speed) b) +10 to –10 rad/s.

At –10 rad/s, the stator voltage vector is rotating in one direction, and at +10 rad/s it is rotating in the opposite direction. When the stator flux vector is changing direction, the frequency of the stator voltage is zero. At rated

load, this occurs at about $\omega = -3\,\mathrm{rad/s}$, and it is clearly seen that there is an error in the estimated speed in a region close to $\omega = -3\,\mathrm{rad/s}$. This could be expected from the results in section *Important Problems at Low Frequencies* of Chapter 5.

In conclusion, the results regarding parameter sensitivity at different observer gains, and the problems at low frequency operation, as well as the general behaviour of the observer discussed in earlier chapters, have been experimentally verified.

9

Conclusion

With mechanical analogies, and simplified examples, many of the hidden mysteries of speed and flux observers have been clarified. With the knowledge acquired from these examples, it has been possible to obtain an observer which does not suffer from integrator drift and other problems reported elsewhere.

This observer can be used in a sensorless vector control drive system, filling the gap between open loop frequency inverter systems and vector control systems using speed measurement. The dynamic performance of the sensorless system with speed estimation is superior to an open loop frequency inverter system. Even though it will never show the same accuracy near zero speed as a system with a speed sensor on the motor shaft, the sensorless system can increase the performance in applications where open loop inverters are used today, and it can be used in many applications which otherwise would require a speed sensor.

The sensorless system uses the same inverter bridge configuration as in an open loop frequency inverter, with little additional hardware, and any standard induction motor can be used. The main difference is that observer and controller calculations are performed by a digital signal processor. As the cost of a suitable fixed point DSP is less than $10 (1995), the overall cost of the sensorless system is equal to the cost of an open loop inverter system.

Future Topics

The remaining problems are two; the lack of information at zero frequency, and the error in estimated speed due to errors in the rotor resistance parameter of the observer.

It is believed that both problems can be reduced by superimposing perturbation signals on the supply voltage. A perturbation in the *d*-axis, parallel to the magnetizing flux, would not directly affect the produced torque of the motor, but would give additional information to the observer. This would only require additional calculations, without any modifications of motors or inverters.

References

1) Baader, U., M. Depenbrock, G. Gierse (1992) ”Direct Self Control (DSC) of Inverter-Fed Induction Machine: A Basis for Speed Control Without Speed Measurement”, *IEEE Transactions on Industry Applications*, vol. 28, no. 3, May/June 1992, pp. 581-588.

2) Bausch H., K. Kanelis, B. Lange, W. Zeng (1994) ”Torque Control of Synchronous and Asynchronous Drives Without Mechanical Sensors”, *Proc. ICEM ’94*, Paris, France, pp. 324-328.

3) Beguenane, R., C. Ghyselen, H. Schoorens (1994), ”A Proposed Induction Motor Speed Sensor Without Contact from Slots Harmonics: Application to Rotoric Time Constant Identification”, *Proc. 1994 IEE Conf.*, London, UK, pp. 90-95.

4) Böcker, J., J. Janning (1991), ”Discrete-Time Flux Observer for PWM Inverter Fed Induction Motors, *Proc. EPE ’91*, Firenze, Italy, pp. 171-176.

5) Carlsson, A. (1993), *Liten, snabb realtidskärna i C* (in Swedish), Department of Automatic Control, LTH, Lund, Sweden

6) Glad, T., L. Ljung (1981), *Reglerteknik* (in Swedish), Studentlitteratur, Lund, Sweden

7) Habetler, T. G., F. Profumo, M. Pastorelli, L. M. Tolbert (1992), ”Direct Torque Control of Induction Machines Using Space Vector Modulation”, *IEEE Transactions on Industry Applications*, vol. 28, no. 5, September/October 1992, pp. 1045-1053.

8) Haemmerli, B. M. (1986), ”Rotor Speed Detection for Induction Machines Utilising Rotor Slots Harmonics”, *Proc. ICEM ’86*, pp. 352-354.

9) Henneberger, G., B.-J. Brunsbach, Th. Klepsch (1991), ”Field-Oriented Control of Synchronous and Asynchronous Drives without Mechanical Sensors Using a Kalman Filter”, *Proc. EPE ’91*, Firenze, Italy, pp. 664-669.

10) Hori, Y., V. Cotter, Y. Kaya (1987), ”A Novel Induction Machine Flux Observer and its Application to a High Performance AC Drive

System", *Proc. IFAC 10th Triennial World Congress*, Munich, FRG, pp. 363-368.

11) Hurst, K. D., T. G. Habetler, G. Griva, F. Profumo (1994), "Speed Sensorless Field-Oriented Control of Induction Machines Using Current Harmonic Spectral Estimation", *Proc. IAS '94 29th Annual Meeting*, Denver Colorado, pp. 601-607.

12) Jansen, P. L., R. D. Lorenz (1994a), "Transducerless Position and Velocity Estimation in Induction and Salient AC Machines", *Proc. IAS '94 29th Annual Meeting*, Denver Colorado, pp. 488-495.

13) Jansen, P. L., R. D. Lorenz (1994b), "A Physically Insightful Approach to the Design and Accuracy Assessment of Flux Observers for Field Oriented Induction Machine Drives", *IEEE Transactions on Industry Applications*, vol. 30, no. 1, January/February 1994, pp. 101-110.

14) Jansen, P. L., R. D. Lorenz (1993) "Accuracy Limitations of Velocity and Flux Estimation in Direct Field Oriented Induction Machines", *Proc. EPE '93*, Brighton, UK, pp. 312-318.

15) Jönsson, R. (1991), *Natural Field Orientation*, Patent Application PCT/SE91/00086.

16) Kim, Y.-R., S.-K. Sul, M.-H. Park (1994), "Speed Sensorless Vector Control of Induction Motor using Extended Kalman Filter", *IEEE Transactions on Industry Applications*, vol. 30, no. 5, September/October 1994, pp. 1225-1233.

17) Kovács, P. K. (1984), *Transient Phenomena in Electrical Machines*, Elsevier, Amsterdam.

18) Krzeminski, Z. (1991) "Speed and Rotor Resistance Estimation in Observer System of Induction Motor", *Proc. EPE '91*, Firenze, Italy, pp. 538-542.

19) Kubota, H., K. Matsuse (1994), "Speed Sensorless Field-Oriented Control of Induction Motor with Rotor Resistance Adaption", *IEEE Transactions on Industry Applications*, vol. 30, no. 5, September/October 1994, pp. 1219-1224.

20) Leonhard, W. (1985), *Control of Electrical Drives*, Springer, Berlin.

21) Lorenz, R. D., T. A. Lipo, D. W. Novotny (1994), *Motion Control with Induction Motors*, University of Wisconsin, Madison, WI.

22) Luenberger, D. G. (1979), *Introduction to Dynamic Systems*, John Wiley & Sons, USA.

23) Menander, F., J. Silvander (1991), *Flödesobserverare för asynkronmotor* (in Swedish), Department of Automatic Control, LTH, Lund, Sweden.

24) Mohan, N., T. M. Undeland, W. P. Robbins (1989), *Power Electronics: Converters, Applications and Design*, John Wiley & Sons, USA.

25) Peterson (1991), *Oscillations in Inverter Fed Induction Motor Drives*, IEA/LTH, Lund, Sweden.

26) Peterson (1996), *DSP Implementation of Induction Machine Speed Observer*, IEA/LTH, Lund, Sweden

27) Pohjalainen. P., P. Tiitinen, J. Lalu (1994), ”The Next Generation Motor Control Method - Direct Torque Control, DTC”, *EPE Chapter Symposium, Electric Drive Design and Applications*, Lausanne, Switzerland, pp. 115-120.

28) Samuelsson, O. (1994), *Point-to-point Position Control using Simple Mechanical Sensors*, IEA/LTH, Lund, Sweden.

29) Schauder, C. (1992) ”Adaptive Speed Identification for Vector Control of Induction Motors without Rotational Transducers”, *IEEE Transactions on Industry Applications*, vol. 28, no. 5, September/October 1992, pp. 1054-1061.

30) Schroedl, M.(1992), ”Sensorless Control of Induction Motors at Low Speed and Stand Still”, *Proc. ICEM ’92*, Manchester, UK, pp. 863-867.

31) Slemon, G., A. Straughen (1980), *Electric Machines*, Addison-Wesley, Reading, Mass.

32) Sugimoto, H., S. Tamai (1987), ”Secondary Resistance Identification of an Induction Motor Applied Model Reference Adaptive System and its Characteristics”, *IEEE Transactions on Industry Applications*, vol. IA-23, no. 2, March/April 1987, pp. 296-303.

33) Tajima, H., Y. Hori (1993), ”Speed Sensorless Field-Orientation Control of the Induction Machine”, *IEEE Transactions on Industry Applications*, vol. 29, no. 1, January/February 1993, pp. 175-180.

34) Takahashi. I., Y. Ohmori (1989), ”High-Performance Direct Torque Control of an Induction Motor”, *IEEE Transactions on Industry Applications*, vol. 25, no. 2, March/April 1989, pp. 257-264.

35) Tamai, S., H. Sugimoto, M. Yano (1987), ”Speed Sensor-less Vector Control of Induction Motor with Model Reference Adaptive

System", *Proc. IEEE Industry Applications Society Annual Meeting 1987*, pp. 189-195.

36) Török, V., J. Valis (1985), *Elektroniska drivsystem* (in Swedish), Tutext, Stockholm.

37) Umeno, T., Y. Hori, H. Suzuki (1990), "Design of the Flux-Observer-Based Vector Control System of Induction Machines Taking into Consideration Robust Stability", *Electrical Engineering in Japan*, vol. 110, no. 6, pp. 53-65.

38) Vélez-Reyes, M., G. C. Verghese (1995), "Subset Selection in Identification, and Application to Speed and Parameter Estimation for Induction Machines", *Proc. 4th IEEE Conf. on Control Applications*, Albany, NY, pp. 991-997.

39) Veltman, A. (1994), *The Fish Method*, Delft University Press, Delft, The Netherlands.

40) Verghese, G. C., S. R. Sanders (1988), "Observers for Flux Estimation in Induction Machines" *IEEE Transactions on Industrial Electronics*, vol. 35, no. 1, February 1988, pp. 85-94.

41) von Westerholt, E., M. Pietrzak-David, B. de Fornel (1992a), "Extended State Estimation of Nonlinear Modeled Induction Machines", *Proc. PESC '92*, Toledo, Spain, pp. 271-278.

42) von Westerholt, E., M. Pietrzak-David, B. de Fornel (1992b), "Extended Kalman Filter based Control of Low-Power Induction Motor Drives for Robotic Applications", *Proc. ICEM '92*, Manchester, UK, pp. 843-847.

43) Yang, G., T.-H. Chin (1993), "Adaptive-Speed Identification Scheme for a Vector Controlled Speed Sensorless Inverter-Induction Motor Drive", *IEEE Transactions on Industry Applications*, vol. 29, no. 4, July/August 1993, pp. 820-825.

44) Zai, L.-C., C. L. DeMarco, T. A. Lipo (1992), "An Extended Kalman Filter Approach to Rotor Time Constant Measurement in PWM Induction Motor Drives", *IEEE Transactions on Industry Applications*, vol. 28, no. 1, January/February 1992, pp. 96-104.

45) Åström, K. J. (1976), *Reglerteori* (in Swedish), Almqvist & Wiksell, Stockholm.

46) Åström, K. J., B. Wittenmark (1984), *Computer Controlled Systems: Theory and Design*, Prentice-Hall, Englewood Cliffs, NJ, USA.

A

List of Symbols

Bold typeface is used for complex quantities, $\mathbf{v} = v_x + jv_y = v\,e^{j\varphi}$ where $v = |\mathbf{v}| = \sqrt{v_x^2 + v_y^2}$ and $\varphi = \arg(\mathbf{v})$

A	system matrix	
B	input matrix	
C	output matrix	
C	capacitance	F
$ç$	real valued constant	
d	viscous damping coefficient	Ns/m
e	controller error	
F	force	N
f_1	stator voltage frequency	Hz
H	rated start time	s
I	identity matrix	
i, $\mathbf{i}$	current	A
J	inertia	kg m^2
j	$\sqrt{-1}$	
k	spring constant	N/m
K, k, $\mathbf{k}$	observer gain	
k_p	controller proportional gain	
L	inductance	H
m	mass	kg
n	mechanical speed of rotor in revs/min	min^{-1}

n_n	rated mechanical speed of rotor in revs/min	min^{-1}
P	power	W
$\mathbf{p}$	pole	
R	resistance	Ω
r	radius	m
$\mathbf{s}$	Laplace variable	
s	slip	
T	torque	Nm
T_i	controller integration time	
u	system input	
u, $\mathbf{u}$	voltage	V
v	velocity	m/s
x	state vector	
$\tilde{x}$	error in estimate, $x - \hat{x}$	
$\hat{x}$	estimate of x	
y	system output	
z_p	no. of pole pairs	
ζ	relative damping	
σ	leakage factor	
τ	time constant	s
φ	flux vector angle	◦
Ψ, $\mathbf{\Psi}$	flux linkage (referred to as ”flux” for simplicity)	Vs
Ω	natural frequency	
ω	angular velocity of rotor (referred to as ”rotor speed” for simplicity)	rad/s
ω_1	angular frequency of stator voltage vector	rad/s

ω_e	angular frequency of rotor flux	rad/s

subscripts

e	parameter of estimator
L, *l*	leakage
M, *m*	magnetizing
n	rated value
r	rotor
ref	reference value
s	stator
stat	steady state value
x	real part, $v_x = \Re(\mathbf{v})$
y	imaginary part, $v_y = \Im(\mathbf{v})$
0	operating point

superscripts

r	rotating reference frame
T	T-model (as opposed to Γ-model)
T	transpose

symbols

*	complex conjugate
^	estimated quantity
~	error in estimate

B

Mechanical Analogy

An electric motor is both an electrical and a mechanical system. The interaction between the electrical and mechanical parts are often complicated to analyse. By representing the electrical part of the system by its mechanical analogy, the complete system becomes mechanical and more intuitive and easier to analyse.

If the product of two quantities in the electrical system yields power, then the product of the corresponding mechanical quantities must be power. In the electrical system, the product of current and voltage is power. If current is represented for example by force the voltage should be represented by speed as the product of force and speed is power. This gives a very useful mechanical analogy. Table B.1 lists some corresponding electrical and mechanical quantities, and Fig. B.1 shows mechanical components corresponding to the electrical ones.

Electrical system	Mechanical equivalent
power P [W]	power P [W]
current i [A]	force F [N]
voltage u [V]	speed v [m/s]
flux linkage Ψ [Vs]	distance x [m]
resistance R [Ω]	inverse of damping $1/d$ [m/Ns]
inductance L [H]	inverse of spring stiffness $1/k$ [m/N]
capacitance C [F]	mass m [kg]

Table B.1 Corresponding electrical and mechanical quantities.

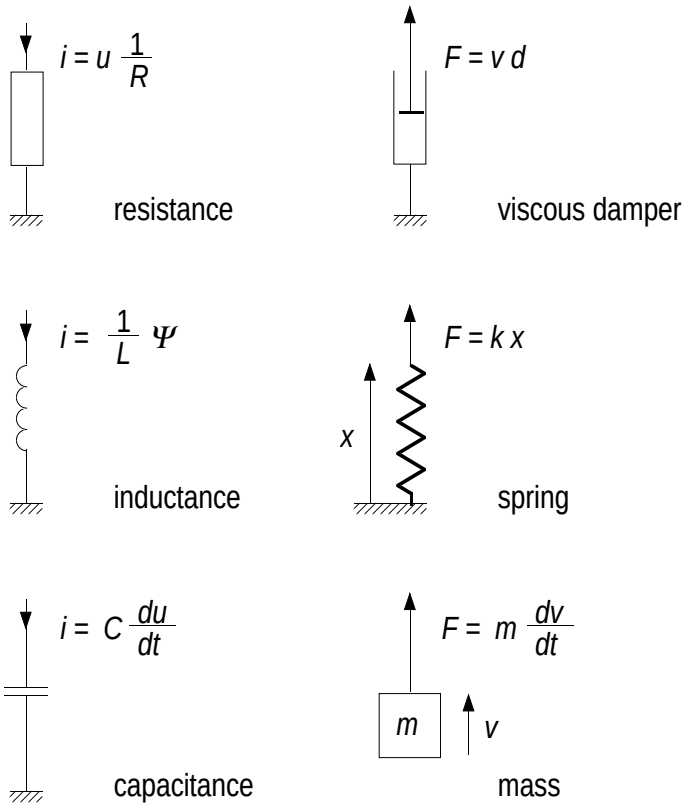

Fig. B.1 Electrical components and corresponding mechanical components.

Note that the equilibrium position of the spring is when the length of the spring is zero and $x = 0$. A negative force results in $x < 0$.

C

Mechanical Model of the Induction Machine

A mechanical equivalent model of equations (2.3) and (2.4) is shown in Fig. C.1, where inductances have become springs and currents are forces pulling the springs (Török et al, 1985). The inductance is the inverse of the stiffness of the spring. (Appendix B gives a complete description of corresponding parameters in the electrical and mechanical models.)

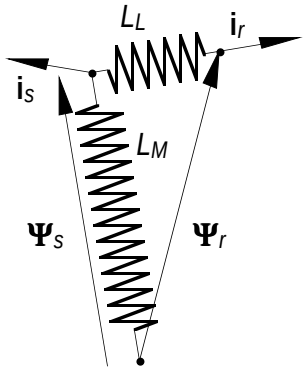

Fig. C.1 Mechanical equivalent model of equations (2.3) and (2.4).

The flux linkages are vectors with a length and a direction corresponding to the original flux linkages. The torque on the springs developed by the force representing the current $\mathbf{i}_s$ is

$$T = \Im\left(\boldsymbol{\Psi}_s^* \mathbf{i}_s\right) \tag{C.1}$$

which for a two pole machine is two thirds of the driving torque in equation (2.8). The point in Fig. C.1 where the force $\mathbf{i}_r$ is attached to the spring L_L follows the restrictions of equation (2.6) if the resistance R_r is represented as a two dimensional viscous damper which can be a drag-pad on an oily surface shown in Fig. C.2. The velocity difference between the drag-pad and the surface is proportional to the force applied to the drag-pad, and the velocity and the force have the same direction. The time derivative of the flux in the mechanical model is the velocity of the tip of the flux vector. If the oily surface is a rotating disc with the angular speed $z_p\ \omega$ (Fig. C.2) then the relative velocity difference between the drag-pad and the disc is

$$\mathbf{v}_{diff} = \frac{d\boldsymbol{\Psi}_r}{dt} - jz_p\omega\boldsymbol{\Psi}_r \tag{C.2}$$

The force on the drag-pad is $-\mathbf{i}_r$ and then the velocity difference between the disc and the drag-pad can be expressed as

$$\mathbf{v}_{diff} = -\mathbf{i}_r R_r \tag{C.3}$$

Combining equations (C.2) and (C.3) gives equation (2.6).

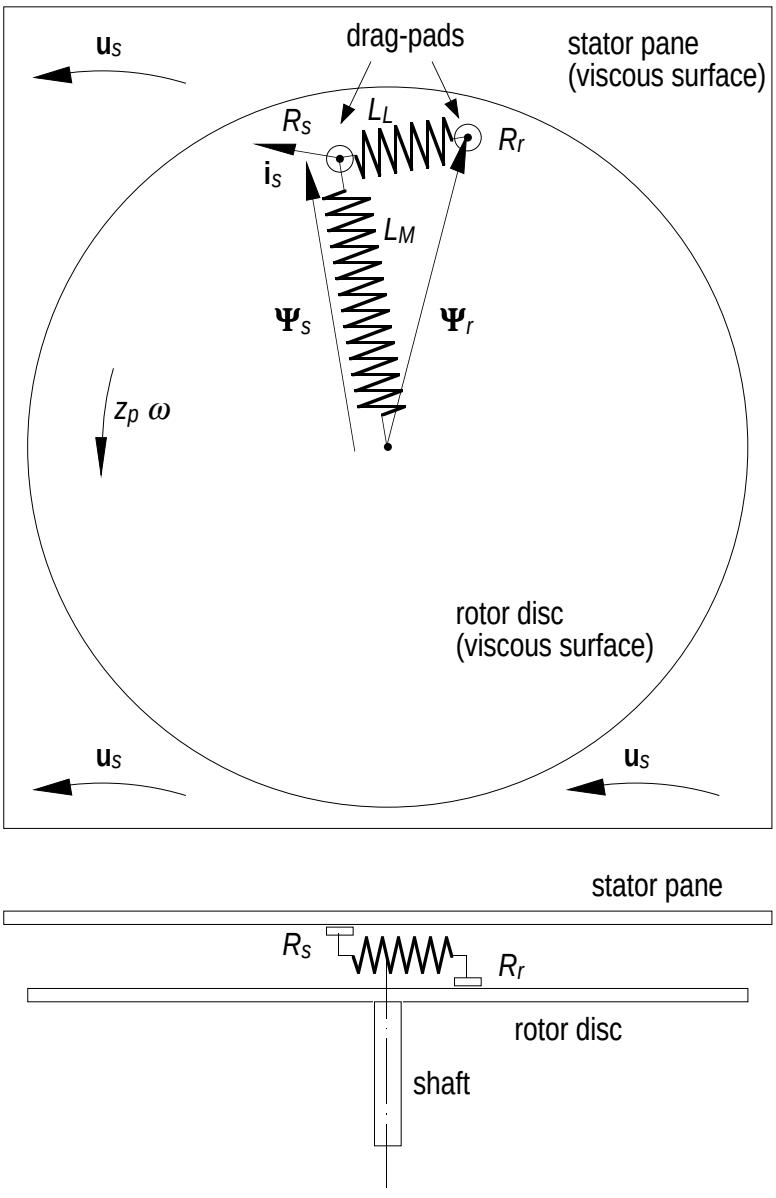

Fig. C.2 Mechanical model of the induction machine.

The torque transferred from the drag-pad to the disc is given by equation (C.1). If the rotating disc represents the rotor and has two thirds of the actual rotor moment of inertia divided by the number of pole pairs

$$J_{disc} = \frac{2}{3z_p} J \tag{C.4}$$

and the same relation holds for the actual load torque and the load torque of the disc,

$$T_{discload} = \frac{2}{3z_p} T_{load} \tag{C.5}$$

we have an *exact* mechanical analogy of the set of equations (2.3), (2.4), (2.6) and (2.7). To get a complete analogy of equations (2.3)-(2.7), the stator resistance must be modelled. Equation (2.5) can also be represented by a mechanical equivalent if R_s is represented as a drag-pad on a viscous surface. The drag-pad is transferring the force $\mathbf{i}_s$ to the springs. The viscous surface is moving with the velocity $\mathbf{u}_s$ independently of the stator flux. All points of this surface are moving in the same direction at the same speed. Contrary to the rotor disc, this surface cannot rotate. The velocity of the tip of the stator flux will be the difference between the stator voltage and the resistive voltage-drop in the stator. Fig. C.2 shows the mechanical model with the stator resistance included. It is important to observe that the equations describing the mechanical system in Fig. C.2 are identical to the equations describing an ideal induction machine.

D

Parameters of Machines

The 0.75 kW machine used in simulations and experiments is not representative to all induction machines. The p.u. stator resistance is much higher for such a small machine than for a larger one. However, as a large stator resistance makes flux estimation and speed estimation more difficult at low frequencies, the chosen machine represents a ”near worst case”.

machine: IMEP type TAM 80-19

rating: 3~ M

Δ/Y 220/380 V 3.63/2.1 A

0.75 kW, 5.2 Nm

1390 r/min 50 Hz cosφ 0.76

parameters of Δ-connected machine:	p.u. parameters
R_s = 3.60 Ω	0.10
R_r = 2.47 Ω	0.070
L_{sl} = 0.0128 H	0.11
L_{rl} = 0.0128 H	0.11
L_m = 0.148 H	1.32
k_γ = 0.920	
L_M = 0.160 H	1.44
L_L = 0.0291 H	0.26

$J = 2.1 \cdot 10^{-3}$ kg m^2

$H = 37 \cdot 10^{-3}$ s

$$\Psi_{sn} = \frac{U_{phase,peak}}{2\pi f_1} = \frac{\sqrt{2}\,U_n}{\sqrt{3}\cdot 2\pi f_1} = \frac{\sqrt{2}\cdot 220}{\sqrt{3}\cdot 2\pi 50} = 0.57 \text{ Vs}$$

$$Z_n = \frac{U_n}{\sqrt{3}I_n} = \frac{220}{\sqrt{3}\cdot 3.63} = 35\,\Omega$$

E

Observer Poles

The dynamic behaviour of the observer described by equation (4.12) is determined by the poles of the system. The poles are eigenvalues of the system matrix $\left(A_e - R_e\, k\, C_e\right)$ and can be calculated as the roots of the characteristic polynomial

$$P(\mathbf{s}) = \det\left(\mathbf{s}I - \left(A_e - R_e\, k\, C_e\right)\right) \tag{E.1}$$

where I is the identity matrix. Equations (E.1), (4.5), (4.7), (4.10) and (4.11) give

$$\begin{aligned} P(\mathbf{s}) = \mathbf{s}^2 + \left(R_{se}\left(\mathbf{k}_s + 1\right)\left(\frac{1}{L_{Me}} + \frac{1}{L_{Le}}\right) + \frac{R_{re}\left(1 - \mathbf{k}_r\right)}{L_{Le}} - jz_p\,\omega \right) s \\ + \frac{R_{se}\left(\mathbf{k}_s + 1\right)\left(R_{re} - jz_p\,\omega\left(L_{Le} + L_{Me}\right)\right)}{L_{Le} + L_{Me}} \end{aligned} \tag{E.2}$$

The required observer gain k for a desired characteristic polynomial,

$$P(\mathbf{s}) = \mathbf{s}^2 + \mathbf{c}_1\mathbf{s} + \mathbf{c}_2 \tag{E.3}$$

with the poles $\mathbf{p}_1$ and $\mathbf{p}_2$ where

$$\mathbf{c}_1 = -\left(\mathbf{p}_1 + \mathbf{p}_2\right) \tag{E.4}$$

$$\mathbf{c}_2 = \mathbf{p}_1\,\mathbf{p}_2 \tag{E.5}$$

is found with the following relation (Åström et al, 1984),

$$\begin{aligned} k &= R_e^{-1}K \\ &= R_e^{-1}P\left(A_e\right)W_o^{-1}\begin{bmatrix}0\\1\end{bmatrix} \\ &= R_e^{-1}\left(A_e^2 + \mathbf{c}_1A_e + \mathbf{c}_2I\right)W_o^{-1}\begin{bmatrix}0\\1\end{bmatrix} \\ &= R_e^{-1}\left(A_e^2 - \left(\mathbf{p}_1 + \mathbf{p}_2\right)A_e + \mathbf{p}_1\mathbf{p}_2I\right)W_o^{-1}\begin{bmatrix}0\\1\end{bmatrix} \end{aligned} \tag{E.6}$$

where W_o is the observability matrix,

$$W_o = \begin{bmatrix} C_e \\ C_e A_e \end{bmatrix} \tag{E.7}$$

With equations (4.2) and (4.4) inserted in (E.7), we have after inversion and multiplication with $\begin{bmatrix} 0 & 1 \end{bmatrix}^T$

$$W_o^{-1}\begin{bmatrix} 0 \\ 1 \end{bmatrix} = \begin{bmatrix} \dfrac{L_{Me}L_{Le}\left(R_{re} + jz_p\,\omega\left(L_{Me}+L_{Le}\right)\right)}{R_{re}^2 + z_p^2\,\omega^2\left(L_{Me}+L_{Le}\right)^2} \\ \dfrac{\left(L_{Le}^2 + L_{Me}L_{Le}\right)\left(R_{re} + jz_p\,\omega\left(L_{Me}+L_{Le}\right)\right)}{R_{re}^2 + z_p^2\,\omega^2\left(L_{Me}+L_{Le}\right)^2} \end{bmatrix} \tag{E.8}$$

The observer gain will be

$$k = \begin{bmatrix} \dfrac{1}{R_{se}} & 0 \\ 0 & \dfrac{1}{R_{re}} \end{bmatrix}\left(A_e^2 + \mathbf{c}_1 A_e + \mathbf{c}_2 I\right)\begin{bmatrix} \dfrac{L_{Me}L_{Le}\left(R_{re} + jz_p\,\omega\left(L_{Me}+L_{Le}\right)\right)}{R_{re}^2 + z_p^2\,\omega^2\left(L_{Me}+L_{Le}\right)^2} \\ \dfrac{\left(L_{Le}^2 + L_{Me}L_{Le}\right)\left(R_{re} + jz_p\,\omega\left(L_{Me}+L_{Le}\right)\right)}{R_{re}^2 + z_p^2\,\omega^2\left(L_{Me}+L_{Le}\right)^2} \end{bmatrix}$$

$$= \begin{bmatrix} \dfrac{\mathbf{c}_2\,\dfrac{L_{Me}L_{Le}}{R_{se}}\left(R_{re} + jz_p\,\omega\left(L_{Me}+L_{Le}\right)\right)}{R_{re}^2 + z_p^2\,\omega^2\left(L_{Me}+L_{Le}\right)^2} - 1 \\ \dfrac{L_{Le}\,\dfrac{L_{Me}+L_{Le}}{R_{re}}\left(R_{re} + jz_p\,\omega\left(L_{Me}+L_{Le}\right)\right)}{R_{re}^2 + z_p^2\,\omega^2\left(L_{Me}+L_{Le}\right)^2} + 1 - \dfrac{L_{Le}}{R_{re}}\left(\mathbf{c}_1 + jz_p\,\omega\right) \end{bmatrix} \tag{E.9}$$

The gain vector k consists of four components,

$$k_{sx} = \frac{\dfrac{L_{Me}L_{Le}}{R_{se}}\left(\Re(\mathbf{c}_2)R_{re} - \Im(\mathbf{c}_2)z_p\,\omega\left(L_{Me}+L_{Le}\right)\right)}{R_{re}^2 + z_p^2\,\omega^2\left(L_{Me}+L_{Le}\right)^2} - 1 \tag{E.10}$$

$$k_{sy} = \frac{\frac{L_{Me} L_{Le}}{R_{se}} \left(\Im(\mathbf{c}_2) R_{re} + \Re(\mathbf{c}_2) z_p \, \omega \left(L_{Me} + L_{Le} \right) \right)}{R_{re}^2 + z_p^2 \, \omega^2 \left(L_{Me} + L_{Le} \right)^2} \tag{E.11}$$

$$k_{rx} = \frac{L_{Le} \frac{L_{Me} + L_{Le}}{R_{re}} \left(\Re(\mathbf{c}_2) R_{re} - \Im(\mathbf{c}_2) z_p \, \omega \left(L_{Me} + L_{Le} \right) \right)}{R_{re}^2 + z_p^2 \, \omega^2 \left(L_{Me} + L_{Le} \right)^2} + 1 - \frac{L_{Le}}{R_{re}} \Re(\mathbf{c}_1)$$

(E.12)

$$k_{ry} = \frac{L_{Le} \frac{L_{Me} + L_{Le}}{R_{re}} \left(\Im(\mathbf{c}_2) R_{re} + \Re(\mathbf{c}_2) z_p \, \omega \left(L_{Me} + L_{Le} \right) \right)}{R_{re}^2 + z_p^2 \, \omega^2 \left(L_{Me} + L_{Le} \right)^2} - \frac{L_{Le}}{R_{re}} \left(\Im(\mathbf{c}_1) + z_p \, \omega \right)$$

(E.13)

Poles of System with Complex Variables

The observer system matrix $\left(A_e - R_e \, k \, C_e \right)$ is a 2×2 matrix with complex coefficients. As the coefficients are complex, complex eigenvalues of this matrix need not be complex conjugates. For a 2×2 matrix with real coefficients on the other hand, complex eigenvalues come in pairs of complex conjugates.

The observer can also be described with a 4×4 matrix with real coefficients. If the observer is described by the real state vector

$$\begin{bmatrix} \hat{\Psi}_{sx} \\ \hat{\Psi}_{rx} \\ \hat{\Psi}_{sy} \\ \hat{\Psi}_{ry} \end{bmatrix}$$

instead of the complex state vector

$$\begin{bmatrix} \hat{\boldsymbol{\Psi}}_{s} \\ \hat{\boldsymbol{\Psi}}_{r} \end{bmatrix}$$

the new observer have the following 4×4 system matrix

$$\begin{bmatrix} \Re\left(A_e - R_e k C_e\right) & -\Im\left(A_e - R_e k C_e\right) \\ \Im\left(A_e - R_e k C_e\right) & \Re\left(A_e - R_e k C_e\right) \end{bmatrix}$$

with real coefficients. The eigenvalues of this matrix are the same as the eigenvalues of $\left(A_e - R_e k C_e\right)$, but there are also two new eigenvalues which are the conjugates of the old ones.

F

Steady State Value of Speed Observer

The following steps give the solution to the system of equations (5.32)–(5.34). The first two equations can be written

$$\hat{\boldsymbol{\Psi}}_s\left(j\omega_1 + R_{se}\left(1+\mathbf{k}_s\right)\left(\frac{1}{L_{Me}}+\frac{1}{L_{Le}}\right)\right) - \hat{\boldsymbol{\Psi}}_r R_{se}\left(1+\mathbf{k}_s\right)\frac{1}{L_{Le}} = \mathbf{u}_s + R_{se}\mathbf{k}_s\mathbf{i}_s \tag{F.1}$$

$$\hat{\boldsymbol{\Psi}}_s\left(R_{re}\mathbf{k}_r\left(\frac{1}{L_{Me}}+\frac{1}{L_{Le}}\right)-\frac{R_{re}}{L_L}\right)+\hat{\boldsymbol{\Psi}}_r\left(j\omega_1 - jz_p\hat{\omega}+\left(1-\mathbf{k}_r\right)\frac{R_{re}}{L_{Le}}\right) = R_{re}\mathbf{k}_r\mathbf{i}_s \tag{F.2}$$

Introduce **a**, **b**, **c**, **d**, **e** and **f** to make the equations more compact,

$$\mathbf{a}\hat{\boldsymbol{\Psi}}_s + \mathbf{b}\hat{\boldsymbol{\Psi}}_r = \mathbf{c} \tag{F.3}$$

$$\mathbf{d}\,\hat{\boldsymbol{\Psi}}_s + \left(\mathbf{e} - jz_p\hat{\omega}\right)\hat{\boldsymbol{\Psi}}_r = \mathbf{f} \tag{F.4}$$

solving this system for the stator and rotor flux estimates gives the functions f_1 and f_2 of equations (5.38) and (5.39),

$$\hat{\boldsymbol{\Psi}}_s = \mathrm{f}_1\left(\hat{\omega}\right) = \frac{\mathbf{ce} - j\mathbf{c}z_p\hat{\omega} - \mathbf{bf}}{\mathbf{ae} - j\mathbf{a}z_p\hat{\omega} - \mathbf{b}\,\mathbf{d}} \tag{F.5}$$

$$\hat{\boldsymbol{\Psi}}_r = \mathrm{f}_2\left(\hat{\omega}\right) = \frac{\mathbf{af} - \mathbf{dc}}{\mathbf{ae} - j\mathbf{a}z_p\hat{\omega} - \mathbf{b}\,\mathbf{d}} \tag{F.6}$$

Inserting this in equation (5.40), and some rearranging give

$$\varsigma = \frac{\mathbf{af} - \mathbf{dc} + L_{Le}\mathbf{i}_s(\mathbf{ae} - \mathbf{bd}) - L_{Le}\mathbf{i}_s j\mathbf{a}z_p\hat{\omega}}{\mathbf{ce} - \mathbf{bf} - j\mathbf{c}z_p\hat{\omega}} = \frac{\mathbf{n} - \mathbf{m}\hat{\omega}}{\mathbf{h} - \mathbf{p}\hat{\omega}} \tag{F.7}$$

As ς is real, it follows that

$$\begin{gathered}\Im\left(\frac{\mathbf{n}-\mathbf{m}\hat{\omega}}{\mathbf{h}-\mathbf{p}\hat{\omega}}\right)=0\\ \Leftrightarrow\\ \frac{\Re\left(\mathbf{n}-\mathbf{m}\hat{\omega}\right)}{\Re\left(\mathbf{h}-\mathbf{p}\hat{\omega}\right)}=\frac{\Im\left(\mathbf{n}-\mathbf{m}\hat{\omega}\right)}{\Im\left(\mathbf{h}-\mathbf{p}\hat{\omega}\right)}\\ \Leftrightarrow\\ \frac{n_x-m_x\hat{\omega}}{h_x-p_x\hat{\omega}}=\frac{n_y-m_y\hat{\omega}}{h_y-p_y\hat{\omega}}\end{gathered} \tag{F.8}$$

where index *x* denotes real parts and index *y* denotes imaginary parts. The estimated speed $\hat{\omega}$ can now be calculated from this equation of the second order. The two solutions are

$$\begin{aligned}\hat{\omega}=&\frac{h_y m_x+p_y n_x-h_x m_y-p_x n_y}{2\left(p_y m_x-p_x m_y\right)}\\ &+\frac{\sqrt{\left(h_y m_x+p_y n_x-h_x m_y-p_x n_y\right)^2-4\left(p_y m_x-p_x m_y\right)\left(h_y n_x-h_x n_y\right)}}{2\left(p_y m_x-p_x m_y\right)}\end{aligned} \tag{F.9}$$

and

$$\begin{aligned}\hat{\omega}=&\frac{h_y m_x+p_y n_x-h_x m_y-p_x n_y}{2\left(p_y m_x-p_x m_y\right)}\\ &-\frac{\sqrt{\left(h_y m_x+p_y n_x-h_x m_y-p_x n_y\right)^2-4\left(p_y m_x-p_x m_y\right)\left(h_y n_x-h_x n_y\right)}}{2\left(p_y m_x-p_x m_y\right)}\end{aligned} \tag{F.10}$$

where

$$\begin{aligned}\mathbf{n} &= \mathbf{af} - \mathbf{dc} + \hat{L}_L \mathbf{i}_s(\mathbf{ae} - \mathbf{bd}) \\ &= \mathbf{u}_s R_{re}\left(\frac{1}{L_{Le}} - \mathbf{k}_r\left(\frac{1}{L_{Me}} + \frac{1}{L_{Le}}\right)\right) \\ &+ \mathbf{i}_s\left(\mathbf{k}_r R_{se} R_{re}\left(\frac{1}{L_{Me}} + \frac{1}{L_{Le}}\right) + \mathbf{k}_s R_{se} R_{re}\frac{1}{L_{Le}} + j\omega_1 R_{re} - L_{Le}\omega_1^2\right) \\ &+ \mathbf{i}_s\left(j\omega_1 R_{se} L_{Le}(1+\mathbf{k}_s)\left(\frac{1}{L_{Me}} + \frac{1}{L_{Le}}\right) + (1+\mathbf{k}_s) R_{se} R_{re}\frac{1}{L_{Me}}\right)\end{aligned} \tag{F.11}$$

$$\mathbf{m} = jz_p L_{Le}\mathbf{i}_s\mathbf{a} = jz_p L_{Le}\mathbf{i}_s\left(j\omega_1 + R_{se}(1+\mathbf{k}_s)\left(\frac{1}{L_{Me}} + \frac{1}{L_{Le}}\right)\right) \tag{F.12}$$

$$\begin{aligned}\mathbf{h} &= \mathbf{ce} - \mathbf{bf} \\ &= j\omega_1 \mathbf{u}_s + j\omega_1 R_{se}\mathbf{i}_s\mathbf{k}_s + \frac{R_{re}}{L_{Le}}\left(\mathbf{u}_s(1-\mathbf{k}_r) + R_{se}\mathbf{i}_s(\mathbf{k}_s + \mathbf{k}_r)\right)\end{aligned} \tag{F.13}$$

$$\mathbf{p} = jz_p\mathbf{c} = jz_p\left(\mathbf{u}_s + R_{se}\mathbf{i}_s\mathbf{k}_s\right) \tag{F.14}$$

G

Non-linear Systems and Linearized Systems

A few simple examples will demonstrate that linearization and calculation of poles of non-linear systems must be done with great caution.

Stability of Non-linear Systems

The non-linear system

$$\begin{aligned} \frac{dx}{dt} &= x^2 + x + u \\ y &= x \end{aligned} \tag{G.1}$$

where u is the input and y is the output will be used to demonstrate some traps. In this example, the input is

$$u = 0.5\sin(10t) \tag{G.2}$$

A linearized approximation of the system can be obtained if x is replaced by $x_0 + \delta x$,

$$x = x_0 + \delta x \tag{G.3}$$

where δx is the deviation from an operating point x_0. As x_0 is constant it follows that

$$\frac{dx_0}{dt} = 0 \tag{G.4}$$

and

$$\begin{aligned} \frac{d}{dt}\delta x &= \frac{dx}{dt} \\ &= \left(x_0 + \delta x\right)^2 + x_0 + \delta x + u \\ &= x_0^2 + 2x_0\delta x + \delta x^2 + x_0 + \delta x + u \\ &= \left(2x_0 + 1\right)\delta x + x_0 + x_0^2 + \delta x^2 + u \end{aligned} \tag{G.5}$$

Neglecting the non-linear term δx^2 gives a linear system,

$$\begin{aligned} \frac{d}{dt}\delta x &= (2x_0 + 1)\delta x + x_0 + x_0^2 + u \\ y_{lin} &= x_0 + \delta x \end{aligned} \tag{G.6}$$

The pole *p* of this system lies in

$$p = 2x_0 + 1 \tag{G.7}$$

resulting in a stable system if

$$x_0 < -0.5 \tag{G.8}$$

Fig. G.1 shows a simulations of the non-linear system of equation (G.1) and the linear system of equation (G.6). The non-linear output *y* is solid and the linear output y_{lin} is dashed.

In Fig. G.1 a) the system is linearized around two operating points, $x_0 = 0.1$ and $x_0 = -0.1$, and the simulations start from the operating points ($x(0) = x_0$ and $\delta x(0) = 0$). Note how the linear system is unstable in both cases while the non-linear system solution is converging if $x_0 = -0.1$. This example shows that the linear model cannot be used to determine if the non-linear system is converging or not. However, the linear system can be used to simulate the non-linear system for a short period of time, as long as the deviation from the operating point is not too large. It is seen that the linear system follows the non-linear for about one or two seconds, depending on the operating point.

If the operating point is close to a point where the non-linear system is at steady state when the input is zero, in this case at *x* = –1, the linear system will provide a better approximation. In Fig. G.1 b) the operating point is $x_0 = -0.8$. Both the linear system and the non-linear system solution are now converging, and their outputs lie close during the complete simulation.

To conclude this example:

- if $x_0 > 0$, neither system is converging
- if $-0.5 < x_0 < 0$, the non-linear solutions, but not the linear system, are converging
- if $x_0 < -0.5$, both systems are converging

A linearized solution gives a faithful description of a non-linear solution only in an immediate neighbourhood of the operating point.

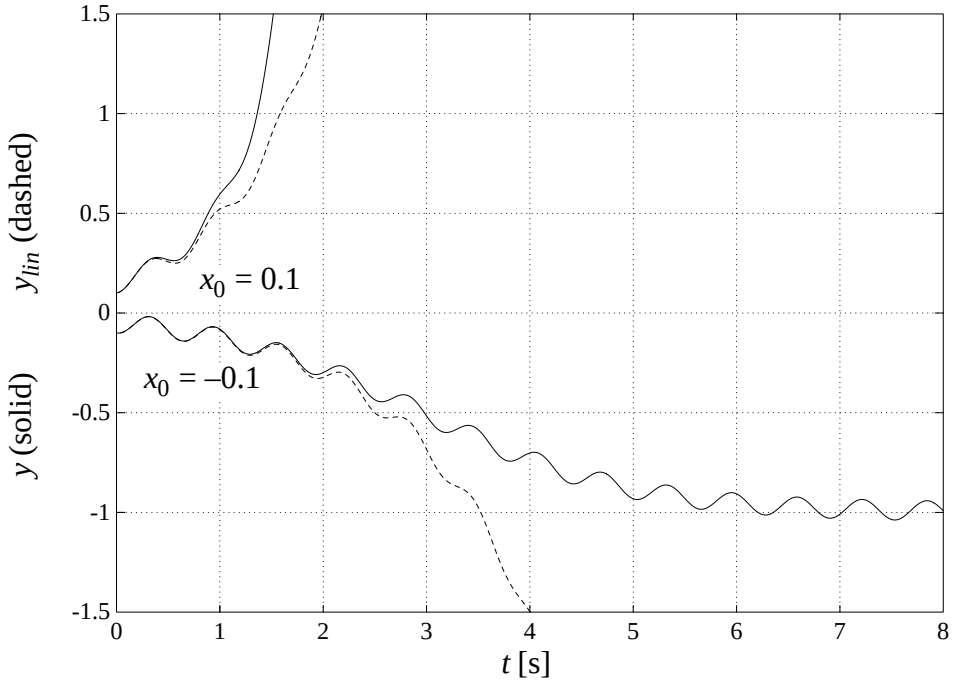

a)

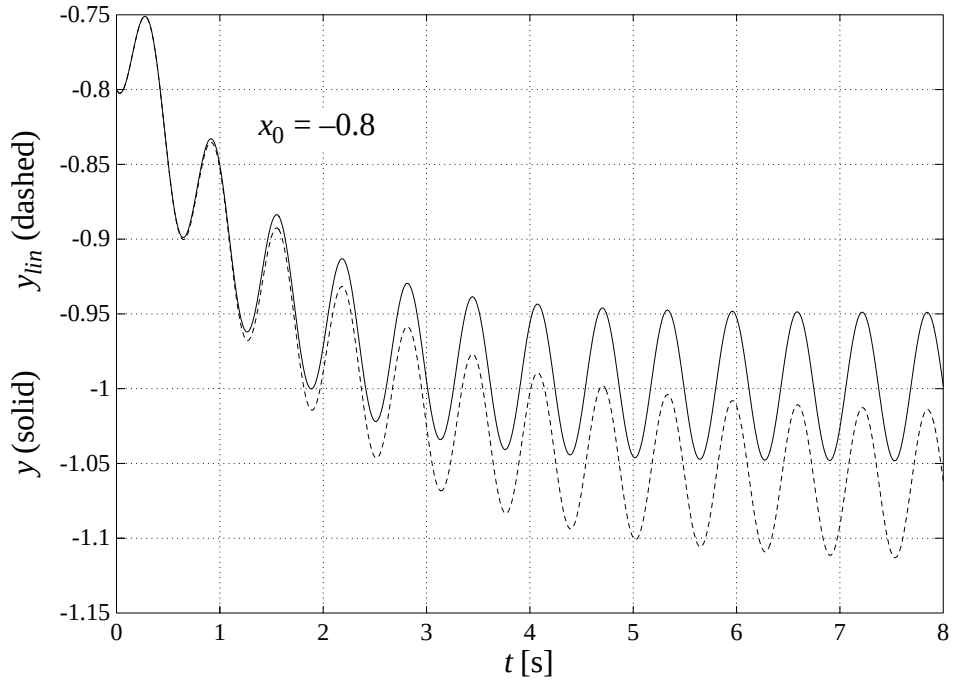

b)

Fig. G.1 Simulation of non-linear (solid) and linearized (dashed) system. a) simulations starting from operating points –0.1 and 0.1 b) simulation starting from operating point –0.8

Non-linearities Introduced by Change of Reference Frame

A linear system with the complex state variable $\mathbf{x} = x_x + j\,x_y$ described by

$$\frac{d}{dt}\begin{bmatrix} x_x \\ x_y \end{bmatrix} = \begin{bmatrix} -k & 0 \\ 0 & -k \end{bmatrix}\begin{bmatrix} x_x \\ x_y \end{bmatrix} + \begin{bmatrix} u_x \\ u_y \end{bmatrix} \tag{G.9}$$

will be used as an example to demonstrate some consequences of changing the reference frame. The system is shown as a block diagram in Fig. G.2.

a)

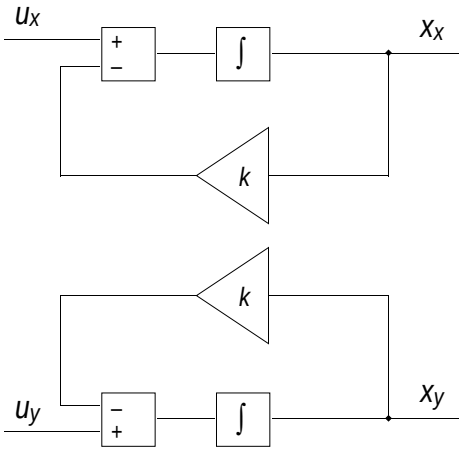

b)

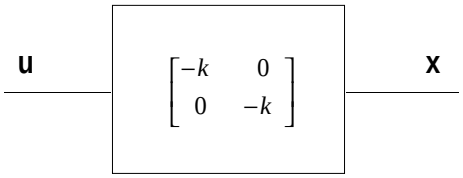

Fig. G.2 Block diagram of a system in a stationary reference frame. a) detail b) overview.

Both poles of this system are equal and real-valued,

$$\mathbf{p}_{1,2} = -k \tag{G.10}$$

Let the input $\mathbf{u} = u_x + j\,u_y$ be rotating with angular velocity ω_1,

$$\begin{bmatrix} u_x \\ u_y \end{bmatrix} = \begin{bmatrix} u\cos\omega_1 t \\ u\sin\omega_1 t \end{bmatrix} \tag{G.11}$$

After the transient, the state **x** will also be rotating with angular velocity ω_1. If instead the reference frame is rotating synchronously with the input **u**, the system is described by equation

$$\frac{d}{dt}\begin{bmatrix} x_x^r \\ x_y^r \end{bmatrix} = \begin{bmatrix} -k & \omega_1 \\ -\omega_1 & -k \end{bmatrix}\begin{bmatrix} x_x^r \\ x_y^r \end{bmatrix} + \begin{bmatrix} u_x^r \\ u_y^r \end{bmatrix} \tag{G.12}$$

where the r-superscripts denote quantities in the rotating frame. The system is also shown as a block diagram in Fig. G.3.

a)

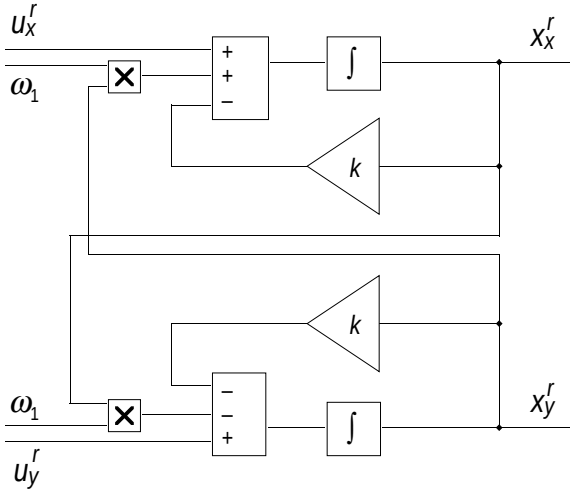

b)

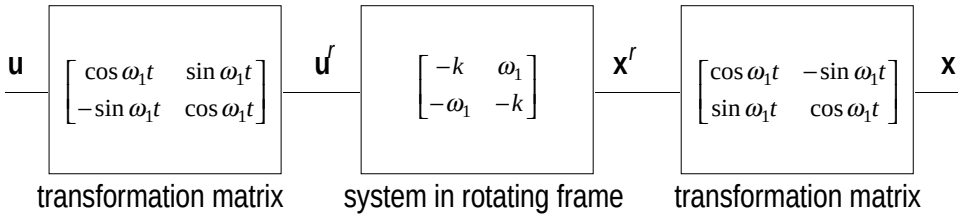

Fig. G.3 Block diagram of a system in a rotating reference frame. a) detail b) overview.

Any vector $\mathbf{v} = v_x + jv_y$ in the stationary frame can be transformed to the rotating frame with the following relation,

$$\begin{bmatrix} v_x^r \\ v_y^r \end{bmatrix} = \begin{bmatrix} \cos\omega_1 t & \sin\omega_1 t \\ -\sin\omega_1 t & \cos\omega_1 t \end{bmatrix}\begin{bmatrix} v_x \\ v_y \end{bmatrix} \tag{G.13}$$

The real and imaginary parts of the input $\mathbf{u}^r = u_x^r + ju_y^r$ will be constant in the rotating frame,

$$\begin{bmatrix} u_x^r \\ u_y^r \end{bmatrix} = \begin{bmatrix} \cos\omega_1 t & \sin\omega_1 t \\ -\sin\omega_1 t & \cos\omega_1 t \end{bmatrix} \begin{bmatrix} u\cos\omega_1 t \\ u\sin\omega_1 t \end{bmatrix} = \begin{bmatrix} u \\ 0 \end{bmatrix} \tag{G.14}$$

and also the state $\mathbf{x}^r = x_x^r + jx_y^r$ will be constant after the transient. If this state is transformed back to the stationary frame as in Fig. G.3 b), using a transformation matrix which is the inverse of the matrix in equation (G.13),

$$\begin{bmatrix} x_x \\ x_y \end{bmatrix} = \begin{bmatrix} \cos\omega_1 t & -\sin\omega_1 t \\ \sin\omega_1 t & \cos\omega_1 t \end{bmatrix} \begin{bmatrix} x_x^r \\ x_y^r \end{bmatrix} \tag{G.15}$$

$\mathbf{x} = x_x + j\,x_y$ will be rotating with angular velocity ω_1. After the transformations, the outputs of both the system in Fig. G.2 and the system in Fig. G.3 will be identical. However, the system in the rotating frame have its poles in

$$\mathbf{p}_{1,2} = -k \pm j\,\omega_1 \tag{G.16}$$

Here we have two systems with the same behaviour, but one of the systems has its poles on the real axis, indicating a well damped system, while the poles of the other system have moved a distance ω_1 from the real axis, indicating a system with less damping. The explanation is that the transformation from the stationary reference frame to the rotating frame introduces a non-linearity to the system. In Fig. G.3 it is seen that states, x_x and x_y are multiplied by an input variable ω_1. As the angular frequency of the input **u** might be changing, ω_1 should be considered an input, and not a constant. The poles are meaningful only for a linear system, i.e. if ω_1 is held constant. Such a limitation does not exist for the system in the stationary frame. The conclusion is that even though equation (G.9) and (G.12) describe the same physical system, the first equation is a linear description, while the second equation is non-linear.